NATIONAL AERONAUTICS AND SPACE ADMINISTRATION

Space Programs Summary No. 37-32, Volume III

for the period January 1, 1965 to February 28, 1965

The Deep Space Network

jpl
JET PROPULSION LABORATORY
CALIFORNIA INSTITUTE OF TECHNOLOGY
PASADENA, CALIFORNIA

March 31, 1965

NATIONAL AERONAUTICS AND SPACE ADMINISTRATION

Space Programs Summary No. 37-32, Volume III

for the period January 1, 1965 to February 28, 1965

The Deep Space Network

JET PROPULSION LABORATORY
CALIFORNIA INSTITUTE OF TECHNOLOGY
PASADENA, CALIFORNIA

March 31, 1965

Preface

The *Space Programs Summary* is a six volume, bimonthly publication designed to report on JPL space exploration programs, and related supporting research and advanced development projects. The subtitles of all volumes of the *Space Programs Summary* are:

Vol. I. The Lunar Program (Confidential)

Vol. II. The Planetary–Interplanetary Program (Confidential)

Vol. III. The Deep Space Network (Unclassified)

Vol. IV. Supporting Research and Advanced Development (Unclassified)

Vol. V. Supporting Research and Advanced Development (Confidential)

Vol. VI. Space Exploration Programs and Space Sciences (Unclassified)

The *Space Programs Summary,* Volume VI consists of an unclassified digest of *appropriate material from* Volumes I, II, and III; an original presentation of the JPL (1) quality assurance and reliability efforts, and (2) environmental- and dynamic-testing facility-development activities; and a reprint of the space science instrumentation studies of Volumes I and II.

W. H. Pickering, *Director*
Jet Propulsion Laboratory

Space Programs Summary No. 37-32, Volume III

Prepared under Contract No. NAS 7-100, National Aeronautics & Space Administration

Contents

I. Introduction

The Deep Space Network (DSN) is a precision communication system which is designed to communicate with, and permit control of, spacecraft designed for deep space exploration. The DSN consists of the Deep Space Instrumentation Facility (DSIF), the Space Flight Operations Facility (SFOF), and the DSN Ground Communication System (GCS).

The DSN is a NASA facility, managed by JPL through a contract between NASA and the California Institute of Technology. The Office of Tracking and Data Acquisition is the cognizant NASA office.

It is the policy of the DSN to continuously conduct research and development of new components and systems and to engineer them into the DSN to maintain a state-of-the-art capability.

The DSN has facilities for simultaneously controlling a newly launched spacecraft and a second one already in flight. Within a few months, it will be able to control simultaneously either two newly launched spacecraft plus two in flight, or the operations of four spacecraft in flight at the same time. The DSIF is equipped with 85-ft antennas having gains of 53 db at 2300 Mc and a system temperature of 55°K, making it possible to receive significant data rates at distances as far as the planet Mars. To improve the data rate and distance capability, a 210-ft antenna is under construction at the Goldstone Mars site, and two additional antennas of this size are scheduled for installation at overseas stations.

The DSIF utilizes large antennas, low-noise phase-lock receiving systems, and high-power transmitters located at stations positioned approximately 120 deg around the Earth to track, command, and receive data from deep space probes. Overseas stations are generally operated by personnel of the respective countries. The DSIF stations are:

I.D. No.	Name	Location
11	Goldstone, Pioneer	Goldstone, California
12	Goldstone, Echo	Goldstone, California
13	Goldstone, Venus (R&D)	Goldstone, California
14	Goldstone, Mars (under construction)	Goldstone, California
41	Woomera	Island Lagoon, Australia
42	Canberra (under construction)	Canberra, Australia
51	Johannesburg	Johannesburg, South Africa
59	MTS	Johannesburg, South Africa
61	Madrid (under construction)	Madrid, Spain
71	Spacecraft Monitoring	Cape Kennedy, Florida

The SFOF is located in a three-story building at the Jet Propulsion Laboratory in Pasadena, California, and utilizes operations control consoles, status and operations displays, computers, data processing equipment for analysis of spacecraft performance and space science experiments, and communication facilities to control space flight operations. This control is accomplished by generating trajectories and orbits, and command and control data, from tracking and telemetry data received from the DSIF in near real-time. The SFOF also reduces the telemetry, tracking, command and station performance data recorded by the DSIF into engineering and scientific information for analysis and use by the scientific experimenters and spacecraft engineers.

The DSN Ground Communication System consists of voice, normal and high data rate teletype circuits provided by the NASA World-Wide Communications Network between each overseas station and the SFOF; teletype and voice circuits between the SFOF, Goldstone Stations, and Cape Kennedy; and a microwave link between the SFOF and Goldstone, provided by the DSN.

II. Tracking Stations Engineering and Operations

A. Flight-Project Engineering

1. Surveyor

Substantial progress on implementation of the *Surveyor* interface with the DSIF has been made. Interface cables were fabricated for the Pioneer site and were installed in February with interface tests scheduled to commence March 1. Procurement of cables for the Canberra and Johannesburg Stations is in progress, the anticipated delivery dates being compatible with the arrival time of the *Surveyor* ground support equipment at the overseas stations which are now prepared to receive and install the *Surveyor* ground support equipment. Selected personnel from all stations supporting *Surveyor* have arrived here for an 8-wk training course at Hughes Aircraft Co.

Compatibility test plans for DSIF-11, -42, and -51 have been published, and a compatibility verification test plan for DSIF-71 has been developed.

2. Pioneer

Further progress has been made on the implementation of the Pioneer Project interface with the DSIF. The Pioneer ground equipment is to be located in a separate room at the Echo site and a suitable raised floor has been constructed. Interface cables for this site have been completed and procurement initiated on cables for DSIF-71, -42, and -51.

The Pioneer telecommunications system design has been evaluated and some deficiencies in spacecraft power margins have been brought to the attention of Ames Research Center. The principal concern is initial acquisition difficulty at Johannesburg due to the low spacecraft power output of 50 mw.

An effort is being made to develop a compatibility test program for the Echo site which will allow for the very late availability of the DSIF equipment there.

3. Mariner

The Venus site is being made ready for support of the *Mariner* Project. In addition to providing receiver capability for *Mariner IV* during the *Ranger VIII* and *IX* missions, the Venus site will stand by with its 100-kw transmitter during the last stages of the *Mariner IV* mission and will provide a back-up receiver for the occultation experiment.

4. Lunar Orbiter

A description of the DSIF *Lunar Orbiter* interface has been written and is undergoing review.

Design reviews of the spacecraft communications package have been completed. Negotiations with the DSN office regarding layout and space at all sites supporting *Lunar Orbiter* are in progress.

5. Ranger

Participating stations reported complete readiness for the support of *Rangers VIII* and *IX*. A method for recording *Ranger* impact time to ± 5 msec has been developed.

6. AC-5 and -6 Missions

Telemetry discriminators, receiver and transmitter crystals and VCO's have been procured for distribution to the stations supporting the two latest *Atlas-Centaur* launches, *AC-5* and *-6*.

B. Systems Engineering and Integration

1. Spacecraft Checkout Facility

The contract for the supply of the shielded enclosure for the spacecraft checkout facility at Goldstone has been let and completion set for May 15.

2. JPL Engineering Planning Document No. 256

Vol. II of Engineering Planning Document No. 256 (described in *SPS 37-31*, Vol. III, p. 5) was printed in February and is scheduled for distribution in March.

3. Spacecraft Monitoring Station

Construction continues on the Control Building at DSIF-71. Walls and roof are in place and joint occupancy of the control room is scheduled for early March. Equipment has been checked out at Goldstone and is scheduled for shipment to the Air Force Eastern Test Range in March. The station is scheduled to be operational with new equipment on May 7, 1965.

4. DSIF-72 (Ascension Island) Implementation

The new space communications station at Ascension Island will provide guidance and command functions and additional tracking and data acquisition support for spacecraft which have direct ascent launchings from Cape Kennedy. This station will not normally be used when other DSIF stations can perform the same functions.

The implementation for this station was placed on an accelerated schedule in December 1964. The revised schedule initially called for station operational readiness by September 15, 1965; however, the new operational readiness date is November 15, 1965.

The system will be GSDS S-band, except for the antenna, which will have a 30-ft azimuth-elevation mount, and the microwave subsystem which must be modified because of the difference in the antennas.

Procurement has been initiated on all major items of equipment and has been completed on approximately 60%. The equipment will be delivered to Goldstone and integrated as a system, using a 30-ft mock-up antenna being procured for this purpose. When the integration and testing are completed, the system will be shipped to and installed at Ascension Island.

5. ECR Panel

An Engineering Change Control Program has been formally initiated for the GSDS S-band system. Of the 12 subsystems, 5 came under the control of the program immediately with the rest to come under its control as cognizant engineering is transferred to the Section 332 Network Engineering Unit.

Once a subsystem becomes operational, no change may be made to the equipment or its documentation without the submission and approval of the *DSIF Engineering Change Requirement* (ECR) form which is submitted to a panel for investigation of the requested change. Its effect on system and subsystem performance and interface, station schedule commitments, and program cost is evaluated. The panel then makes a recommendation to the Change Control Board which makes a decision on each ECR, and if approved, assigns a job number, cognizant engineer, and implementation completion schedule. The ECR panel then follows the progress of the modification until completion.

During the first 2 mo after initiation, 19 ECRs were received and processed by the panel.

C. Goldstone Operations

The tracking of *Mariner IV* continues to be the prime activity at Goldstone. Preparation for, and participation in, the *Ranger VIII* mission was accomplished on a time-share basis. *Ranger VIII* was launched from Cape Kennedy on the morning of February 17, 1965, and impacted on the Moon in the early morning of February 20, 1965. The Echo site participated in the launch standby and three view periods, recovering the transmitted video at the end of the third view period. The Pioneer site provided backup during the third view period and also was successful in recovering the video information. The Venus site tracked *Mariner IV* during the *Ranger VIII* mission.

1. Mariner IV

a. Pioneer site. Tracking activities for the long voyage of *Mariner IV* have progressed to the efficiency of routine operation, with the S-band tracking system requiring only periodic adjustments. A continual flow of spacecraft engineering and scientific data are being recorded and forwarded to JPL for reduction and analysis.

Since the Pioneer S-band system was designated the original development system, new equipment and operating techniques are operationally tested at Pioneer prior to incorporation into other systems. Assembly of all S-band systems continues to be accomplished at the Pioneer site, with limited operational testing being performed, when possible, by the operating personnel of the station involved.

The S-band system of the Madrid Station (DSIF-61) was shipped during January, with several of the station's personnel accompanying it. Most of the Madrid Station personnel remained at Pioneer until late February, and were given additional operating experience by participating in the *Mariner IV* passes.

b. Venus site. Originally programmed to provide high power command transmission to the *Mariner* spacecraft (*SPS 37-30*, Vol. III, p. 4; *SPS 37-31*, Vol. III, p. 17), the Venus site will also provide a full receive capability as additional backup for the Pioneer site. The 100-kw transmitter cone assembly has been modified with the addition of a traveling wave maser and a closed-cycle refrigeration system to enable the standard Venus S-band receiver to receive *Mariner IV* signals. To expedite the Venus S-band receive capability during the *Ranger VIII* mission, a suitcase receiver was installed in the transmitter cone, and an operator rode inside while *Mariner IV* was being tracked. Interfaces with the Pioneer site were accomplished through the Goldstone microwave system.

2. Ranger VIII

a. Echo site. Preparations for *Ranger VIII* began in December 1964 with equipment preparation and minor subsystem testing. With the completion of the *Mariner IV* midcourse maneuvers, additional personnel were available for comprehensive testing and operation of the Echo L-band system. No major changes were made to the system after *Ranger VII*, and testing consisted primarily of insuring full operational capability.

Station personnel participated in six major tests simulating full tracking operation: one acceptance test, January 14; one command procedure test, January 22; two SFOF/DSIF integration tests, January 26 and February 2; and two operational readiness tests on February 8 and 12. Results of these tests indicated the L-band system was in good condition, and that the Echo site, except for minor peaking adjustments, was ready for the *Ranger VIII* launch.

Ranger VIII was launched at 17:05:00 GMT, February 17, 1965, on schedule. It impacted on the Moon's Sea of Tranquility at 09:57:38 (Echo-recorded time) February 20, 1965. Both video channels turned on at the same time and photographs were received simultaneously by Echo and Pioneer sites for 23 min, from 09:34:34 to impact. Except for the erratic signal levels during the midcourse maneuver of the first Echo site pass, a normal tracking mission was accomplished.

The tracking of *Ranger VIII* was different from usual tracking missions in that another spacecraft, *Mariner IV*, was being tracked simultaneously from Goldstone. In Australia, the Woomera Station (DSIF-41) had been relieved of duty in the *Mariner* mission by the new Canberra Station (DSIF-42) in January. Just prior to the launch of *Ranger VIII*, the Johannesburg Station left the *Mariner* track and converted from S- to L-band for final testing and participation in the *Ranger VIII* mission. Removal of the Johannesburg station in South Africa from the *Mariner* track caused an approximate 7-hr nonview period between the end of the Canberra view period and the start of the Pioneer view period.

Since the Pioneer site would be used to back up the Echo site during the third view period of *Ranger VIII*, its removal from the *Mariner* track could add an additional

10 hr of nonview to the Johannesburg 7 for a total of approximately 17 hr. Fig. 1 illustrates the tracking coverage provided for the two spacecrafts during the third and last view period of *Ranger VIII*. The Venus site, using the suitcase receiver assembly, assumed the Pioneer track of *Mariner IV*. Thus, *Ranger VIII* received full coverage from the three DSIF stations, and *Mariner IV*, tracked by Venus, had only the 7-hr, nonview period caused by the absence of Johannesburg.

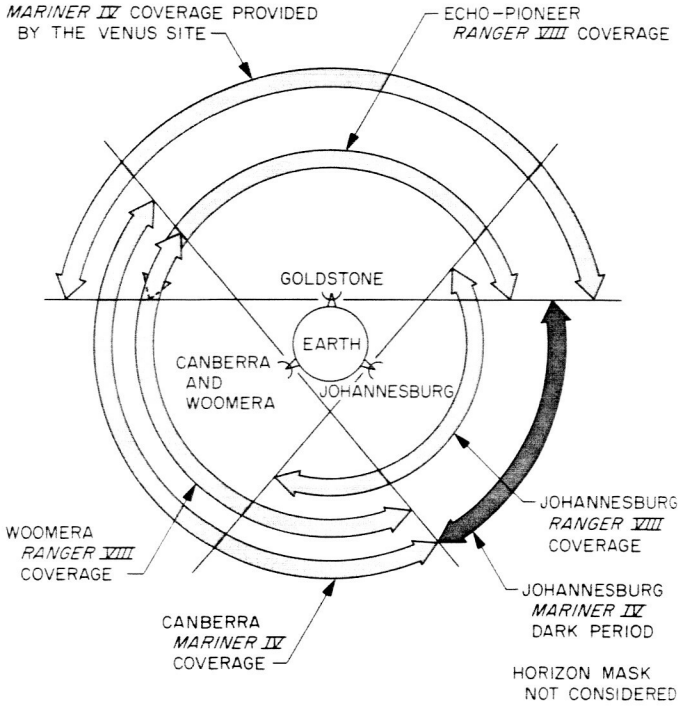

Fig. 1. *Mariner IV–Ranger VIII* DSIF tracking conditions

b. Pioneer site. The Pioneer L-band receiver was installed in the new west wing of the Control Building, while the backup video equipment remained in the original location (Fig. 2). Tests were performed to determine the time necessary to remove the hyperbola and change the antenna feed from S- to L-band so that Pioneer could track *Mariner IV* until just before impact of *Ranger VIII*. Pioneer made the S- to L-band change prior to acquisition and provided full backup for the entire third pass.

3. Additional Projects

a. Surveyor. At the Pioneer site, preparations for the *Surveyor* Project are continuing. All cabling between the *Surveyor* control room and the Pioneer S-band building is completed. The interim compatibility tests between the *Surveyor* installation and the Pioneer S-band system are completed.

b. Atlas-Centaur 5. The Pioneer site was scheduled to participate in the *AC-5* mission scheduled for early

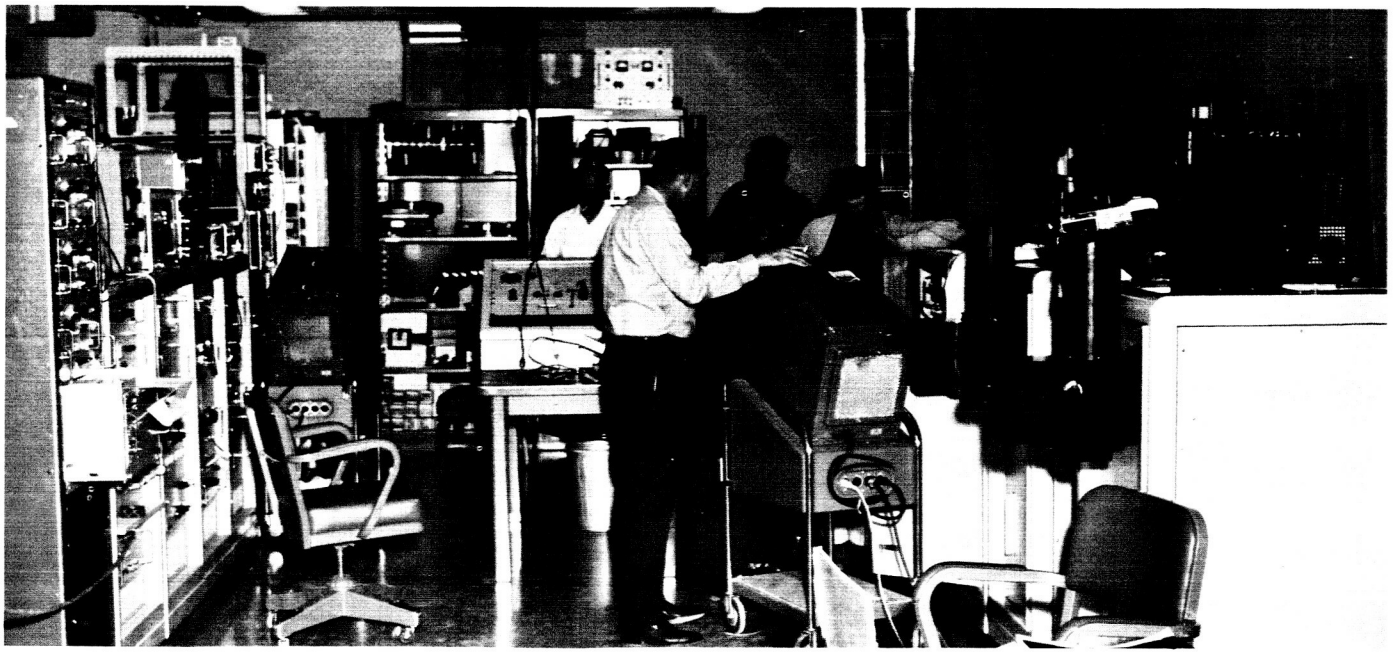

Fig. 2. Video equipment installation testing at Pioneer site

March. A special discriminator was installed in the analog instrumentation system, and the RF subsystem was modified to enable the No. 2 S-band receiver to angle track. Tests in preparation for the tracking support included an integration test between the Pioneer and Venus sites and the SFOF at JPL. A final operational readiness test was held in February.

c. Echo site S-band system. Equipment for the Echo S-band system has begun to arrive at Goldstone. Testing was limited to power turn-on for the units, but full operational tests will be conducted after final installation of the equipment.

4. Construction

Construction of the S-band wing of the Echo site Control Building (G-26) is nearing completion; the walls and roof slabs are now in place. Fig. 3 illustrates the placement of the precast slabs. Interior nonload-bearing walls are being installed, and primary power installation is in progress.

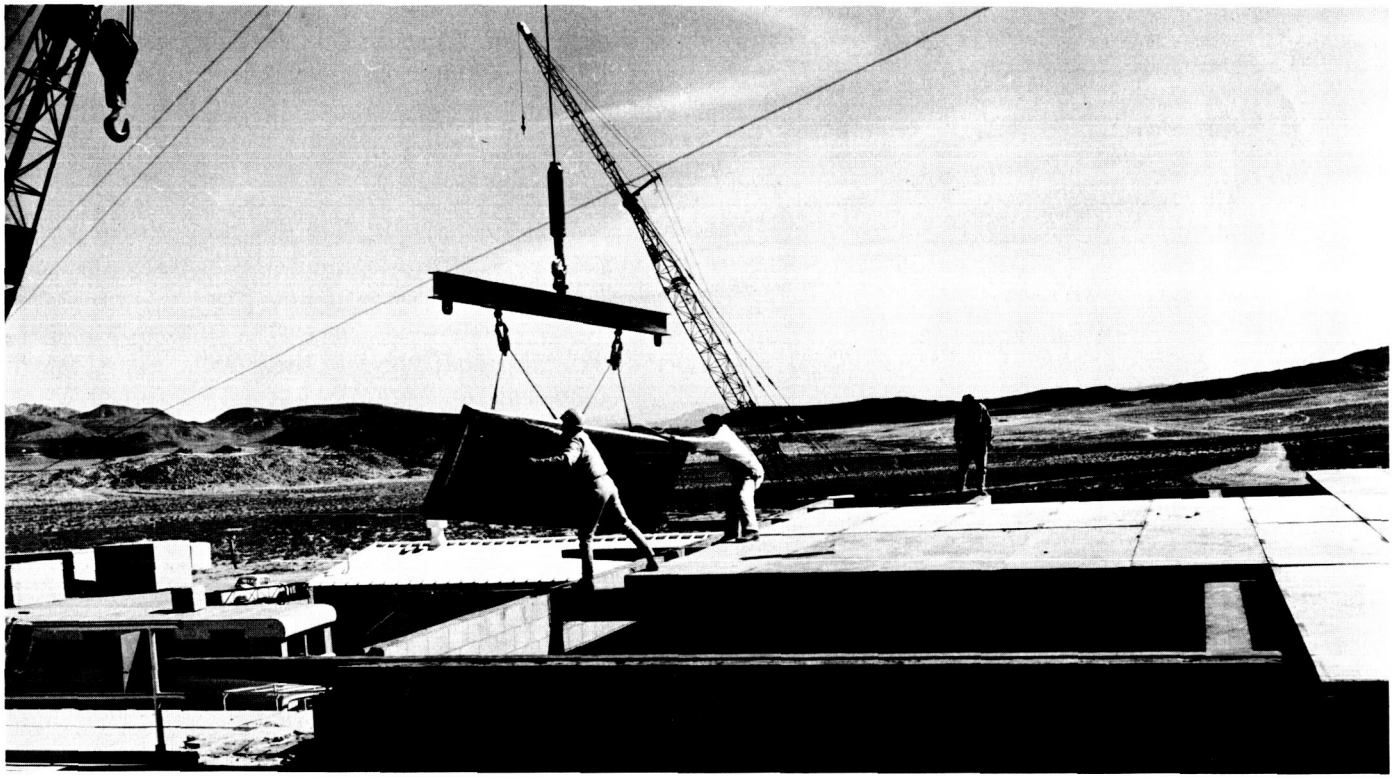

Fig. 3. Placing of S-band wing roof slabs at Echo site

III. Communications Engineering Developments

A. S-Band Implementation for DSIF

1. TWM for DSIF

Problems with the closed cycle refrigerators (CCR's) in the traveling wave maser (TWM) subsystem are gradually being overcome. In most cases problems have been solved through telephone communication between the operators and JPL consultants.

a. Recent activities. A principal problem with the CCR is a result of inadequate separation of oil (compressor lubricant) from the helium gas; the oil eventually clogs the Joule-Thomson circuit. While this problem is being solved, two steps have been taken to alleviate the situation:

(1) Two charcoal traps are being used in each installation; normally one is kept as an idle spare.

(2) Attempts are being made to operate the compressor at reasonably low ambient temperatures to minimize the oil carry-over problem.

The oil contamination problem can be monitored for each station by careful analysis of the varying operating parameters. A weekly report of the daily station log is sent to JPL; the pertinent pressures are plotted on a graph for continuing analysis. It is anticipated that this will mitigate the operational problems and also help in establishing a systematic schedule for servicing and maintenance of the equipment at all stations.

2. Mariner IV Feed Cone Installation

a. Introduction. The *Mariner IV* feed cone installation on the 85-ft antenna at the Venus site was initiated to provide backup support for the *Mariner IV* program (see Section H, p. 32, this volume). This project was originally planned to provide 100-kw transmitter backup, but in December, 1964, it was decided that it would also provide receiver backup which required the installation of a maser, two additional RF switches and associated waveguide changes in the *Mariner* cone. This system was used with the "suitcase" telemetry receiver to track *Mariner IV* on several test trials. It also provided the

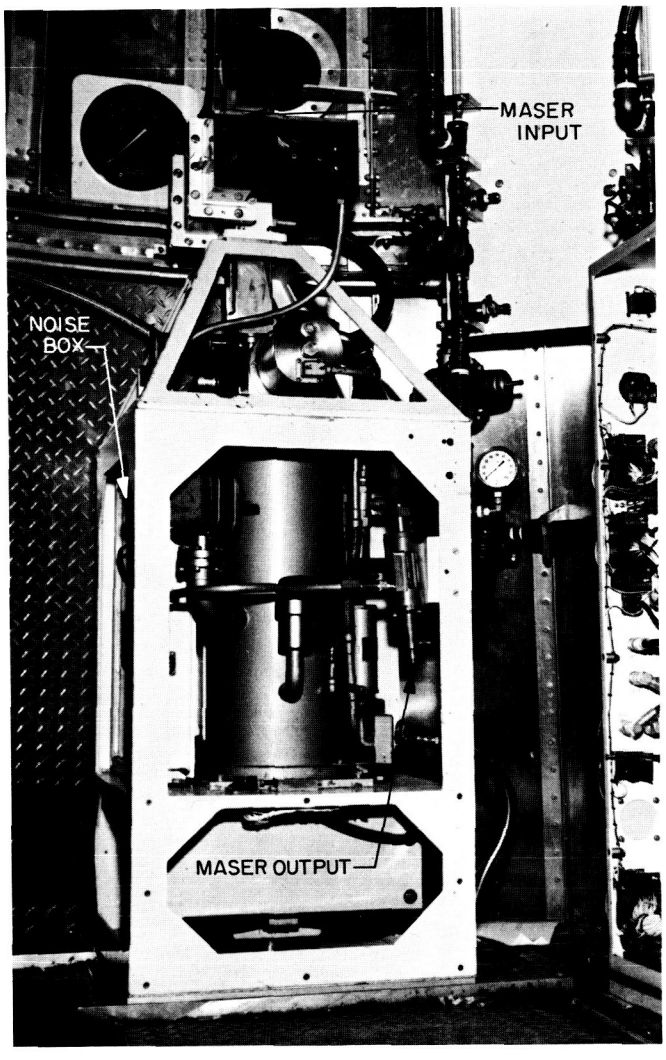

Fig. 1. 2295-Mc DSIF maser installation in *Mariner IV* cone

prime receiving system at Goldstone on February 20, 1965, when the Pioneer site provided the backup for *Ranger VIII* receiving at 960 Mc.

b. Maser installation. The 2295-Mc maser at the Echo site was moved to the Venus site and installed in the *Mariner IV* cone (Fig. 1). The control instrumentation and CCR compressor were installed adjacent to the Venus site cone storage area. Fig. 2 is a block diagram of the RF plumbing and maser instrumentation. A new noise box was fabricated to provide the VSWR load measurement capability. This system can be operated in the Venus site cone storage area with the original DSIF instrumentation or on the antenna with the R&D cable installation and instrumentation in the control room.

The noise source was evaluated in the cone storage area using an ambient and liquid helium cooled waveguide termination to be 62.0 ±2°K at the input to the maser. The system temperature measured in the cone storage area with the cone pointed at zenith was approximately 25.1°K. The system temperature with the cone on the antenna pointed at zenith was 27.7°K.

B. Antenna Servo

Redesign of the high-pressure hydraulic rotary joint for the Venus site 30-ft antenna was described in *SPS 37-31*, Vol. III, pp. 36–38. The dynamic testing and installation is now complete. Fig. 3 shows the installation on the azimuth axis of the antenna; the restraint arms that were discussed previously are shown. For expediency of installation and any future adjustment, turnbuckles with jam nuts were used as a portion of the restraint tension and compression members.

The sizing of the back-up rings in the joint required several assembly and test cycles. Table 1 shows the results of the testing on the final configuration. During the test program the leakage between cavities was checked. Leakage between the drain cavity and atmosphere and to the return cavity was nil; leakage between the return cavity and the pressure cavity was nil with pressure on both ports. However, with pressure on the return port

Table 1. Rotary joint rotational torque

Test pressure, psi	Torque, ft-lb CW[a] and CCW[b]
Zero	75
Normal operating:	
Supply: 1800	
Return: 25	275
Drain: 5	
Special high velocities:	
Supply: 2700	
Return: 65	300
Drain: 25	
Proof test:	
Supply: 3500	
Return: 200	Not applicable
Drain: 100	

[a]CW: clockwise
[b]CCW: counterclockwise

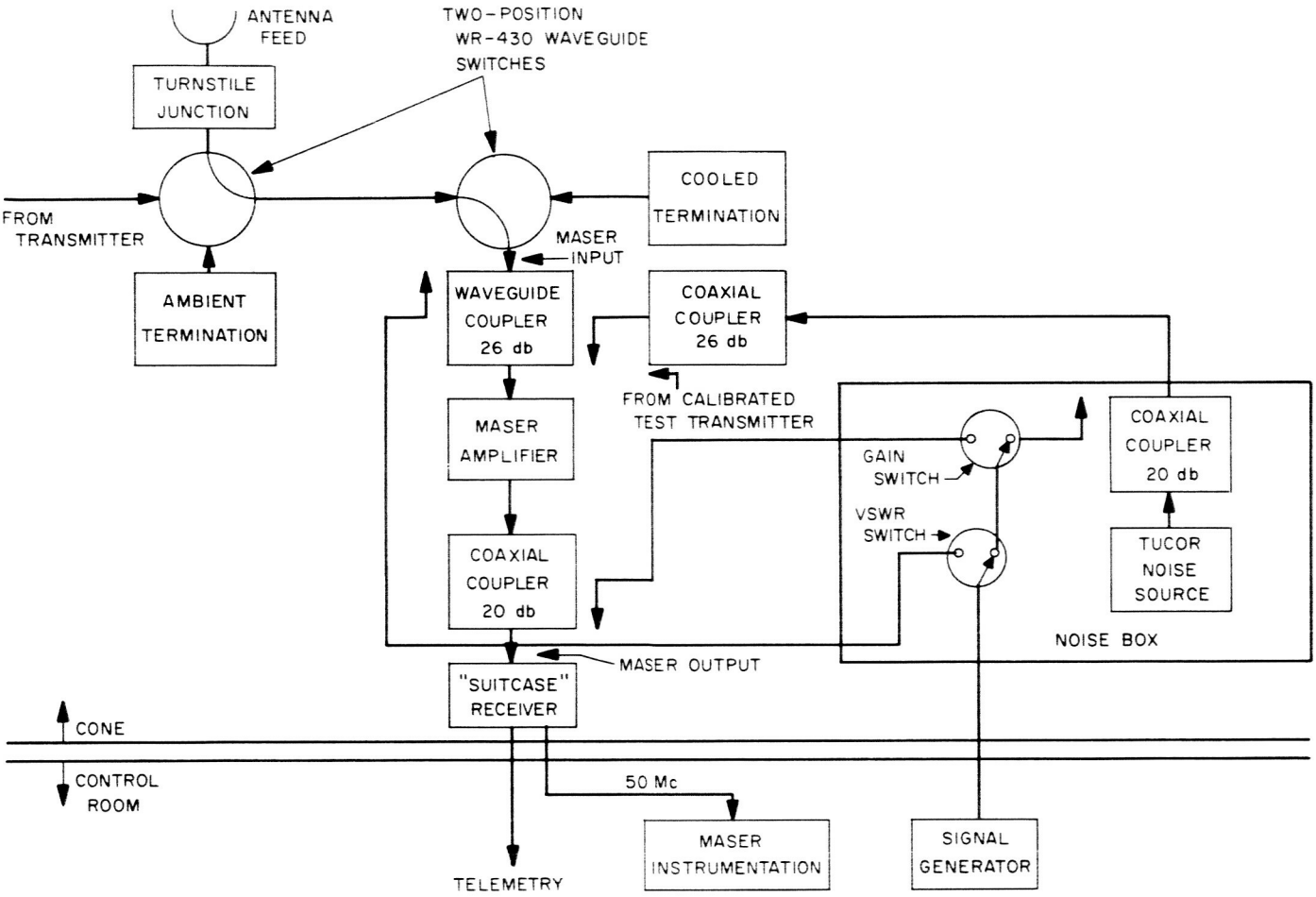

Fig. 2. 2295-Mc maser waveguide and instrumentation configuration

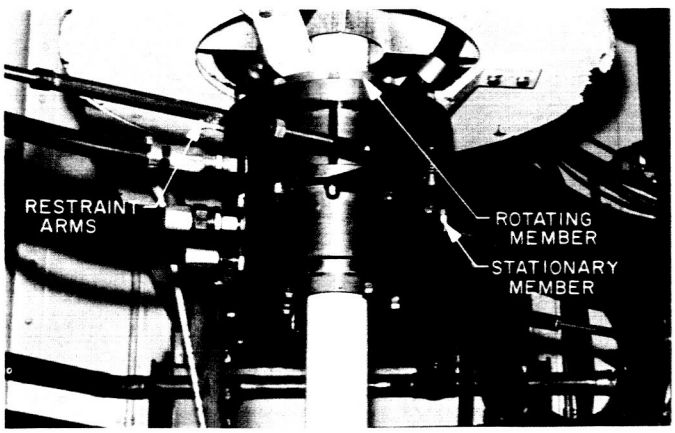

Fig. 3. Rotary joint installed

only, there was leakage at a rate of about 2 cm^3/min to the pressure cavity; this occurs because pressure is being applied in the reverse direction of the chevrons. The leakage of the pressure port to atmosphere was nil.

The cable wrap up and the servo system were both designed to accept a torque component of 500 ft-lb from the rotary joint. The test results show a maximum value of 300 ft-lb, well below the allowable maximum.

C. Ground Instrumentation for *Mariner IV* Occultation Experiment

1. Summary

The *Mariner IV* occultation experiment places unique demands on the measurement capabilities of the DSIF. The principal quantities to be measured in the occultation experiment are doppler frequency and received

power of the *Mariner* spacecraft S-band radio signal versus time.

One channel of the DSIF S-band receiver at the Pioneer site and at the Canberra Station will be used in the standard phase lock configuration to measure doppler and amplitude (by using AGC data). The second channel of the Pioneer receiver will be used in a constant frequency, constant gain mode. The configuration of the receiver at the Pioneer site is described in *SPS 37-30*, Vol. III, pp. 34–35. The receiver at the Venus site will be used as a backup and will be operated in the constant gain, constant frequency mode.

2. Recent Work

Frequency stability data are being obtained from one- and two-way doppler data taken during *Mariner IV* tracking at the Pioneer site. These data are being reduced to obtain spacecraft auxiliary oscillator crystal frequency drift rates as well as random fluctuations.

Preliminary measurements have been made at the Pioneer site using the dynamic AGC voltage from the S-band receiver which is low-pass filtered and digitized on the DIS computer. This digitized data is then used to compute the audio amplitude modulation spectrum of the received signal.

Measurements are being made to determine vehicle transponder lock-on time using the type-approval radio system in the environmental test chamber. Lock-on time is being determined as a function of frequency offset and power of uplink signal.

D. DSN 1964 S-Band Receiver–Exciter System

1. Introduction

The functional description of the Deep Space Network (DSN) 1964 S-band RF receiver–exciter system and preliminary characteristics was published in *SPS 37-28*, Vol. III, pp. 30–39. Ten of these systems have been produced by Motorola, Inc.; seven have been assigned to the DSN and three to the Manned Space Flight Network (MSFN). The systems assigned to the MSFN are identical to the present DSN but are tuned to an MSFN channel frequency. They do not fulfill all the requirements of the MSFN but are adequate for making preliminary compatibility tests with the complete communications system. The design of the improvements to the DSN 1964 system to make it adequate for the MSFN has been completed and is being incorporated into System 11. These design changes are also applicable to the DSN and will be included in subsequent DSN systems. Except for frequency channel assignments and loop noise bandwidths, the DSN and MSFN systems will be essentially identical.

The receiver–exciter subsystem consists of 11 cabinets (Fig. 4), with 8 cabinets installed in the control room and 3 mounted in the antenna structure. The control room cabinets are identified in the figure as C1–C8. The general function of each cabinet is as follows:

Control room cabinets

C1 Exciter control and system monitoring.

C2 Receiver 1 control, range receiver control, and system monitoring.

C3 Receiver 2 control and system monitoring.

C4 Exciter, doppler extractor, and range receiver.

C5 Receiver 1, angle receivers, microwave RF loop, and Receiver 1 telemetry.

C6 Test instrumentation and isolation amplifiers.

C7 Microwave control panel and isolation amplifiers.

C8 Receiver 2, acquisition aid angle receivers and Receiver 2 telemetry.

Antenna-mounted cabinets

1AC1 Test transmitter, test transponder, and test instrumentation.

1AC2 The high frequency portion of the exciter, receivers, and the angle receivers.

1AC3 Receivers 1 and 2 input switching circuit.

2. Receiver–Exciter Subsystem Performance

Performance data of the DSN 1964 subsystem (Table 2 and Figs. 5–12), taken primarily from the final test of Subsystem 10, are presented and are typical of the performance of Subsystems 1–10. Some of the test data are presented in graph form. To avoid duplication, Receiver 1 data only have been plotted. The performance of both

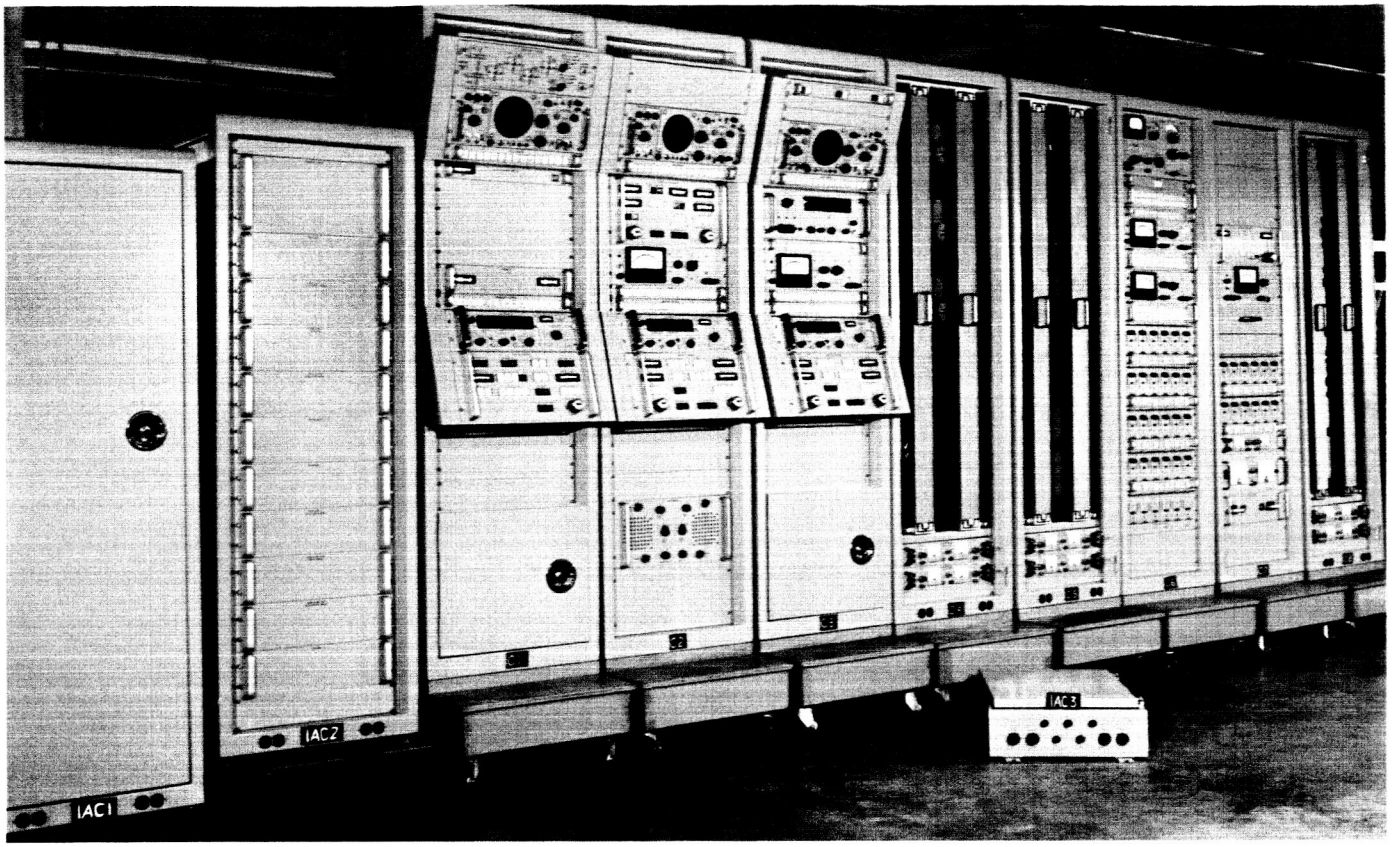

Fig. 4. Receiver-exciter subsystem

receivers is essentially the same. The following comments clarify the discrepancies between the test data and the specification.

The marginal exciter output power level and RF bandwidth are the result of the limitations of the UHF buffer amplifier. This marginal performance condition is being corrected by the use of two buffer amplifiers in cascade. Evaluation of these cascaded amplifiers indicates that the bandwidth will be increased to a value of 18 to 20 Mc and the power output level will increase 1 to 2 db.

The exciter test output is low but will be increased by the removal of an attenuator pad. The output level will then be equal to the test signal output of the final amplifier for compatible use in other subsystems.

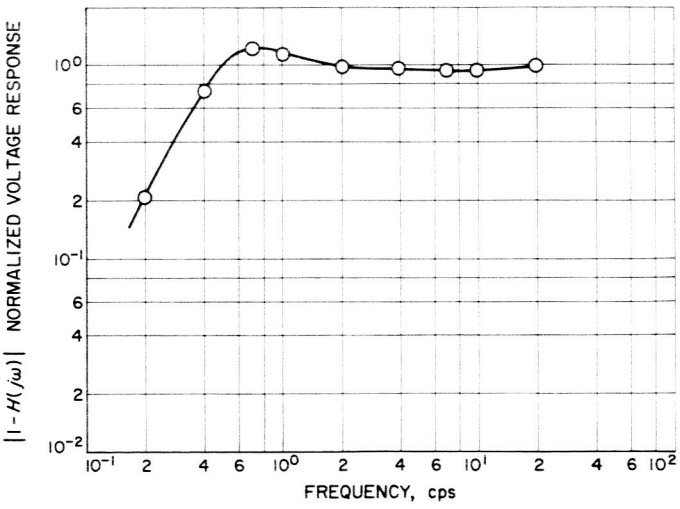

Fig. 5. Synthesizer loop frequency response

The plot of the synthesizer loop frequency response (Fig. 5) indicates the loop to be too narrow. This is a general problem evident in the automatic phase control (APC) loops in the subsystem (Figs. 7, 11, 12) and is caused by using an incorrect value for open-loop gain in calculating the loop filter parameters. The major error is the calculation of detector gains from peak output voltages, assuming the output response to be sinusoidal. Data show that the response in the various detectors deviates from sinusoidal by as much as 15%. At present, data from

Table 2. Receiver–exciter Subsystem 10 test data

Item	Data		Specifications
Exciter:			
1. Power	+33.1		+33 dbm (+3, −0) db
2. RF bandwidth (−3 db)	13.5		10.1 Mc minimum
3. Test output	+3.4		+7 dbm (+3, −1) db
4. Spurious outputs	−31 db		−30 db minimum
5. Modulation			
Command			
Sensitivity	3.16		3.0 (+0.3, −0) rad/v
Bandwidth	3440		100 kc minimum
Ranging			
Sensitivity	5.2		5.0 (+0.5, −0) rad/v
Bandwidth	2.8		2 Mc minimum
Null	41		30 db minimum
Incidental AM	1.1		2 db maximum
6. Synthesizer loop response	(Fig. 5)		
7. Phase jitter exciter and receiver in $2B_{Lo}$ = 12 cps			
Receiver 1	1.8		5 deg rms
Receiver 2	2.8		5 deg rms
Receiver:	Receiver 1	Receiver 2	
1. Noise figure			
Reference channel	9.8	9.7	10.6 db maximum
Hour angle channel	8.8	8.9	10.6 db maximum
Declination channel	9.1	9.0	10.6 db maximum
2. Image rejection	60.0	61.3	45 db minimum
3. AGC characteristic response	(Fig. 6)		
4. Threshold			
($2B_{Lo}$ = 12 cps)	−156	−153	−154 dbm ±1 db
($2B_{Lo}$ = 48 cps)	−149	−147	−148 dbm ±1 db
($2B_{Lo}$ = 152 cps)	−145	−146	−143 dbm ±1 db
5. RF loop response	(Fig. 7)		
6. AGC loop response	(Fig. 8)		

Item	Data		Specifications
7. Angle channels			
Phase tracking	±10 deg	±9 deg	±15 deg maximum
Gain tracking	±1.7	±1.95	±2 db maximum
8. Doppler tracking rate 30-deg phase error −100 dbm			
($2B_{Lo}$ = 12 cps	97.6	124	100 cps/sec
($2B_{Lo}$ = 48 cps)	790	944	920 cps/sec
($2B_{Lo}$ = 152 cps)	4852	5640	5000 cps/sec
9. Telemetry			
Predetected bandwidth			
Channel A (−3 db)	5.60	5.38	6 Mc minimum
S + N to N	(Fig. 9)		
Channel B (−1 db)	3.70	4.04	2.8 Mc minimum
	432	443	420 kc minimum
	24	26	20 kc minimum
	5.3	4.6	4.5 kc minimum
Detected			
Bandwidth (−1 db)	715	780	710 kc minimum
Output level	−4	−2.1	0 dbm ±2 db
S + N to N	(Fig. 10)		
10. Biased doppler			
Bandwidth	1.69		1.5 Mc minimum
	0.433		0.5 Mc maximum
Output level	1.54		1.29 ± 0.29 v rms
Phase jitter	1.4	1.5	8 deg rms maximum
11. RF doppler			
Bandwidth (−2 db)			
0-deg output	197.9		200 kc minimum
90-deg output	360		200 kc minimum
Phase jitter	1.8	1.9	2 deg rms maximum
12. CCTL response	(Fig. 11)		
13. Range receiver			
Loop response	(Fig. 12)		
Noise bias	0.15		0.2 v maximum
Phase jitter	1.4	1.3	5.0 deg rms

the subassemblies which control loop gain (detectors and VCOs) are being evaluated to determine the actual performance characteristics. Loop filter parameters will be corrected accordingly.

The effect of narrow noise bandwidths of Receiver 1 RF loop (Fig. 7) is evident in the reduction in doppler tracking rate capability and improvement in the RF threshold (Fig. 6).

In addition to the narrow noise bandwidth of all APC loops, the data indicate an overshoot in the frequency response curve. This is more pronounced in some of the loops and is caused by RF filtering time constants in the loop in the vicinity of the loop filter. The effect of the additional time constants depends on their magnitude relative to the loop filter time constant. Therefore, in the response curves for the RF loop the overshoot is more pronounced in the 152-cps noise bandwidth position.

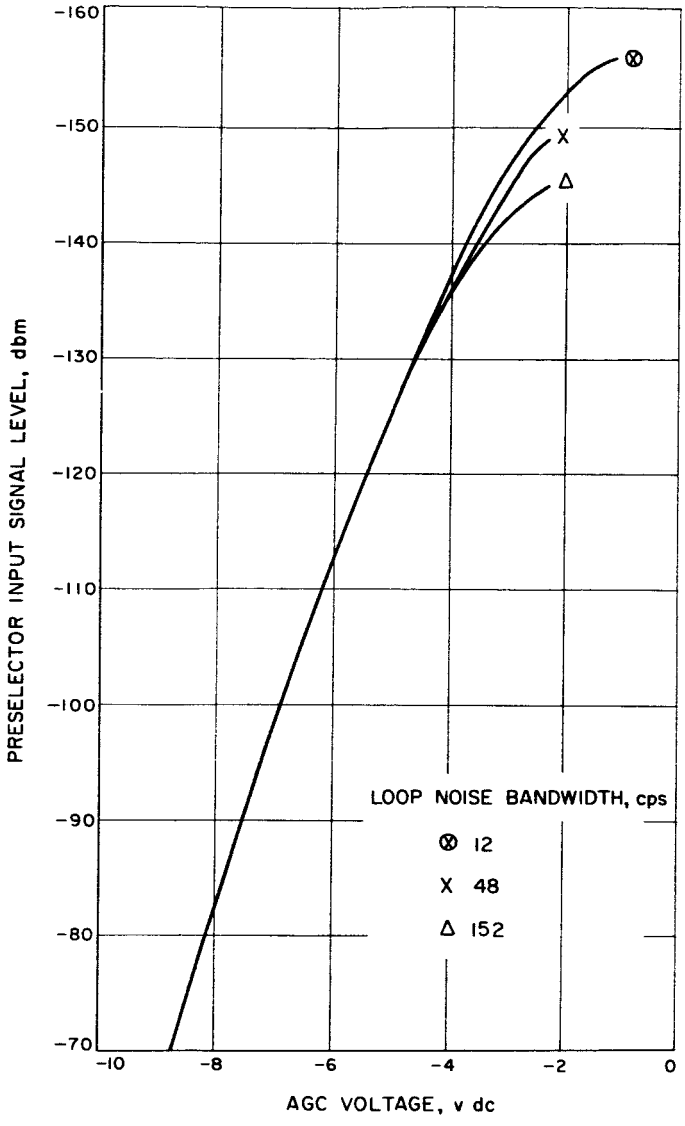

Fig. 6. AGC characteristics

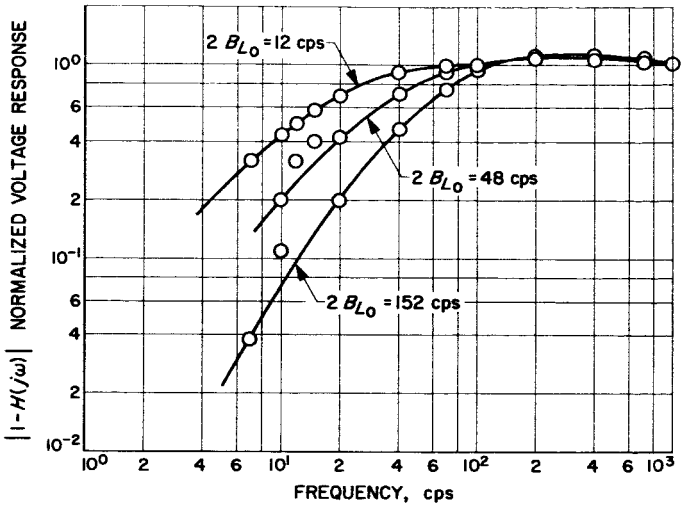

Fig. 7. RF loop frequency response

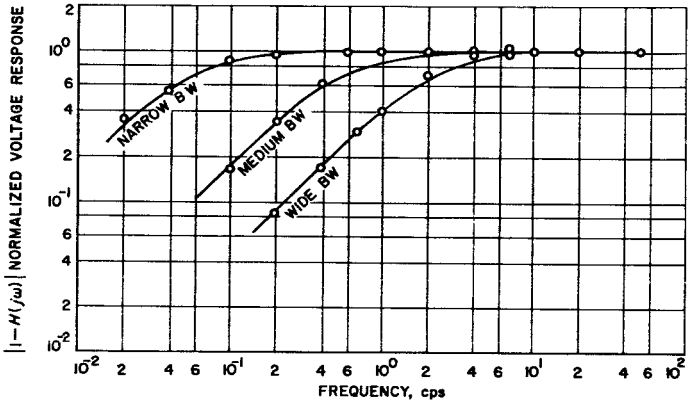

Fig. 8. AGC loop frequency response

Since some RF filtering was removed in the VCO input circuit, starting with Subsystem 4, the overshoot in the RF loop on Subsystem 10 is less than that experienced in the first few systems. Additional filtering is being removed on subsequent systems.

In the response of the ranging receiver (Fig. 12) the fall-off at the higher frequencies is due to the limited response at the phase detector output. This response is being increased to greater than 2000 cps to eliminate the problem.

The discrepancies between the data and specification are of no major consequence and do not adversely affect the performance of the receiver–exciter subsystem in supporting existing or anticipated programs. These discrepancies were noted on Subsystem 1, and the data on Subsystems 1–10 indicated the performance to be consistent. It was decided not to effect any design change until a major redesign such as the MSFN modifications is incorporated.

3. Subassembly Test Fixtures

Adequate alignment and testing of the RF subassemblies or modules require special test equipment in addition to the use of some other subassemblies and commercial test equipment. To this end, a set of ten fixtures was developed at JPL and built by Resdel Engineering Corp. A set of these fixtures will be supplied to subassembly repair centers for use in maintaining the

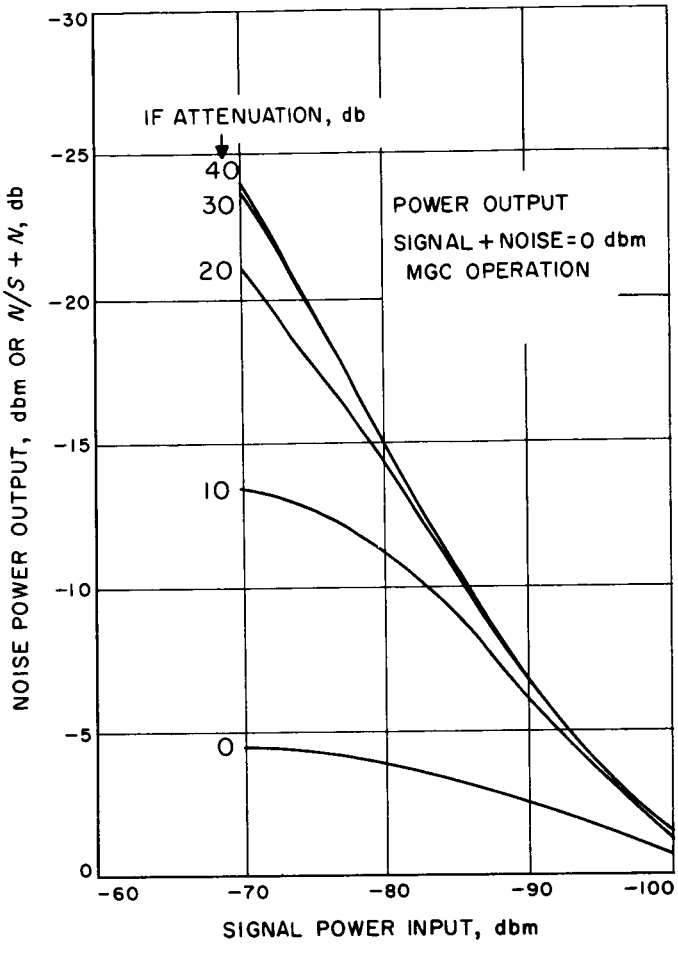

Fig. 9. Wide-band telemetry output signal plus noise-to-noise ratios

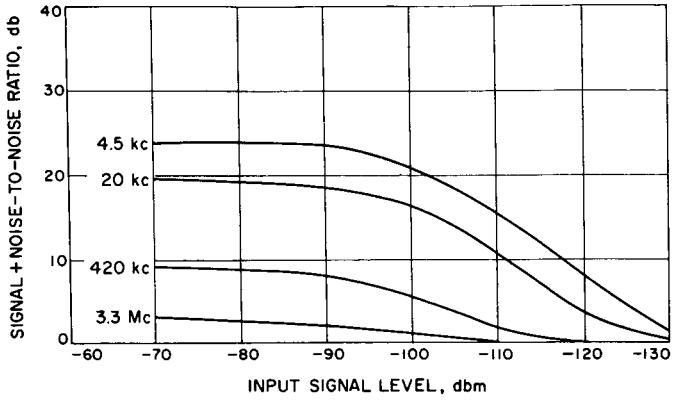

Fig. 10. Narrow-band telemetry output signal plus noise-to-noise ratios

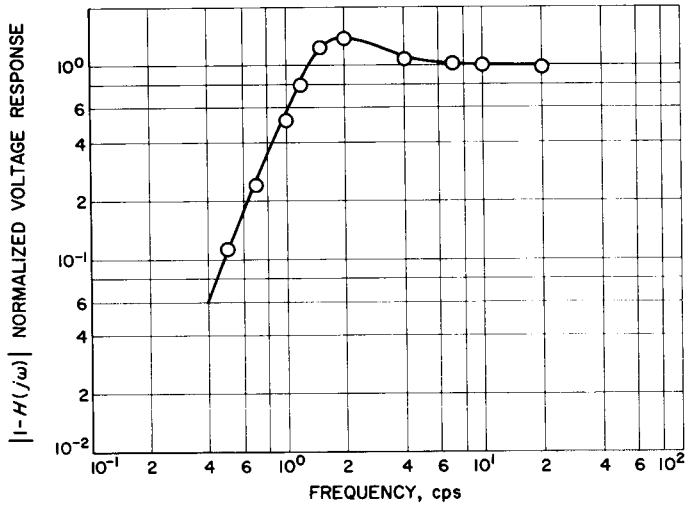

Fig. 11. Code clock transfer loop (CCTL) frequency response

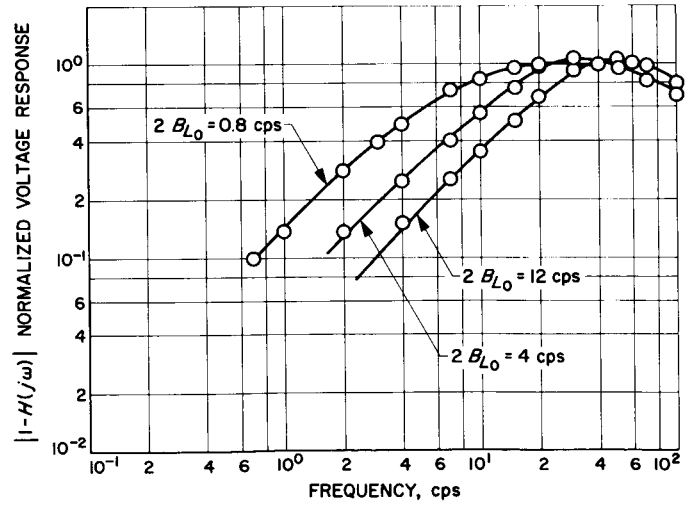

Fig. 12. Range receiver loop frequency response

equipments. These, or similar fixtures, also are used during the production phase. A brief description of the fixtures follows:

(1) A stable DC variable voltage source was designed to supply VCO and AGC test voltages free from AC ripple and capable of vernier control. A battery-powered bridge network was selected because its short-circuit immunity outweighed the disadvantage of its inherent voltage nonlinearity. The general network (Fig. 13) was analyzed, and the following equations of voltage range, voltage linearity, input impedance (as seen by the battery), and output impedance were plotted using an analog computer:

$$y \triangleq \left(\frac{E_{out}}{V}\right) = \frac{x(1-2\alpha)}{1+x+x^2-(\alpha x)^2} \qquad (1)$$

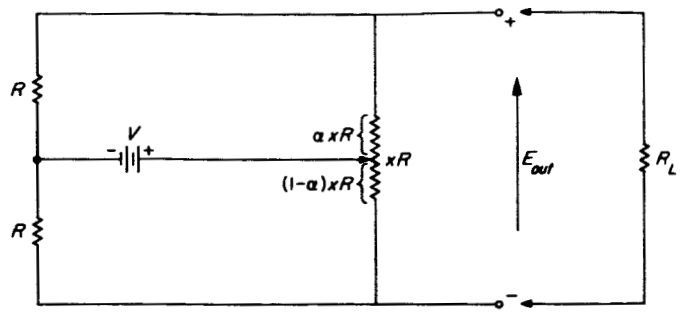

Fig. 13. Stable DC variable voltage source schematic

$$\frac{dy}{d\alpha} = -\frac{2x\left[1 + x + \alpha x^2 - (\alpha x)^2\right] + x^3(1-2\alpha)^2}{\left[1 + x + \alpha x^2 - (\alpha x)^2\right]^2} \tag{2}$$

$$\left(\frac{Z_{in}}{R}\right) = \frac{x + 2\alpha x^2 - 2(\alpha x)^2 + z\left[1 + x + \alpha x^2 - (\alpha x)^2\right]}{2x + z(2 + x)};$$

$$z \triangleq \frac{R_L}{R} \tag{3}$$

$$\left(\frac{Z_{out}}{R}\right) = \frac{x(1 + 2\alpha x - 2\alpha^2 x)}{1 + x + \alpha x^2 - (\alpha x)^2} \tag{4}$$

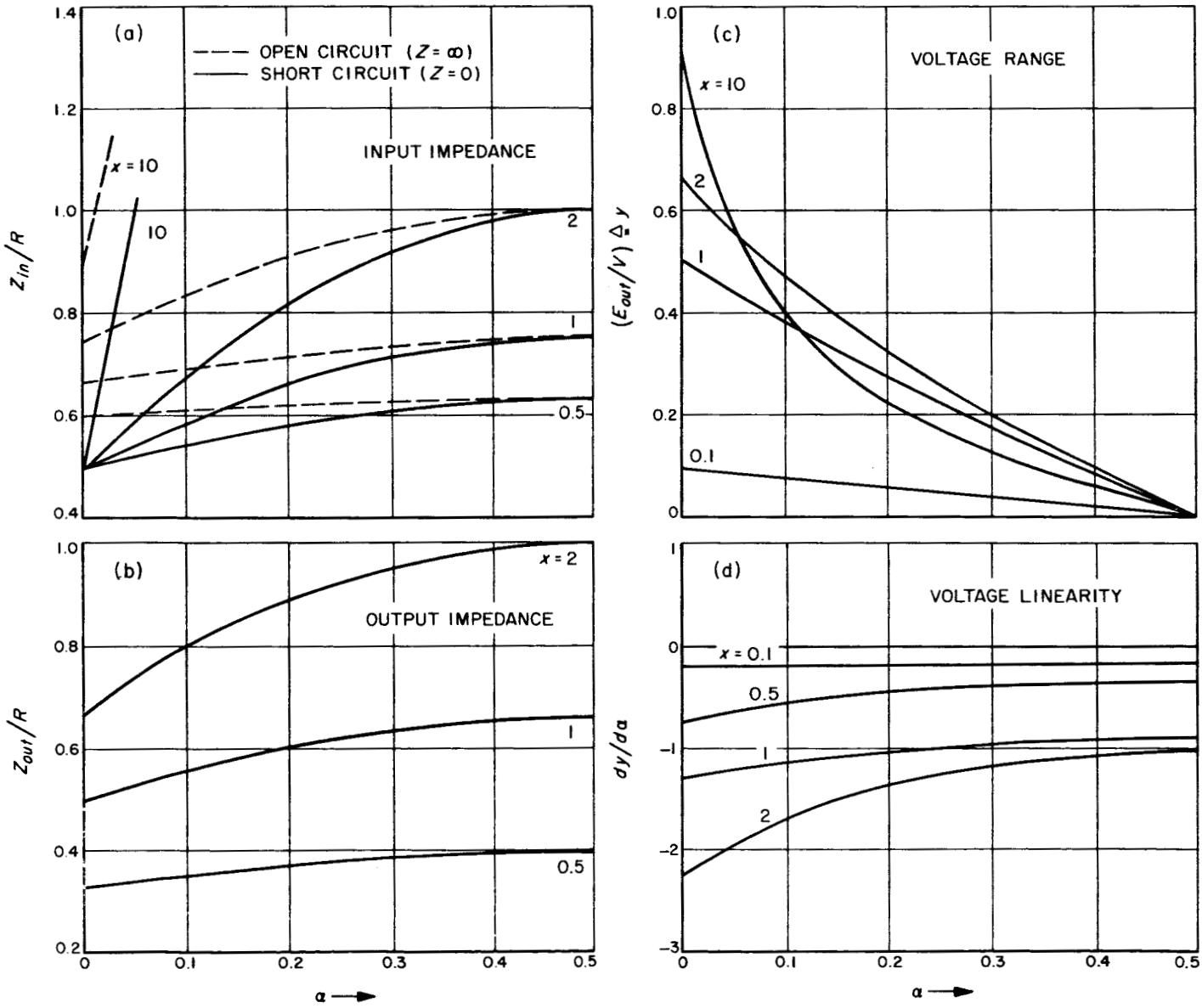

Fig. 14. Stable DC variable voltage source characteristics

As the curves (Fig. 14) illustrate, linearity may be improved at the cost of voltage range and current drain by decreasing the relative potentiometer resistance. Battery drain is increased only slightly when the output is short-circuited. A value of $x = 1$ was selected in the final design trade off of voltage range versus linearity. One unit (Fig. 15) was designed with $R = 300\ \Omega$ to supply low impedance loads ($R_L \leq 2K$) with a continually variable voltage of $\pm 11\frac{1}{2}$ v dc. It was designed to plug into a high-current commercial $22\frac{1}{2}$-v dc source to preclude the need for an excessively large battery. To supply VCO and AGC control voltages a second unit was required, capable of driving impedances of 100 MΩ or more over a voltage range of $\pm 11\frac{1}{2}$ v dc. The AGC control voltage must be capable of a ± 10-μv adjustment around a value of 1 v; to effect so fine an adjustment, an additional variable resistor control was added in series with the battery. Fig. 16 is a schematic of the final unit.

(2) A passive series-resonant load was developed to measure output impedance without the need to inject a signal into the output port of the active device under test. This passive technique is more accurate, especially when transistors are the active elements. When a signal is injected into the output port of a semiconductor device, its characteristics may differ from those obtained under normal operating conditions. Referring to Fig. 17, C is first adjusted for resonance with the 50-Ω reference pad inserted; then retuned for resonance while being driven directly by the unit under test. The readjustment or change in capacity, as read on a vernier dial, can then be correlated to the disparity in the source impedance from a true 50-Ω resistance, i.e.:

$$X_S = X_{C_X} - X_{C_o}$$

where

$X_{C_o} = \frac{1}{2\pi f C_X} \triangleq$ reactance of the capacitor when tuned with a 50-Ω source (pad)

$X_{C_X} = \frac{1}{2\pi f C_X} \triangleq$ reactance of the capacitor when tuned with the unknown source

$X_S =$ source reactance

The absolute source impedance, $|Z_S|$, can be obtained by the standard resistive impedance measuring technique; R_S is then deduced from the relation

$$|Z_S| = (R_S^2 + X_S^2)^{1/2}.$$

Fig. 15. Stable DC variable voltage source

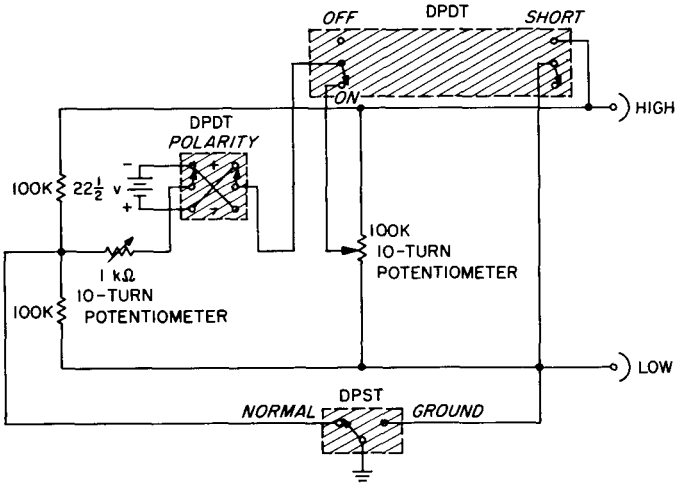

Fig. 16. Low-current variable voltage source

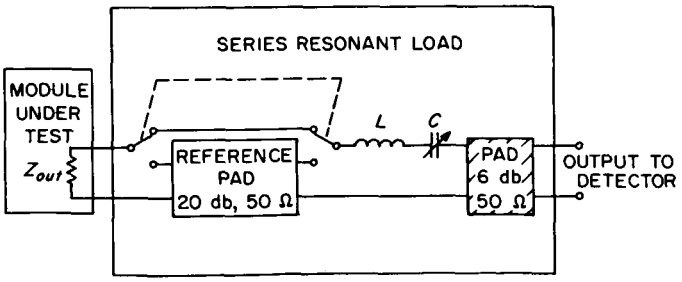

Fig. 17. Passive series resonant load

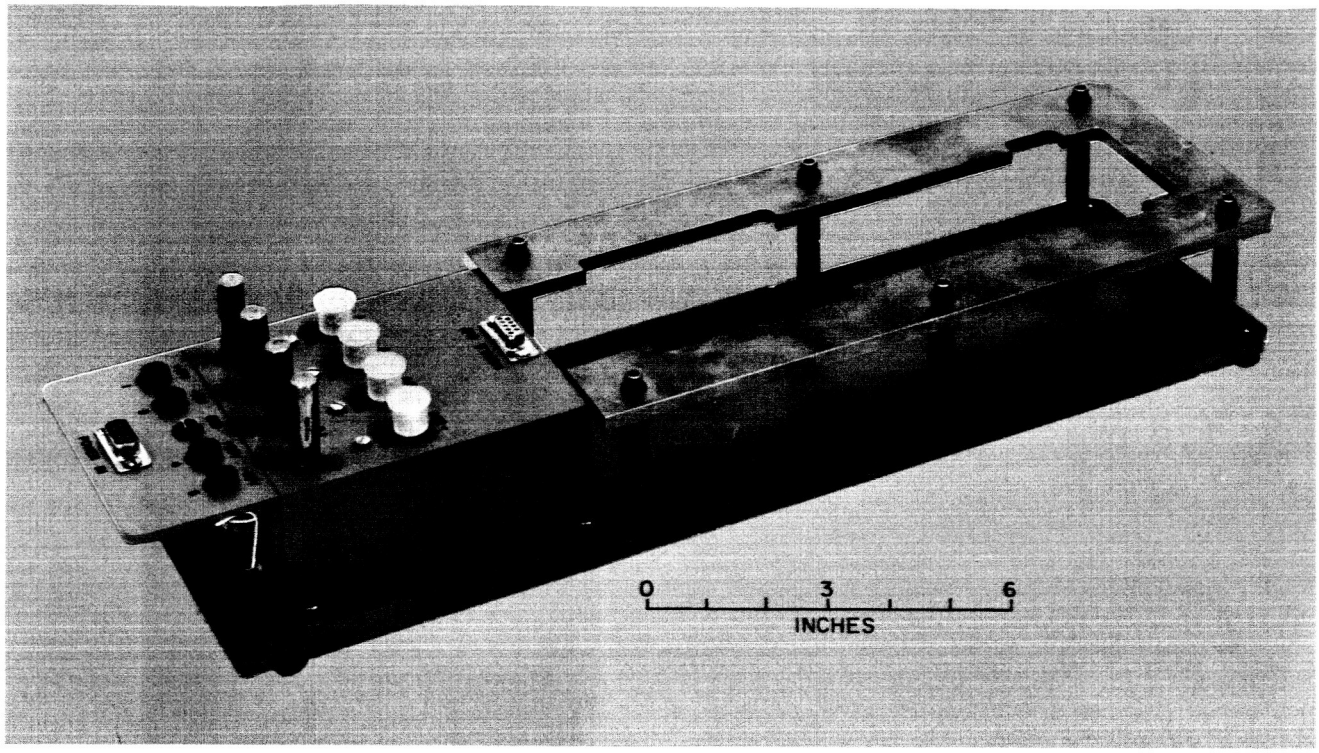

Fig. 18. Line stabilization network test fixture

Various coils may be interchanged to cover special frequencies of interest within the band of 3.8 to 72 Mc. An RF voltmeter or a sensitive receiver is used as the detector, depending on the signal level encountered which ranges from −90 to +30 dbm. The measurement accuracy varies with frequency and signal level, but tolerances in X_s of $\pm j$ 10 Ω are possible, and at frequencies below 25 Mc, $\pm j$ 5 Ω has been achieved. The unit accommodates all of the subassemblies in the frequency range of 3.8 to 72 Mc whose output impedances must be specified.

(3) High-frequency leakage onto the DC power leads of the modules can be detected by a sensitive receiver if they are isolated from power supply filtering by a relatively high impedance. A line stabilization network (Fig. 18) was built to present a load of at least 500 Ω to RFI above 150 kc and, in addition, to furnish convenient BNC pick-off points for the receiver.

(4) The unique waveforms (Fig. 19) needed to test the phase switch subassembly were synthesized by using existing ranging subsystem logic cards which

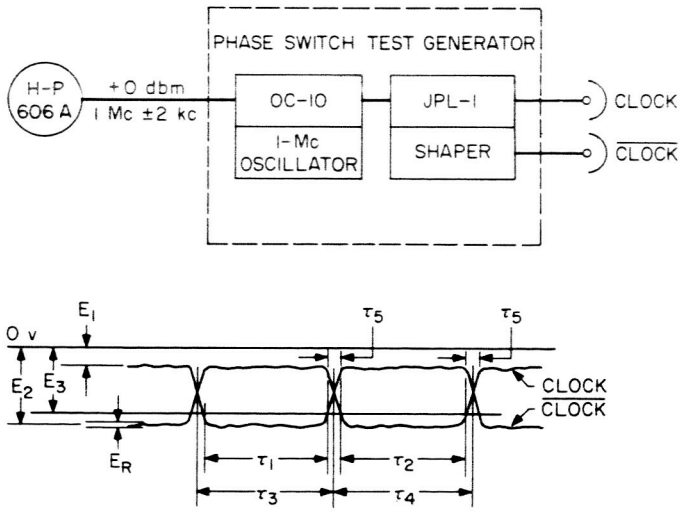

E_1 = −0.55 ±0.1 v
E_2 = −1.35 ±0.1 v
E_3 = −1.15 ±0.02 v (τ_1 AND τ_2 REFERENCE LEVEL)
E_R = 100 mv MAXIMUM (RIPPLE)
$\tau_3 + \tau_4$ = 2 ±0.1 μsec
$|\tau_3 - \tau_4|$ = 0.04 μsec MAXIMUM (~4% OF τ_1)
$|\tau_1 - \tau_2|$ = 0.04 μsec MAXIMUM (~4% OF τ_1)
τ_5 = 0.03 μsec MAXIMUM = TYPICAL 10 TO 90% RISE/DECAY TIME

Fig. 19. Phase switch test generator

were modified as required (the OC-10 oscillator was changed from a free-running to a triggered oscillator), then assembled in a well-shielded box.

(5) Subassemblies with narrow bandwidth crystal filters (20 kc at 50 Mc and 2 kc at 10 Mc) require an extremely frequency-stable generator to trace out their band-pass characteristics. A special source (Fig. 20), capable of supplying signals over the ranges of 10 Mc ±50 kc, 50 Mc ±250 kc, and 60 Mc ±300 kc was designed, whose short-term frequency stability was better than ±1 ppm. A commercial generator operated in its low-frequency range, where an absolute stability of ±10 cps is easily realized, is translated to 10 Mc by mixing it with a crystal-controlled 9.5-Mc reference. Since variations in the signal generator frequency are not multiplied by the translation process, the result is very low-frequency jitter and very fine-frequency control about 10 Mc. Frequency multipliers are then introduced to supply the 50- and 60-Mc outputs.

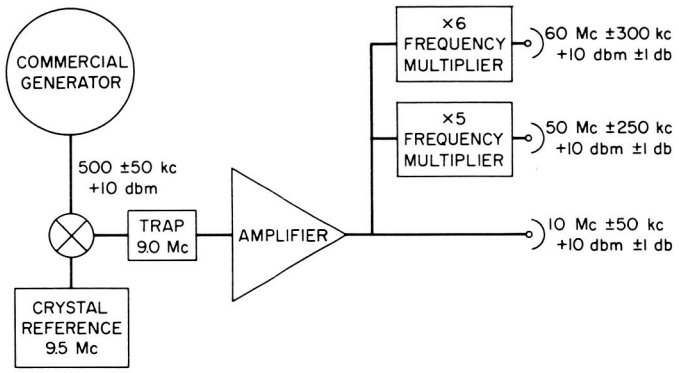

Fig. 20. Frequency stable signal generator

The other fixtures, which required considerably less design effort, are:

(6) A precision resistor set, to supply the special values required by the tests.

(7) An R-C integrator set, to filter unwanted AC from low-voltage DC measurements.

(8) A power pin access fixture (Fig. 21), to effect convenient access of subassembly power leads (e.g., to measure current drain).

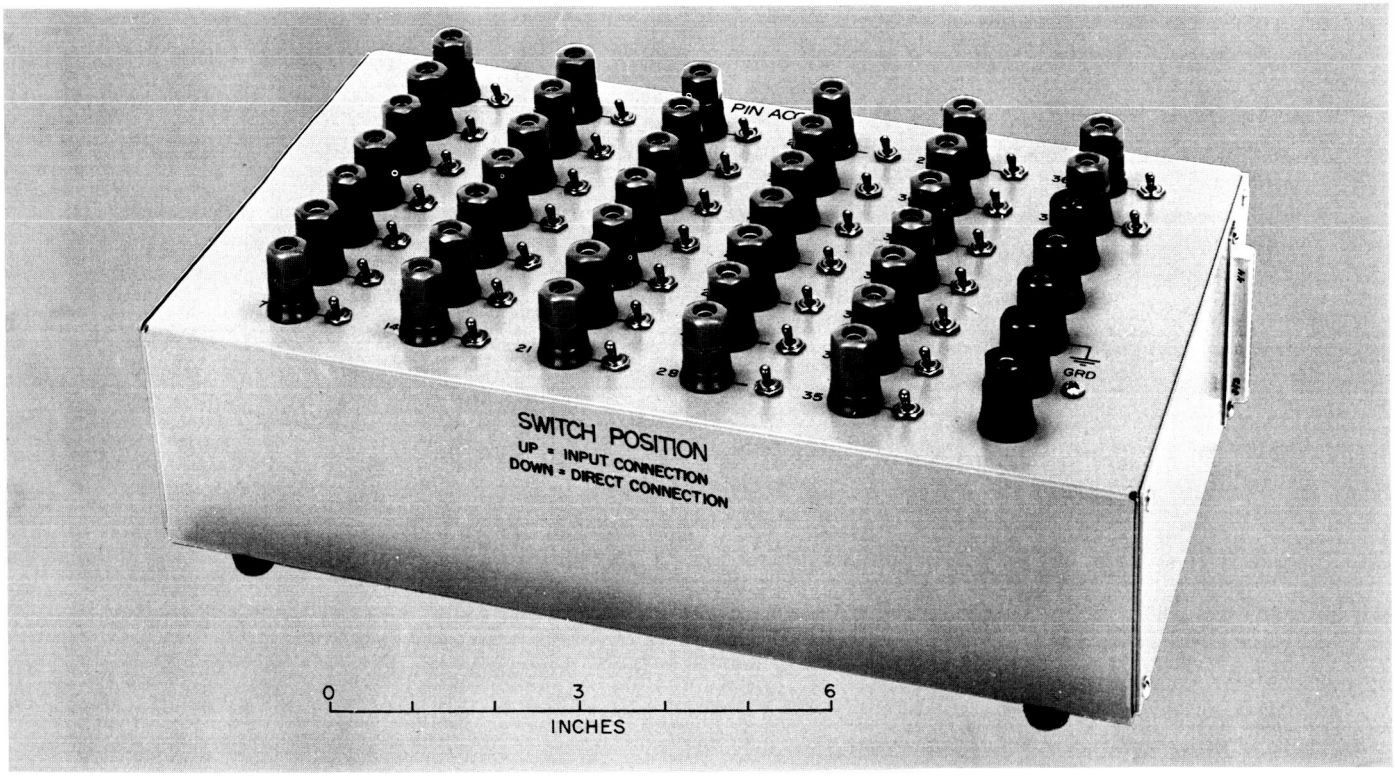

Fig. 21. Power pin access test fixture

(9) A 22-Mc phase shifter, patterned after the 10-Mc subsystem phase shifter, used in the measurement of the transfer function of the exciter loop phase detector.

(10) A variable τ loop filter set, simulating the subsystem noise bandwidths of the various loops for $\times 1$ closed-loop bench configurations. These loop filters combined with existing subassemblies and the VCO's under test provide all the necessary special test facilities required to evaluate phase stability in the threshold noise bandwidths of the loops.

E. Test Transmitter–Transponder

1. Introduction

The specialized RF test equipment used with the receiver–exciter subsystem is contained in two primary subassemblies–the test transmitter and the test transponder. These two subassemblies, with associated equipment, provide the capability of: (1) accurate signal level calibration of the DSN receiver, and (2) simulation of the spacecraft-to-ground link or two-way link between the spacecraft and ground.

One set of these two subassemblies is mounted in the antenna racks of the receiver–exciter subsystem and, when connected by a hard line to this subsystem, one- and two-way tests over cable can be performed. Another set is mounted in the collimation tower for similar tests over an air link. In addition, the test transponder can be installed in an aircraft for acquisition tests, doppler and range measurements, and operator training.

A complete set of equipment for the test transmitter–transponder consists of: test transmitter, test transponder, Harrison Labs 129/802B power supply, Hewlett-Packard 431B power meter, and interconnecting cables.

2. Test Transponder

The test transponder consists of a fully coherent transponder, transmitter, and associated microwave components as shown in Fig. 22. The transmitter has the

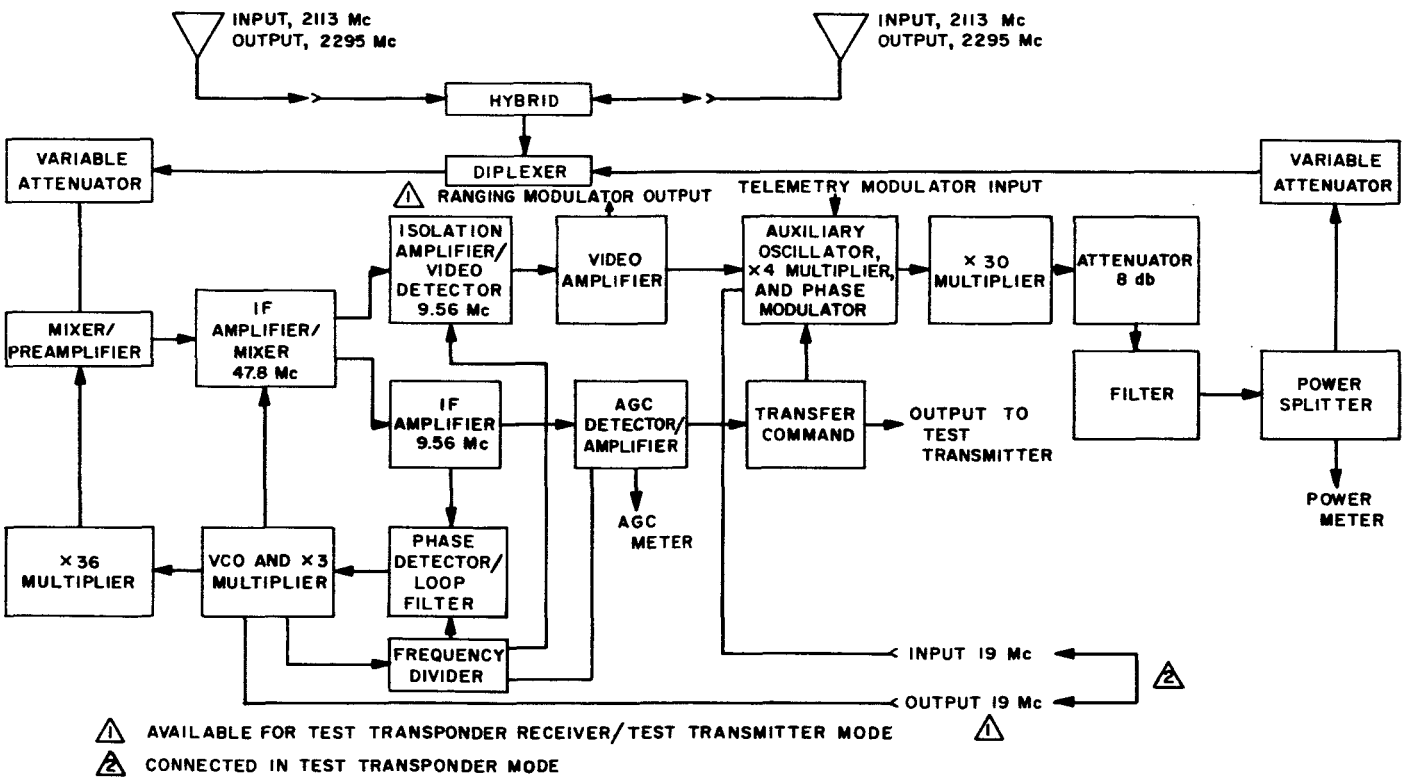

Fig. 22. Test transponder functional block diagram

capability of being driven by a fixed frequency auxiliary oscillator in a noncoherent mode or by the receiver VCO in a coherent mode. In addition, the VCO output is available to drive the test transmitter in a two-way coherent mode with the test transponder receiver. Turn-around ranging capability is also provided.

The transponder in the test transponder subassembly is similar to the *Mariner C*. Frequency agility is attained by omission of the 4500-cps noise bandwidth predetection filter, thus eliminating the necessity of changing the filter each time the frequency is changed to another channel. The penalty of this design is that the threshold is limited by the capability of the receiver to perform under the high levels of noise in the predetection noise bandwidth of approximately 1 Mc. The degradation in performance in this configuration can be seen in the comparison of the AGC curves of a *Mariner C* transponder receiver and the test transponder receiver (Fig. 23). The threshold, however, is adequate for the range of signal levels used in test, which are primarily strong signals. Performance characteristics of the test transponder are listed in Table 3.

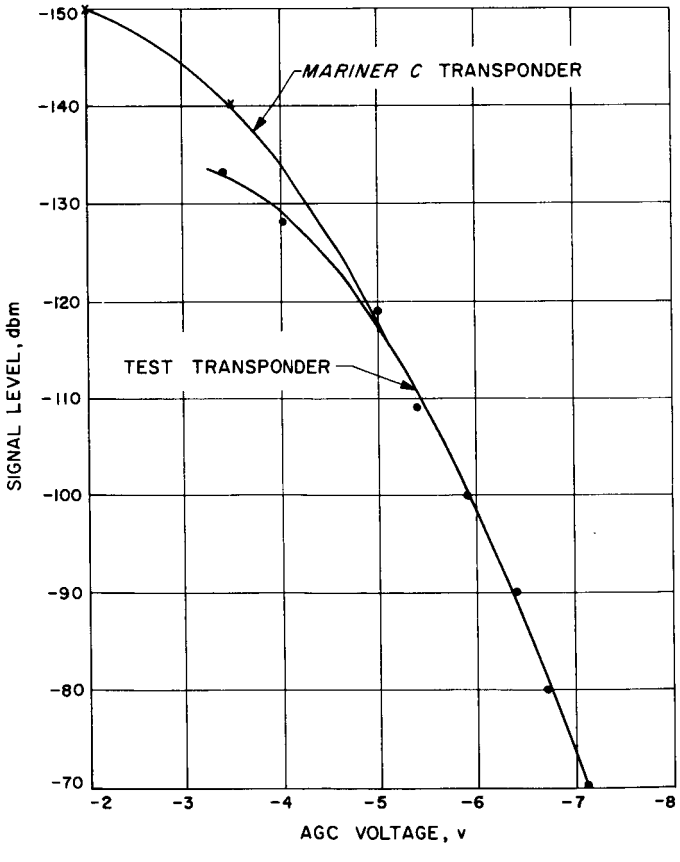

Fig. 23. Test transponder, AGC characteristics

Table 3. Test transponder performance characteristics

Receiver:	
Frequency	2113.3125 Mc (nominal) operational from 2110 to 2120 Mc
Tracking capability	± 3 parts in 10^8
Noise figure	<11 db without variable attenuator
Input signal range	-50 dbm to threshold
RF loop	
Design noise bandwidth ($2B_{L_0}$) in predetection	
N/S ratio = 23.5 db	20 cps
AGC loop	
Design noise bandwidth	<2 cps
Loop filter time constant	23 sec
IF frequencies	47.8 and 9.56 Mc (nominal)
VCO stability, phase frequency (at constant temperature)	<9-deg peak in $2B_{L_0} = 20$ cps
	1 ppm, long-term
Ranging channel	
Bandwidth (-3 db) video out	100 cps to 1.65 Mc (minimum)
Video response	140 nsec rise and fall (maximum)
Transmitter:	
Frequency	2295 Mc (nominal)
Output power	-20 to -120 dbm
Phase stability	<9-deg peak in $2B_{L_0} = 20$ cps
Frequency stability	
Auxiliary oscillator	1 ppm, long-term
Modulation	
Type	Phase
Deviation	Variable to 2.5 rad
Sensitivity	
Telemetry	1 rad peak/v peak
Ranging	2 rad peak/v peak

The test transponder subassembly chassis, or drawer (Fig. 24), constructed of welded aluminum plates contains the transponder subchassis which houses the transponder modules. The remaining components in the drawer include a diplexer, hybrids, attenuators, filters, and a power decoupling box.

All controls are on the front panel. Two connectors on the rear panel provide DC power input and RF input–output. Front panel connectors are: 19-Mc output, 19-Mc input, ranging modulation output, telemetry modulation input, transfer command, telemetry output, and RF input–output.

3. Test Transmitter

The test transmitter provides a stable, accurately calibrated signal source. The signal is generated by one of

the two selectable VCO's (Fig. 25) which is then multiplied 120 times by solid-state amplifiers and multipliers to give the required S-band output. This circuitry is the same as the transmitter portion of the test transponder. Accurately calibrated step and variable attenuators, and a power monitor at a high power level, permit precise control of the output power level. The power is then split by a hybrid to provide outputs at both the front and rear panels. Shielded compartments, extensive use of filters, and power decoupling keep leakage to a minimum.

Provision for modulation is made through front panel connectors for both telemetry and ranging.

The VCO contains a variable voltage source to control its frequency. A front panel switch is available to select either VCO 1 or 2.

Table 4 lists the performance characteristics of the test transmitter.

The transmitter drawer (Fig. 26) is a dip-brazed aluminum chassis. The drawer is divided into ten compartments; four on the top, and six on the bottom. These compartments are used to separate the input and output circuits, power monitoring circuits, DC supply, and circuits at different frequencies from each other. Coaxial filters are used whenever low-frequency energy is passed from one compartment to another.

The S-band compartment, containing high-level S-band energy, is provided with a double cover as added insurance against RF leakage. All covers are rimmed with double bead, rubberized RFI gasket material. To provide good conductive surfaces and reduce RF leakage to a

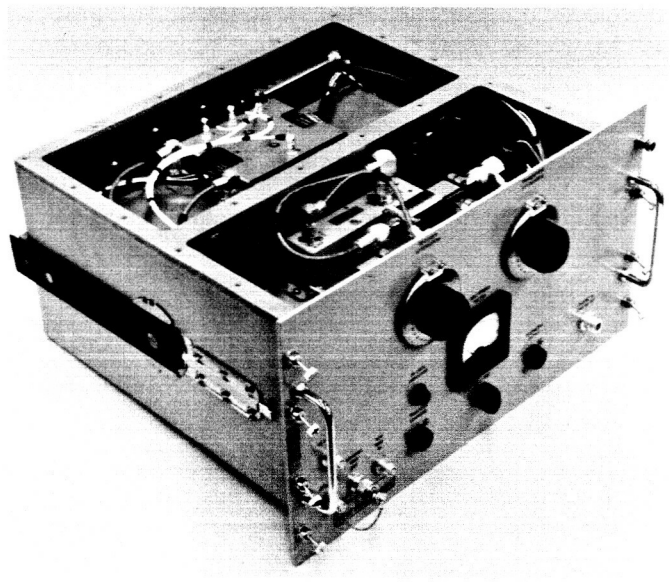

Fig. 24. Test transponder

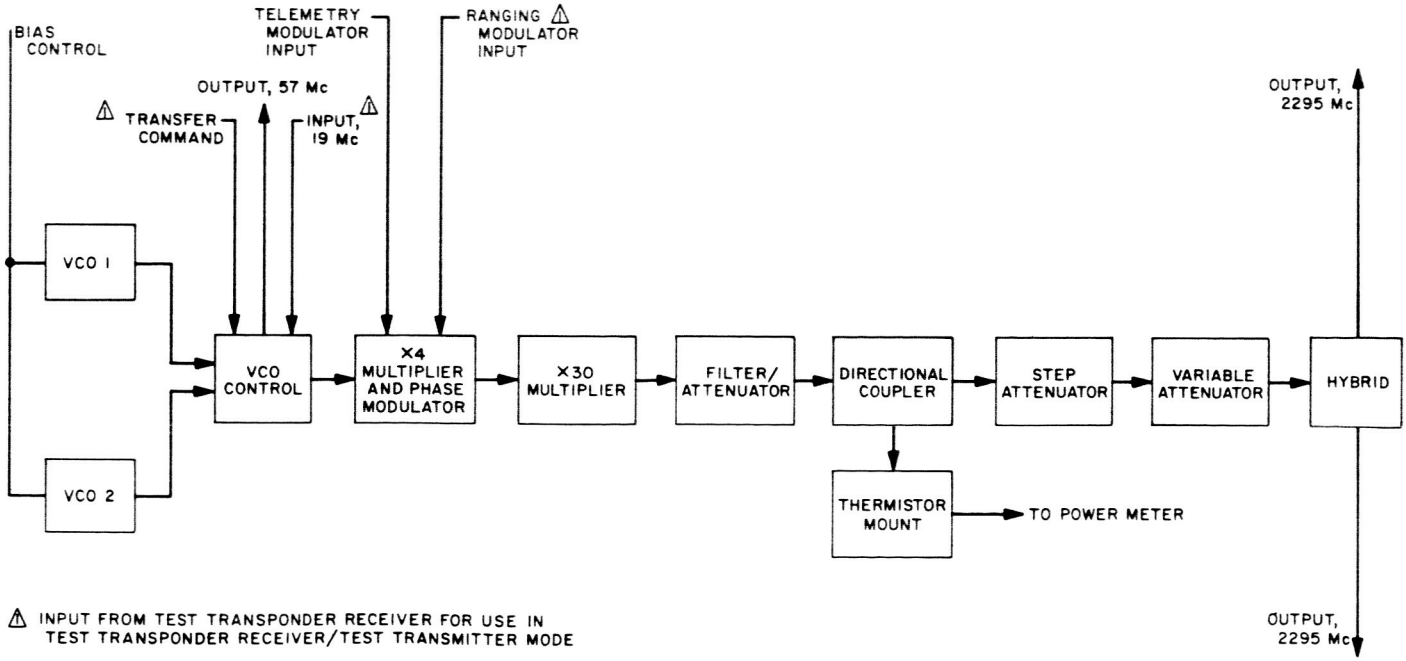

Fig. 25. Test transmitter functional block diagram

Table 4. Test transmitter performance characteristics

Frequency	2295 Mc (nominal)
Bandwidth	>15 Mc
Power output	−45 to −195 dbm
Power output accuracy	Settable to ±0.5 db of absolute
Phase stability	<9-deg peak in $2B_{L_0}$ = 20 cps
VCO	
Frequency	19.125 Mc (nominal)
Tuning range	±3 parts in 10^6 with a single VCO crystal
Frequency stability (at constant temperature)	1 ppm, long-term
Output monitor	3 times VCO frequency
Modulation	
Type	Phase
Deviation	Variable to 2.5 rad
Sensitivity	1 rad peak/v peak telemetry 2 rad peak/v peak ranging
Stability	±5% from 0 to 50°C
Bandwidth	1.8 Mc (minimum)
Radiation level	Less than −150 dbm as detected by a tuned dipole 1 m from the test transmitter
Spurious signal level	At least 40 db below the CW signal level

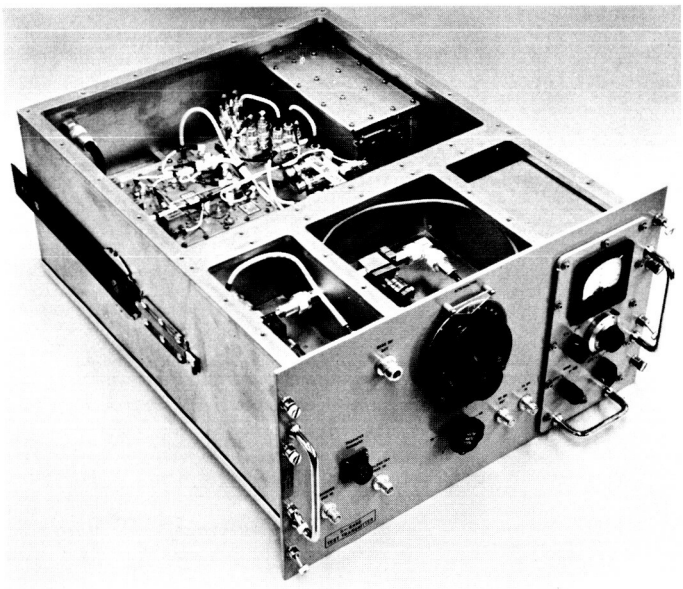

Fig. 26. Test transmitter

minimum, the drawer is silver-plated after proper treatment of the aluminum, and then a gold flash is added to protect the silver.

All controls are on the front panel. Three connectors on the rear panel provide: S-band output, ±28-v input, and power meter output. Six connectors on the front panel are: 19-Mc input, 57-Mc output, ranging modulation input, telemetry modulation input, transfer command, and S-band output.

F. S-Band Cassegrain Monopulse Feed Development

1. Summary

Development of an S-band Cassegrain monopulse (SCM) feed has been completed. The present SCM feed is a modification of a prototype feed described in *SPS 37-18* and *-19*, Vol. III. It is a dual frequency (2110 and 2295 Mc), dual polarization (right and left circular), diplexed, monopulse (simultaneous lobing) tracking feed that utilizes higher-order waveguide modes to: (1) achieve sidelobe suppression in the sum channel, and (2) obtain dual-plane error channels from a single feed horn. The design of the feed is illustrated and discussed, and a brief outline of the theory of operation is presented.

2. Background

The prototype SCM feed was a dual polarization, monopulse feed utilizing a multimode matching section in order to propagate both sum and difference modes through a single, square cross section, pyramidal horn. The resulting primary patterns were acceptable (*SPS 37-16*, Vol. III, p. 18), and produced a secondary antenna efficiency as measured on several radio sources of approximately 47%. The zenith antenna temperature was about 25°K.

Although the performance of this prototype feed was acceptable, and represented a considerable improvement in the performance of tracking feeds, the S-band development schedule permitted some further research to be carried out before finalizing the design of the complete SCM cone assembly. A contract was awarded in June 1963 to Hughes Aircraft Co., Fullerton, California, to explore the possibility of utilizing higher-order waveguide modes for the sum channel in order to achieve partial or complete sidelobe suppression comparable to that obtained at JPL for a circular cross section listening feed (Ref. 1).

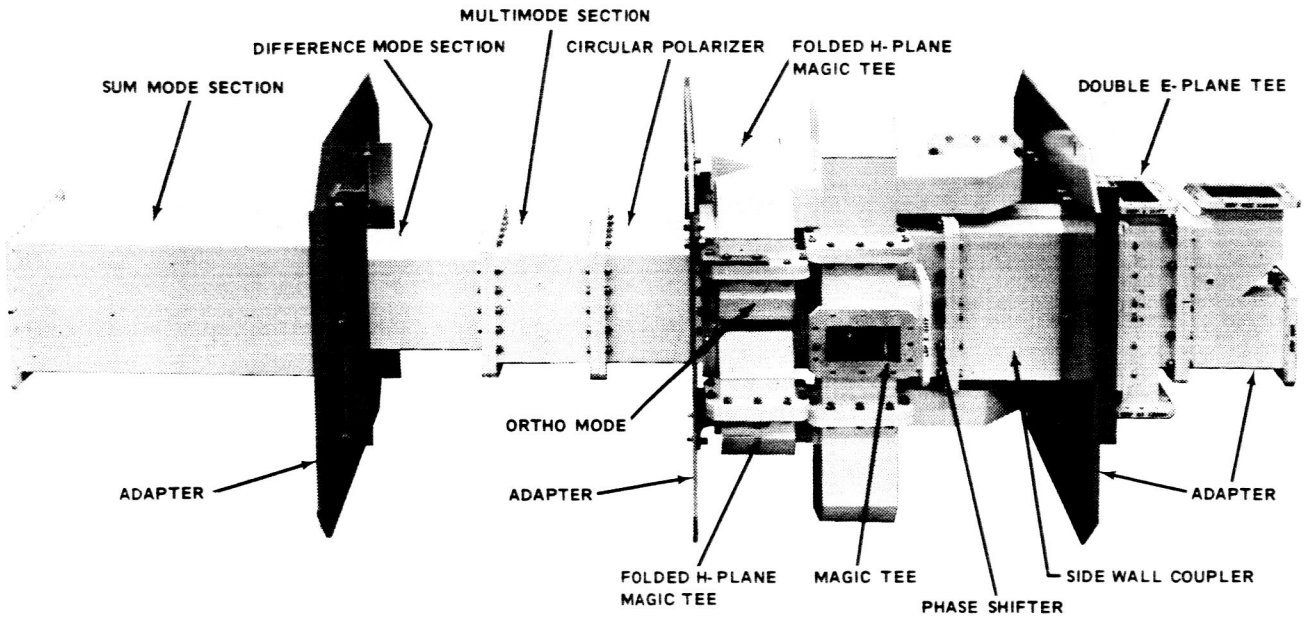

Fig. 27. SCM feed assembly

3. *Production (Suppressed-Sidelobe) SCM Feed*

This short research program was highly successful and resulted in a modified SCM feed (Fig. 27) with the primary patterns shown in Fig. 28. These representative patterns may be compared with those of the prototype feed previously referenced. All patterns shown are right-hand circular polarization (RCP); the left-hand circular polarization (LCP) patterns are essentially identical.

The assembled feed shown in Fig. 27 does not include the horn (Fig. 29) which connects directly to the sum mode control section in Fig. 27.

Fig. 30 is an exploded view of the SCM feed and Figs. 31, 32, and 33 are close-ups of three of the more unusual feed components.

Fig. 34 illustrates the model operation of the SCM feed; each connecting line represents an independent waveguide mode essential to the operation of the feed. Table 5 details these 14 waveguide modes, together with 8 other modes which must be closely controlled to prevent serious degradation of the feed performance.

As the figure and table suggest, the theory of operation of the SCM feed is quite complicated and will not be discussed in detail here. Several specific points are worth noting, however.

The lowest cutoff modes (TE_{31}, etc.) shown in the table effectively determine the upper frequency limit of the feed and are one of the most important design constraints. If any of these modes is allowed to propagate, it will seriously degrade the radiation patterns.

Table 5. SCM feed waveguide modes

Polarization[a]	Suppressed sidelobe sum modes	Elevation error modes	Azimuth error modes	Other modes above cutoff	Lowest cutoff modes
Vertical Linear	TE_{10} TE_{12} TM_{12} TE_{30}	TE_{11} TM_{11}	TE_{20}	TE_{22} TM_{22} TE'_{22} TM'_{22}	TE_{31} TM_{31} TE_{13} TM_{13}
Horizontal Linear	TE_{01} TE_{21} TM_{21} TE_{03}	TE_{02}	TE'_{11}[b] TM'_{11}		

[a]RCP and LCP obtained by combining vertical and horizontal linear modes simultaneously at + and −90-deg phase angles
[b]Primes denote orthogonal (independent) modes with same subscripts

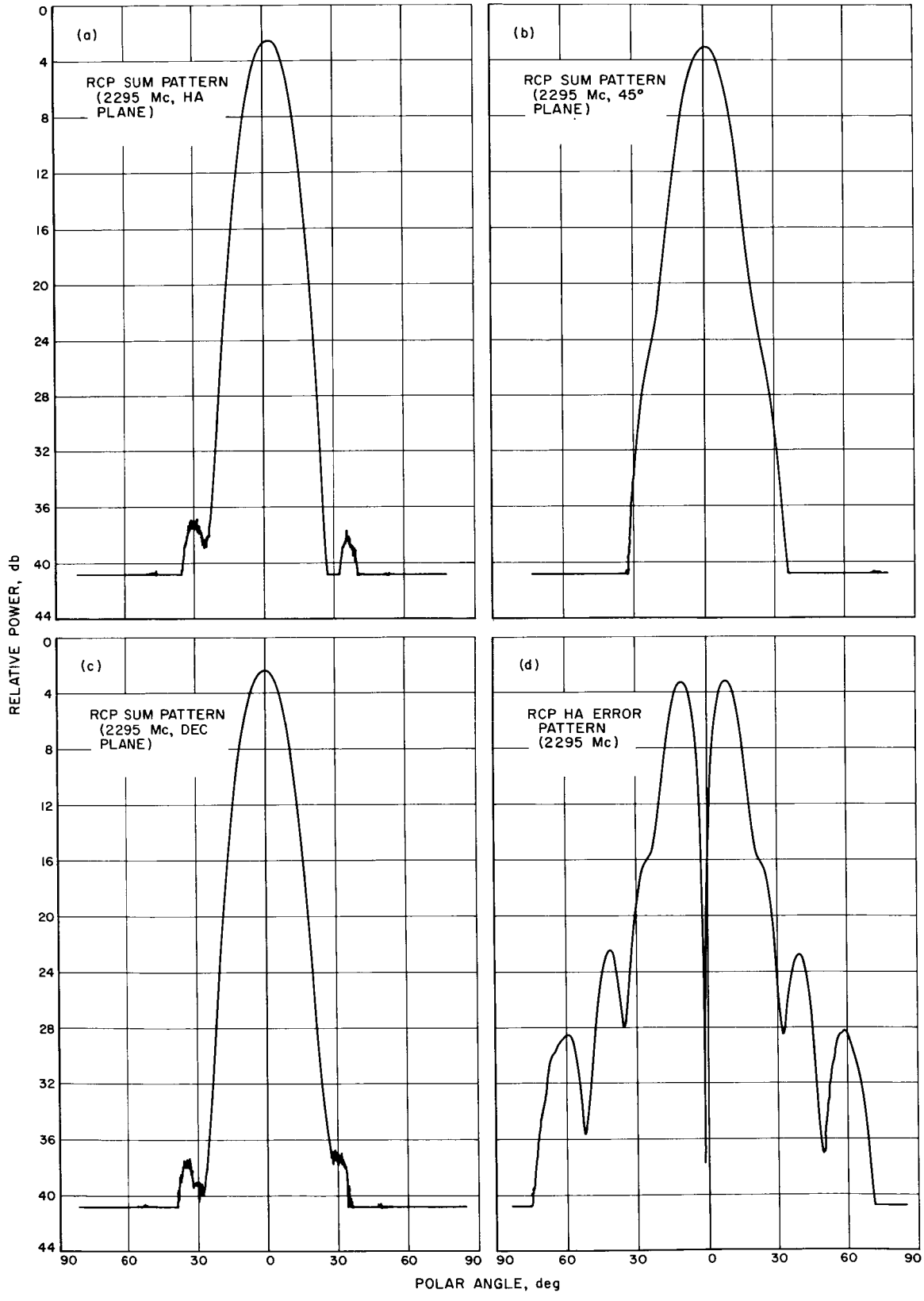

Fig. 28. RCP feed radiation patterns

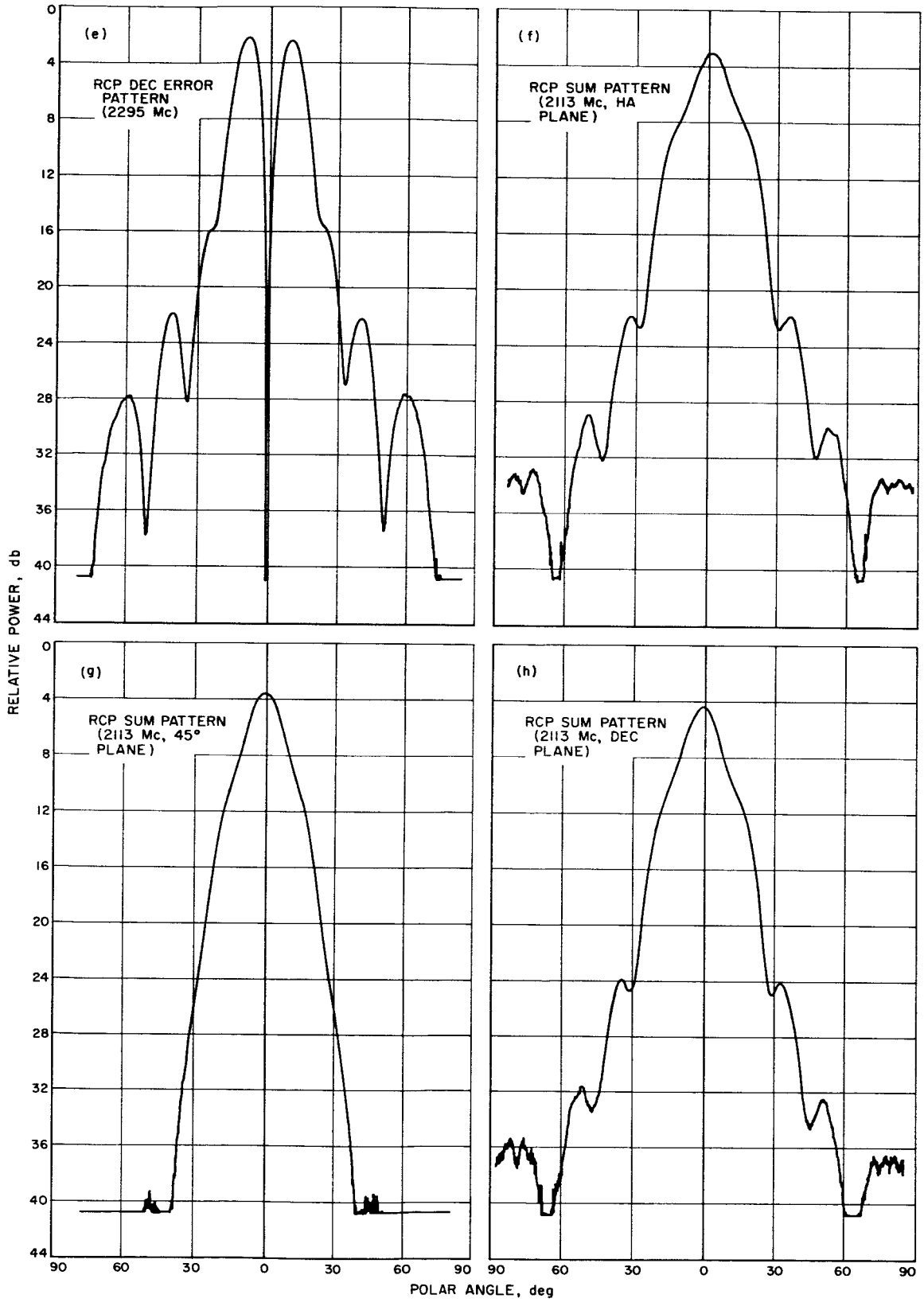

Fig. 28. RCP feed radiation patterns (cont'd)

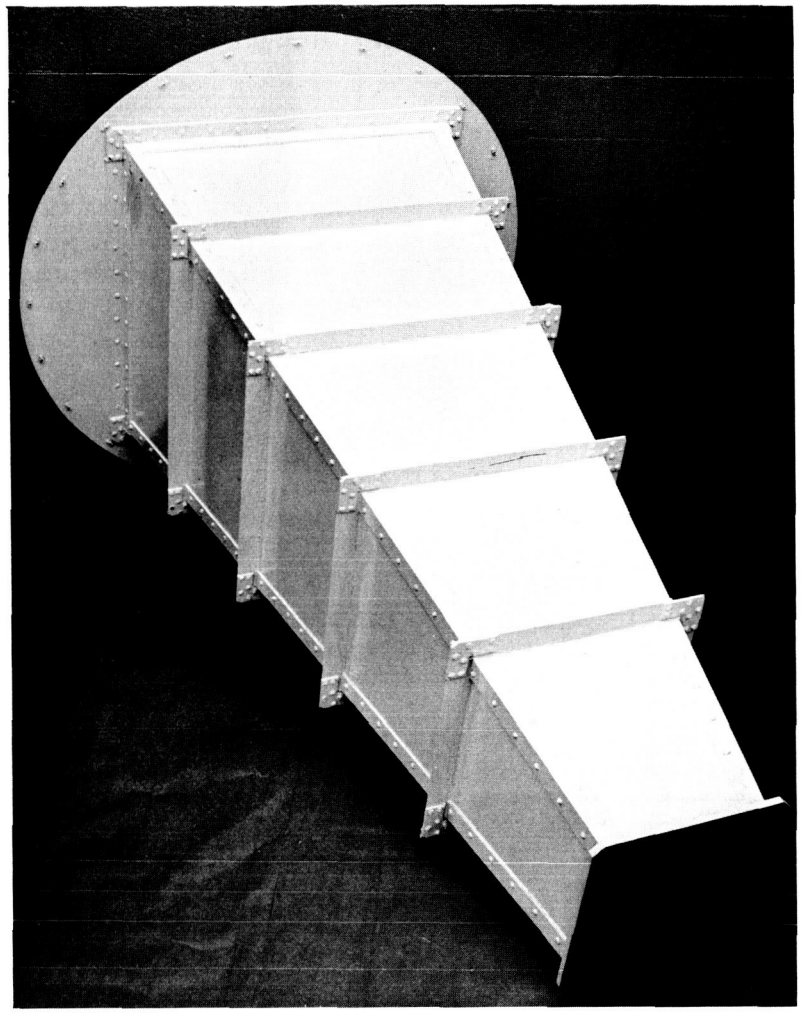

Fig. 29. SCM feed horn

Because the various modes have, in general, different propagation constants, it is necessary to phase the modes carefully, both for proper sidelobe suppression and to obtain circular polarization. For example, to obtain an RCP elevation error pattern, the TE_{11} and TM_{11} modes (which have identical propagation constants in square waveguide) must be properly phased with the TE_{02} mode (which has a different propagation constant) *at the horn aperture*. The relative phase of these modes will, however, vary throughout the horn and the various feed sections, requiring the evaluation of integrals of the form

$$\Delta\phi = \int_{s_1}^{s_2} [\beta_{11}(s) - \beta_{02}(s)]\, ds$$

where $\Delta\phi$ is the differential phase shift between the modes, $\beta_{11}(s)$ and $\beta_{02}(s)$ are the propagation constants of the modes, and s is the linear distance down the guide. For the square waveguide sections, the propagation constants do not vary with s so that the calculation of $\Delta\phi$ is simple. For the pyramidal horn, however, the propagation constants depend upon the cross-sectional dimension, which in turn is a function of the horn flare angle and the distance along the horn. For certain basic system parameters such as frequency, paraboloid and hyperboloid focal lengths, and hyperboloid subtended angle, simultaneous solutions to the various phase integrals may be impossible within reasonable constraints on the Cassegrain cone mechanical layout. Thus, mode phasing calculations are important design inputs early in the antenna system layout.

Measured performance data on the SCM feed is being tabulated and will be presented and compared with the prototype feed data in a future *SPS*.

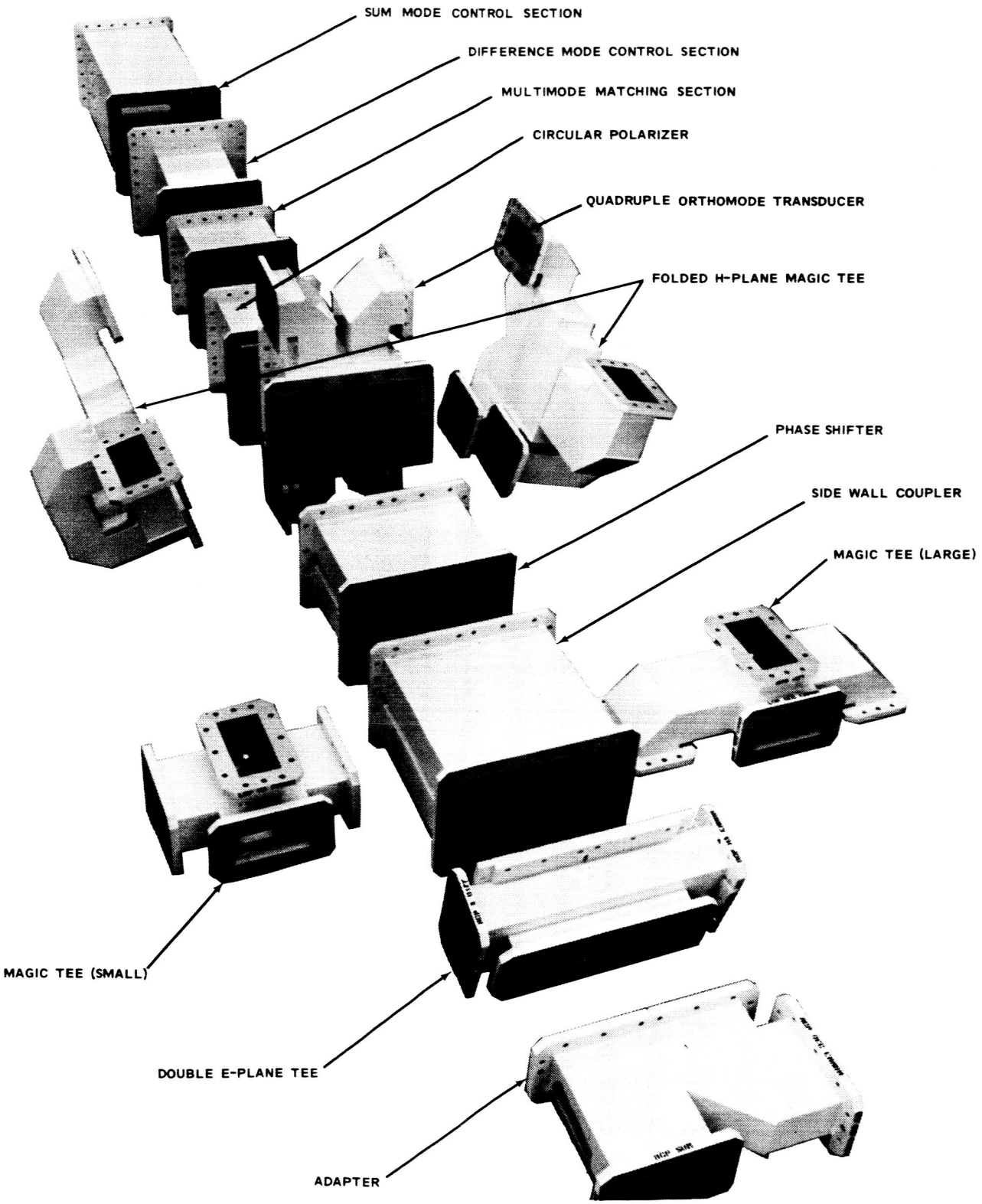

Fig. 30. Exploded view of SCM feed

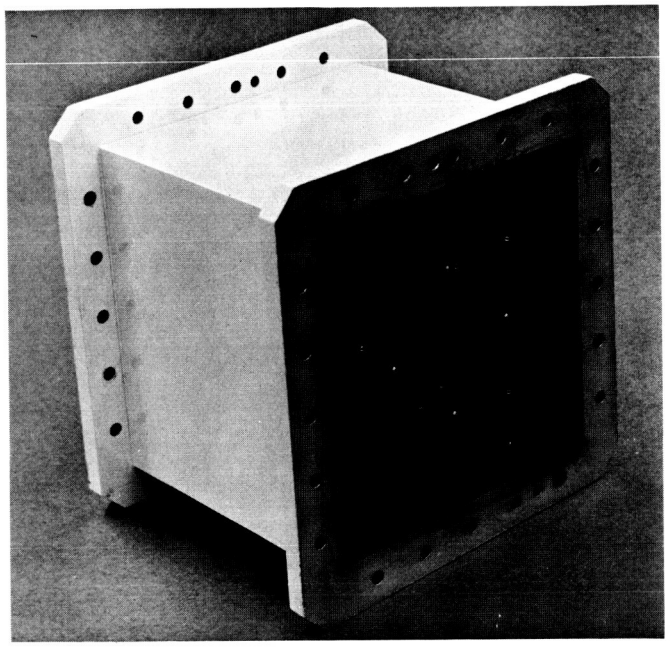

Fig. 31. Multimode matching section

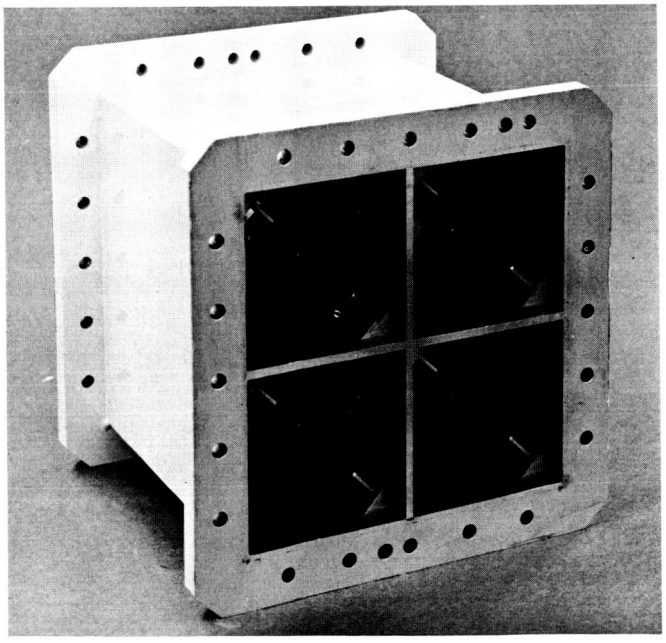

Fig. 32. Quadruple circular polarizer

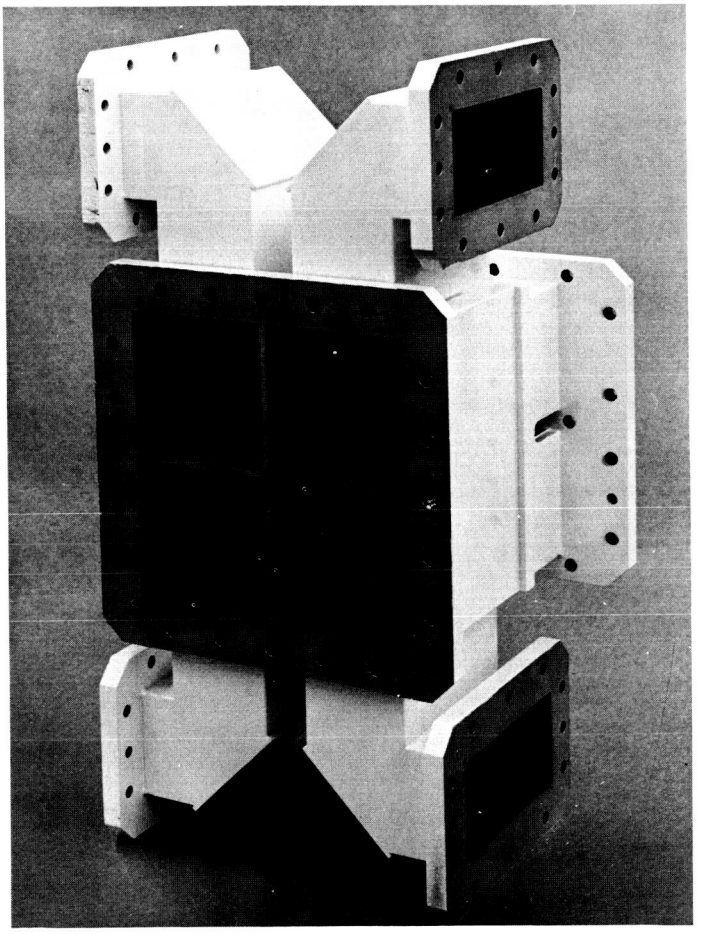

Fig. 33. Quadruple orthomode transducer

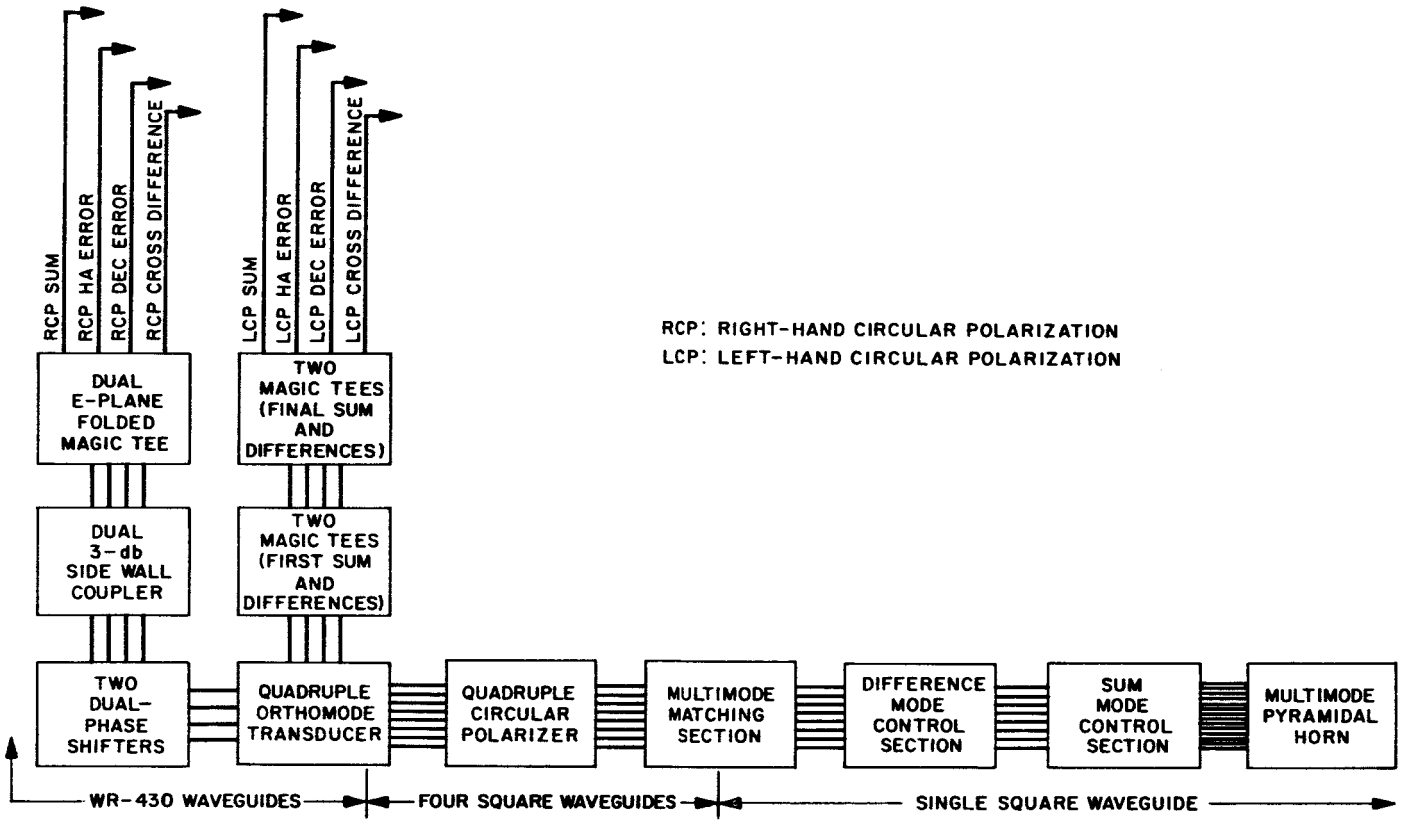

Fig. 34. SCM feed operation block diagram

G. Pilot Signal Radiometer

Radiometric measurements play an important role in the evaluation and calibration of DSIF microwave components and systems. Although a radiometer system is included in the DSIF S-band microwave subsystem, an improvement in that area would provide a capability of making measurements which are not possible at present, as well as improving the accuracy of the measurements which are. The goal in this program is to develop a radiometer which provides a stability of 0.01 db peak-to-peak or better for a period of at least 1 hr under all testing conditions. The present DSIF system may drift from 0.03 to 0.5 db peak depending upon the test being performed.

A radiometer which provides this stability will yield improvements in accuracy and ease of measurement for several calibrations at 2295 Mc. For example, improvements will occur in such areas as antenna gain measurements and noise temperature calibrations. Included under the heading of noise temperature calibrations is the mapping of antenna noise temperature as a function of position and time, as well as the usual system calibrations taken with the antenna at zenith. Possibly more important than the improvements at 2295 Mc are the possibilities of making new measurements. Included in this list is the measurement of antenna gain at 2113 Mc, the calibration of radio stars (using small antennas) at 2295 and 2113 Mc, and the determination of antenna gain as a function of position at both frequencies.

Functionally, the radiometer is designed to permit changes in output only when there is a change in the input noise power. The servo loop corrects for gain changes which occur in the RF or IF amplifiers. Fig. 35 is a block diagram of the pilot signal radiometer. Briefly, the operation is as follows: The output of the first VHF oscillator is multiplied and delivered to a directional coupler at the input of the system. The portion of the pilot signal which is not coupled into the RF amplifier is detected at S-band and compared to the output of the 50-Mc signal detector. Gain changes which occur between the input coupler and the output of the second IF amplifier give rise to error voltages at the output of the differencing junction. These error voltages are then integrated

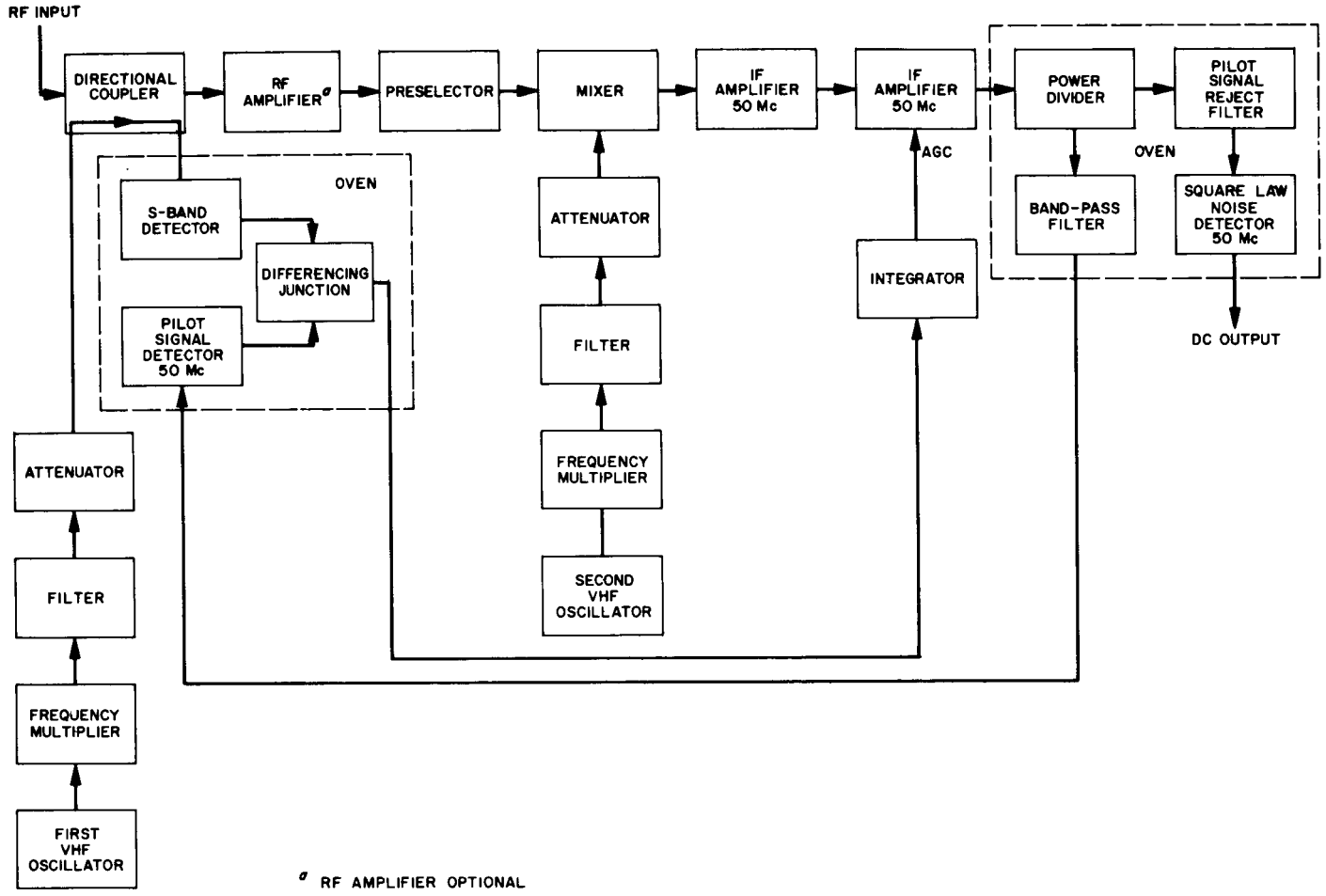

Fig. 35. Pilot signal radiometer

and fed back to the second IF as AGC changes which correct for the initial gain changes. Since the gain is constant, the square law noise detector provides a DC output which is directly proportional only to the system equivalent input noise temperature.

Expected loop performance, based on measurements made on components, is of interest. In order to predict performance, an expression for loop error is derived here. Fig. 36 shows the block diagram and the signals linearized in db as they exist around the loop. The correction which occurs is shown in Fig. 36 as $C(s)$ where

$$C(s) = -S_3/ks\,[P(s)(S_2 - S_1) - S_1G(s) + S_1C(s) - Vd(s)]. \quad (1)$$

Solving Eq. (1) for $C(s)$ explicitly,

$$C(s) = -\frac{S_3/k}{s + (S_3S_1/k)}[P(s)(S_2 - S_1) - S_1G(s) - Vd(s)]. \quad (2)$$

Going back to the basic function of the radiometer, changes in output noise in db $[N'(s)]$ should be equal to changes in input noise in db $[N(s)]$. Then,

$$N'(s) - N(s) = \varepsilon(s)$$

where $\varepsilon(s)$ is the magnitude of the loop error. Since $N'(s) = N(s) + G(s) - C(s)$ (Fig. 36), $\varepsilon(s) = G(s) - C(s)$. The expression for loop error becomes

$$\varepsilon(s) = G(s) + \frac{S_3/k}{s + (S_3S_1/k)}[P(s)(S_2 - S_1) - S_1G(s) - Vd(s)]. \quad (3)$$

To solve for the error caused by a gain change, assume $Vd(s) = 0$ and $P(s) = 0$. For a step gain change G, Eq. (3) gives

$$\varepsilon(s) = \frac{G}{s} - \frac{GS_3S_1/k}{s\,[s + (S_3S_1/k)]}$$

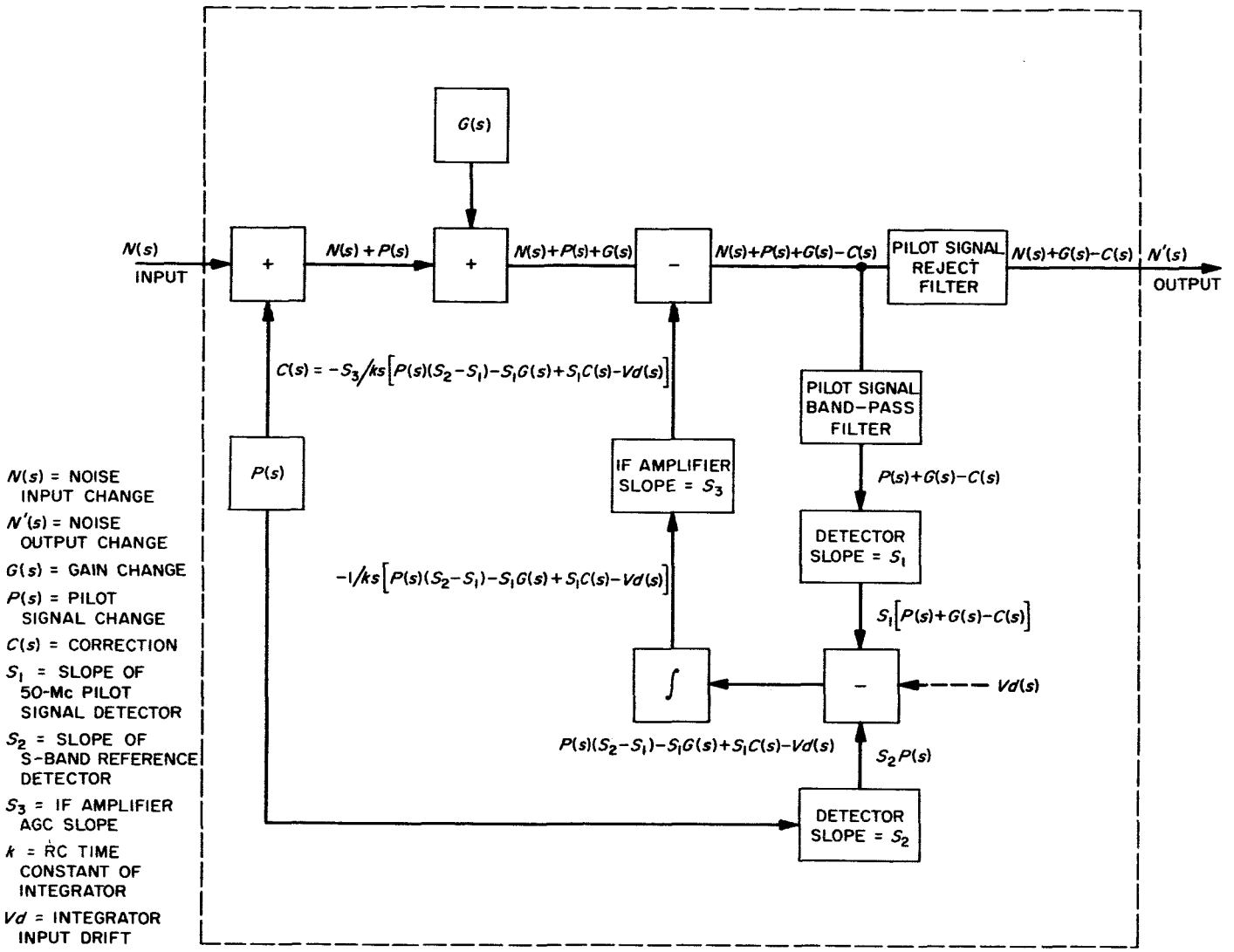

Fig. 36. Pilot signal loop

and

$$\varepsilon(t) = Ge^{-(S_2S_1/k)t} \tag{4}$$

Eq. (3) yields an expression for error caused by integrator input drift when $G(s) = 0$ and $P(s) = 0$. For a step change Vd, Eq. (3) becomes

$$\varepsilon(s) = -\frac{Vd\,S_3/k}{s(s + S_3S_1/k)}$$

and

$$\varepsilon(t) = -\frac{Vd}{S_1}[1 - e^{-(S_2S_1/k)t}] \tag{5}$$

If the pilot signal amplitude changes, tracking error between the S-band reference and 50-Mc pilot signal detector gives rise to a loop error. The tracking error voltage $Ve = P(S_2 - S_1)$ where P is the pilot signal change, and $Ve(s) = P(s)(S_2 - S_1)$. For a step change in P, $Ve(s) = Ve/s$. Eq. (3) becomes

$$\varepsilon(s) = \frac{Ve\,S_3/k}{s(s + S_3S_1/k)}$$

and

$$\varepsilon(t) = \frac{Ve}{S_1}[1 - e^{-(S_2S_1/k)t}] \tag{6}$$

For the purpose of evaluation $\varepsilon(t)$ in Eq. (4), (5), and (6), tests have been made on the components which affect $\varepsilon(t)$. The results are shown in Table 6.

Table 6. Variables in loop equation

Variable	Actual component measured value
S_1	0.04 v/db
S_3	6.6 db/v
k	1×10^{-3} sec
Vd	4×10^{-6} v
Ve (at $P = \pm 0.05$ db)	1.6×10^{-5} v

Eq. (4) describes the effect of a step gain change as an exponentially decaying transient whose peak amplitude is the same as the gain change. However, in actual use, the DC output is filtered before it is fed into the recording device. If a filter time constant of 1 sec is used, calculation shows that the peak change in the DC output is less than 0.002 db for a step gain change of 0.5 db.

Because the loop error given by Eqs. (5) and (6) approaches its maximum value as t increases, the exponential terms in those equations are neglected in the following computations. Error caused by integrator input drift may be calculated by using Eq. (5) and data from Table 6. The loop error (ε) is 0.0001 db. Error caused by pilot signal amplitude changes may be calculated by using Eq. (6) and data from Table 6. The result is $\varepsilon = 0.0004$ db. Clearly, these errors are much less than the design goal of 0.01 db.

Table 7 shows the performance of the 50-Mc filters used in the loop. The data on the signal reject filter notch width (300 cps at 38-db points) establishes an IF frequency stability of ± 150 cps if the pilot signal suppression is to be 38 db. In order to achieve this stability, crystal-controlled VHF oscillators (71 Mc) and frequency multipliers are used in the pilot signal and local oscillator chains. Test results show that the IF frequency stability is better than ± 10 cps. The VHF frequencies (71 Mc) were chosen so that leakage would not be at the IF frequency and present a severe suppression problem.

Based on the calculations made using the test data in Table 6, and on further analysis now being carried out, it appears that the original stability design goal of 0.01 db will be met, if not exceeded.

Table 7. Filter performance

Band-pass filter bandwidth (3 db)	7 kc
Signal reject filter	
Noise bandwidth	2 Mc
Notch depth at center	39 db
Notch width (38-db depth)	300 cps

H. Venus Site *Ranger–Mariner IV* Support

1. Introduction

A ground transmitter power of 100-kw continuous wave (CW) will be required for the *Mariner IV* program under certain operating conditions. A further decision was made, during this reporting period, to provide receive capability at the Venus site (DSIF-13) for *Mariner IV*.

2. 100-kw CW Transmitter

As reported in *SPS 37-30*, Vol. IV, p. 36, the 100-kw amplifier subsystem has been completed and is capable of providing the required support for *Mariner IV*. There was a limited amount of testing time during the reporting period; most of the time was used in reconfiguring the Cassegrain feed cone in order to provide the receive capability to be discussed.

During ground closed-loop tests with the read, write and verify equipment at the Venus site, an excessive amount of incidental phase modulation at 2400 cps was measured on the transmitter signal. Measurements of the ripple on the 32.5-kv klystron beam voltage indicated a

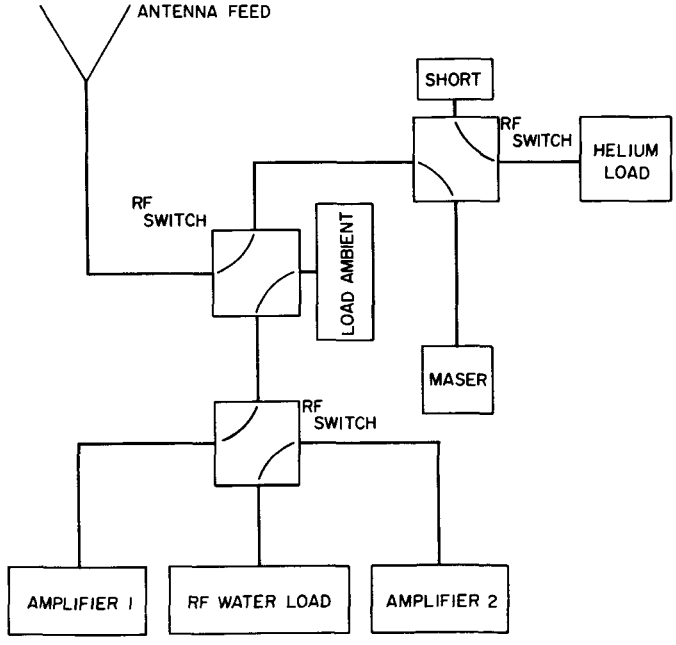

Fig. 37. *Mariner IV* Cassegrain cone, receive capability configuration

value of 180 v peak-to-peak. The ripple at the output of the power supply filter was only 18 v peak-to-peak, and it was determined that the excessive ripple was being produced by the series limiter tube. This tube will be replaced by a resistor in the beam voltage cable near the klystron which will provide klystron protection and will not introduce additional ripple to the power supply output. With 18 v peak-to-peak ripple on the beam voltage, the incidental phase modulation due to the klystron will be approximately 1 deg peak-to-peak.

Tests will be conducted with the *Mariner IV* vehicle to obtain a two-way lock using the 100-kw transmitter at the Venus site and the receiver at the Pioneer site.

3. *Mariner IV* Receive Capability

The original configuration of the *Mariner IV* Cassegrain cone is shown in *SPS 37-31*, Vol. III, p. 33. To provide receive capability, two additional RF switches and a maser were installed. Fig. 37 is a block diagram of this new configuration. Work in progress to provide receive capability, as a backup to the Pioneer site during Mars encounter, is reported elsewhere in this volume.

An immediate requirement exists to receive *Mariner IV* telemetry at the Venus site during periods when the Pioneer site is committed to other programs such as backup support to *Rangers VIII* and *IX*. To provide this support, a "suitcase" telemetry receiver has been installed in the *Mariner* Cassegrain cone. The telemetry output of the receiver is transmitted to the Venus control building by cable and then over the microwave link to the Pioneer site. At this point, the telemetry is demodulated and transmitted to the Space Flight Operations Facility (SFOF) by microwave. A block diagram of this arrangement is shown in Fig. 38. This installation has just been completed and tested. To provide a complete test of the

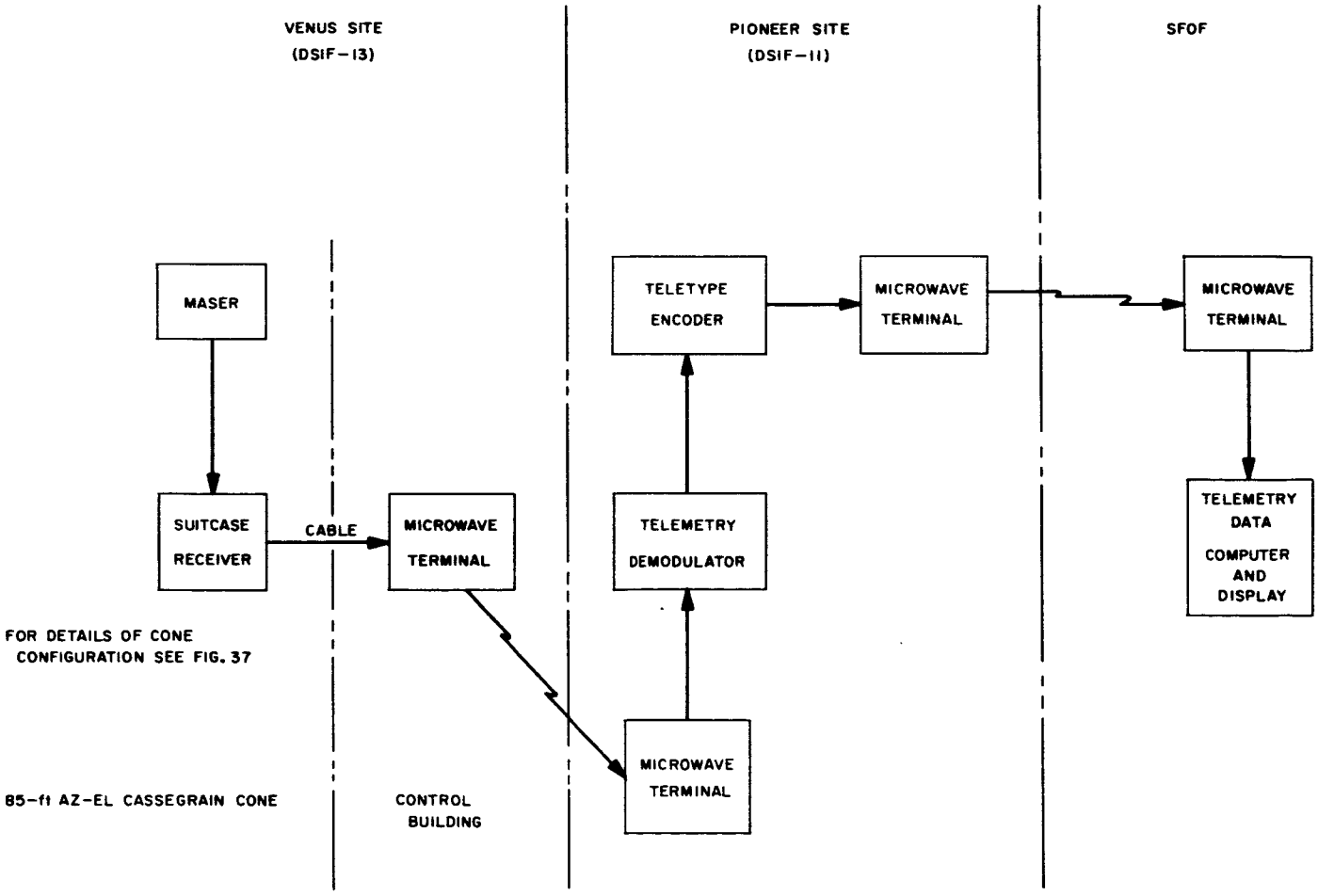

Fig. 38. Receive system block diagram with "suitcase" telemetry receiver

system, the Venus site received the telemetry from the spacecraft simultaneously with Pioneer. Telemetry from both sites was alternately sent to the SFOF; the telemetry from the Venus site was acceptable to the computer at the SFOF and was in complete agreement with that from the Pioneer site.

Reference

1. Potter, P., *A New Horn Antenna with Suppressed Sidelobes and Equal Beamwidths*, Technical Report No. 32-354, Jet Propulsion Laboratory, Pasadena, California, February 25, 1963.

IV. Communications Research and Development

A. Ground Antennas

1. Radio Calibration Techniques: Gain Measurement of the Venus Site 85-ft Antenna

The 85-ft antenna at the Goldstone Tracking Station Venus site will be used to track the *Mariner* Mars vehicle during the period that the Goldstone Pioneer site will be used for tracking *Rangers VIII* and *IX*. The *Mariner* tracking will be at 2297 Mc.

Later in the *Mariner* Mars mission, the 85-ft antenna will also be used for command transmission of 100-kw signals at 2115 Mc, as well as reception at 2297 Mc. The antenna gain at 2297 Mc was measured by using radio stars as calibration sources. The measurements indicate that the antenna gain is 52.6 $\pm$0.5 db absolute.

On February 13, 1965, the gain of the Venus site 85-ft antenna of the Goldstone Tracking Station was measured. The measurement was made using radio astronomical techniques with the *Mariner C* cone in place on the antenna, and a DSIF "suitcase" receiver connected to the maser.

The gain of the antenna was measured by tracking two different radio sources, Virgo A and Cygnus A, and comparing the effective source temperatures seen by the antenna to the best estimates of what the source temperatures would have been for an 85-ft antenna with 100% aperture efficiency. Virgo A was tracked at an elevation angle of about 70 deg with an on-source system temperature of about 38°K. The off-source system temperature at this elevation angle was measured to be about 28°K (the difference, approximately 10°K, being the effective source temperature as seen by the antenna). Since the best estimate of the source (Virgo A) temperature at this frequency and a 100% efficiency is 21°K, the efficiency of this system is found to be about 47.6%. Similarly, Cygnus A, at an elevation of about 30 deg, was found to produce a temperature of about 69.5°K (T_{on} = 99.6°K; T_{off} = 30.2°K). Again, the best estimate of the temperature of Cygnus A is 150°K, leading to an efficiency of 46.3%. The gain of a 100% efficient 85-ft dish at the receiver frequency, 2297 Mc, is 55.88 db [20 log ($\pi D/\Lambda$)]. This, together with the measured efficiency, leads to a measured antenna gain of 52.6 db (Table 1). The measured efficiency, about 47%, is rather low. This low efficiency is a result of optimization of the feed system at the 2115-Mc transmitter frequency.

Table 1. Parameters used in calculating the 2297-Mc gain of the Venus site 85-ft antenna

Source	$\frac{1}{Y_{on}-1}$	$\frac{1}{Y_{off}-1}$	η, %	ΔT_s for $\eta = 100\%$, °K	G^a, db	G^b, db
Virgo A	0.6084 ±0.0035	0.4463 ±0.0026	48 ±5	21 ±2.1	52.7 ±0.5	52.7 ±0.2
Cygnus A	1.5963 ±0.0104	0.4834 ±0.0044	46 ±5	150 ±15	52.5 ±0.5	52.5 ±0.2
Average	—	—	—	—	52.6 ±0.5	52.6 ±0.2

Note: Gas tube $\Delta T = 62.0°K \pm 2°K$.
[a] ±0.5-db tolerance, based on a 10% tolerance for the absolute source temperatures.
[b] ±0.2-db tolerance, based on a 0% tolerance for the absolute source temperatures.

B. Experimental Closed-Cycle Refrigerator for Masers

Commercially available compressors have been studied for possible application to helium gas. The two general approaches are:

(1) Dry compressors in which helium gas, once purified, remains clean.

(2) Oil lubricated compressors in which oil has to be separated continuously from the gas.

Dry compressors make use of organic synthetic materials (like Teflon) in the piston rings and bearings and have been under development for several years. A significant problem in this type of compressor is the removal of the heat of compression from the gas. Air Products and Chemicals, Inc., of Allentown, Pa., has made significant advances in these compressors.

The oil lubricated compressors have the advantage of low mechanical wear and the added feature of easy removal of the heat of compression from the gas. In fact, it is mandatory in this type of compressor to inject adequate oil into the upper cylinder to keep the peak temperature below the flash point of the oil. In other words, a "wet" compressor must be truly wet and a dry one completely dry. The Arthur D. Little Co. has developed the wet type of system which is used in the S-band TWM/CCR subsystem.

The problem with the oil lubricated compressor is, of course, the difficulty of achieving complete separation of the oil from the gas. A compromise system in which the bearings are oil lubricated with dry upper cylinder is probably worthy of consideration for a long term (5000 hr or more) continuous system.

C. Frequency Generation and Control

1. Programmed Exciter

An introductory report on the programmed exciter (PE) appeared in *SPS 37-30*, Vol. III, pp. 84–86. Since that time the basic system design has undergone extensive simplification. The new design eliminates most of the RF modules and more nearly utilizes the full capability of the HP 5100A/5110A frequency synthesizer.

a. System redesign. A system diagram showing the complete PE appears in Fig. 1. Of the 21 modules that appeared in Fig. 54 of the above-referenced article, only 4 appear in Fig. 1. The functions of the remaining modules are now performed by the HP synthesizer. In addition the job of the central frequency synthesizer (*SPS 37-30*, Vol. III, pp. 86–87) is simplified, since the only reference signal now required is 1 Mc.

The digital portion of the system will employ integrated circuit modules with the exception of the computer.

Further explanation of the system is dependent upon an understanding of the operation of the HP synthesizer.

b. The HP 5100A/5110A frequency synthesizer. Using a 1-Mc reference standard, the Hewlett-Packard frequency synthesizer can provide frequencies from 0 to 50 Mc in 0.01-cps steps. The output frequency can be selected by local pushbutton control or remote programming. In addition, a continuously variable search oscillator can be used in any decade from 0.01 cps to 100 kc.

A diagram showing the operation of the 5100A portion of the synthesizer for a given setting of the push-

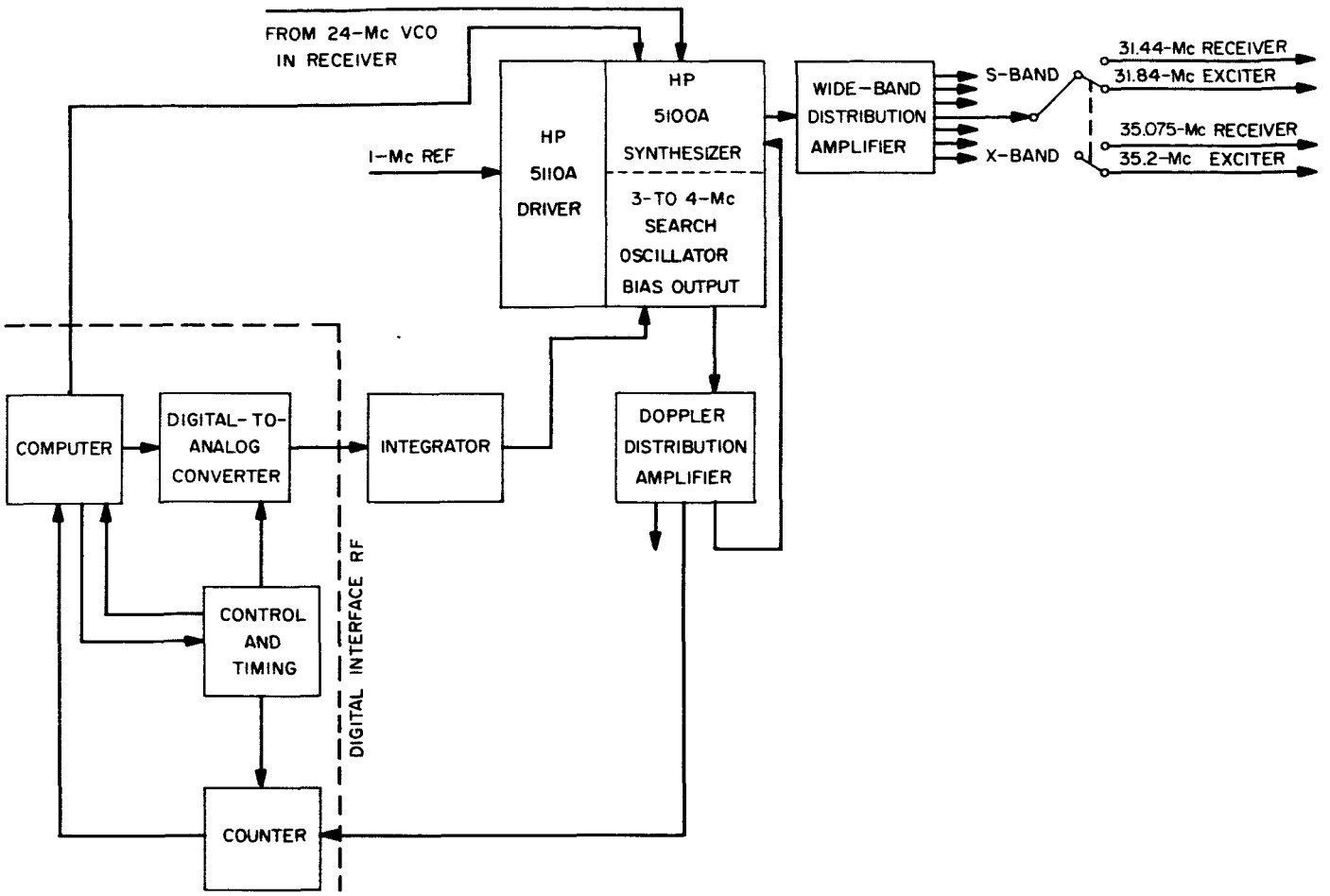

Fig. 1. Programmed exciter block diagram

buttons appears in Fig. 2. The key mixing frequencies in the HF section are 24 Mc and 3.0 to 3.9 Mc in 0.1-Mc steps. The search oscillator varies continuously from 3 to 4 Mc and can be substituted in a decade for the 3.0 to 3.9 Mc. The search oscillator, which will give a total vernier control of 100 cps, is shown in the 10-cps column.

The application of the HP synthesizer to the PE system follows directly. The PE has three basic modes of operation as follows:

(1) Programmed.

(2) Synchronous.

(3) Synchronous with programmed assistance.

In the *programmed mode*, the search oscillator will be digitally controlled by ephemeris tape. The output of the synthesizer can then follow the doppler shift of the received or the transmitted signal.

In *synchronous mode* operation, the 24-Mc VCO to be located in the receiver (presently Mod IV) could, for example, be switched into the synthesizer as shown in Fig. 2. The search oscillator will be switched off. The output of the synthesizer will be a VCO with a nominal output at any frequency from 1 to 50 Mc. The sensitivity of the synthesizer VCO in this mode will always be the sensitivity of the receiver VCO. For present operation, the nominal output will be either 31.44 Mc or 35.075 Mc. This eliminates the necessity of changing receiver VCOs or offsetting the VCO frequency in switching from one frequency band to another.

Operation in the *synchronous mode with programmed assistance* is simply a combination of the above two modes. A portion of the doppler shift is programmed, and the remainder is synchronously controlled. The search oscillator and the 24-Mc VCO will be employed simultaneously to perform their respective operations as indicated previously.

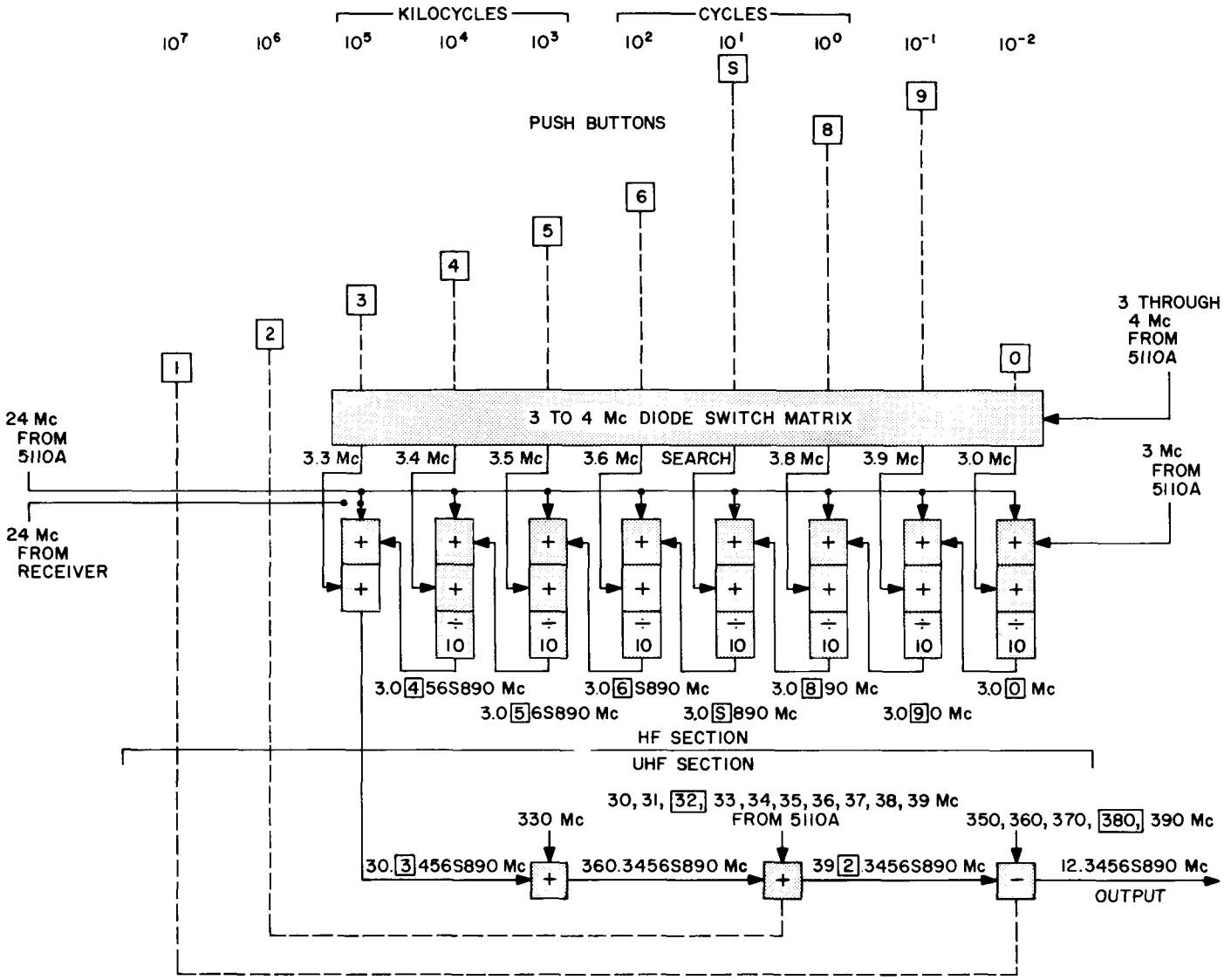

Fig. 2. Operation of the 5100A synthesizer

The search oscillator in the HP 5100A synthesizer has been tested to determine its operating characteristics and its stability. The sensitivity curve is shown in Fig. 3; the variation of the slope of the sensitivity curve with bias voltage is shown in Fig. 4. The nominal sensitivity is 100 kc/v, and the slope remains within 5% of this value from -1 to -11 v, the specified operating range.

The output of the VCO is nominally 0.1 v rms into 50 ohms over its entire frequency range with an adjustable gain control. The voltage–current characteristic of the bias input appears in Fig. 5. The nonlinear nature of the curve is due to a diode shaping network which provides the 5% linearity of the sensitivity curve.

A typical stability curve at 3.0 Mc appears in Fig. 6. Also shown is the low-frequency noise of the bias supply. The peak-to-peak deviation of the VCO is indicated to be 8 cps. The bias supply has peak-to-peak noise of 30 μv, which corresponds to 3 cps at a sensitivity of 100 kc/v. Therefore, the net deviation of the VCO is 5 cps. This is a stability of better than 2 parts in 10^6. Since the swing of the VCO from 3 to 4 Mc is 1 Mc, the resolution for digital control can be 5 parts in 10^6.

2. Control System Synthesis for Programmed Exciter

Feedback systems utilizing digital computer control elements are particularly amenable to synthesis and

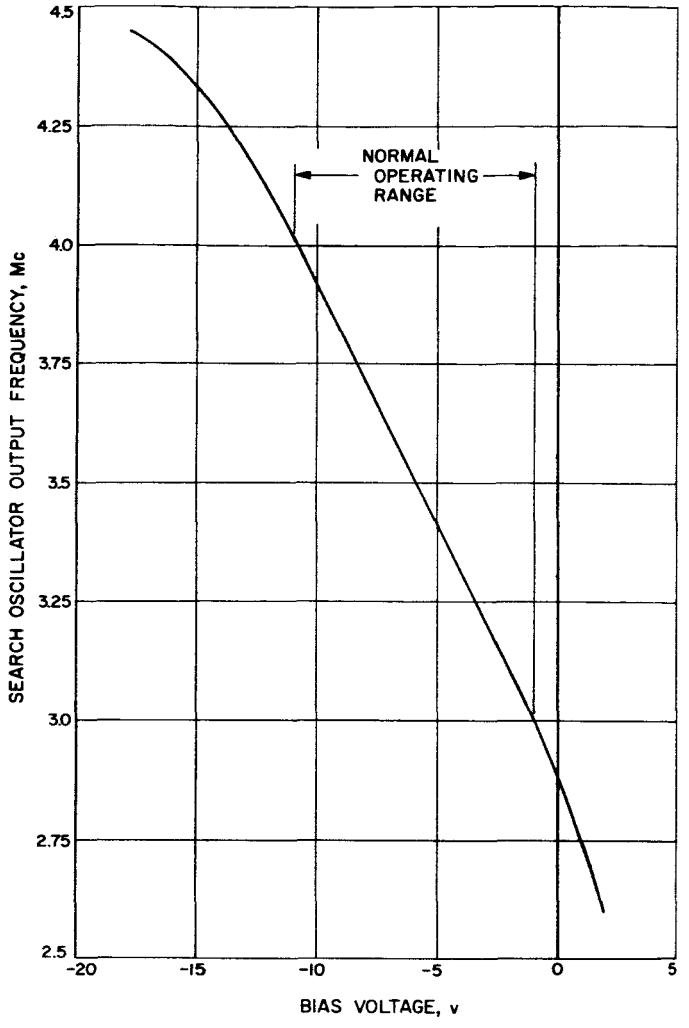

Fig. 3. Search oscillator sensitivity curve

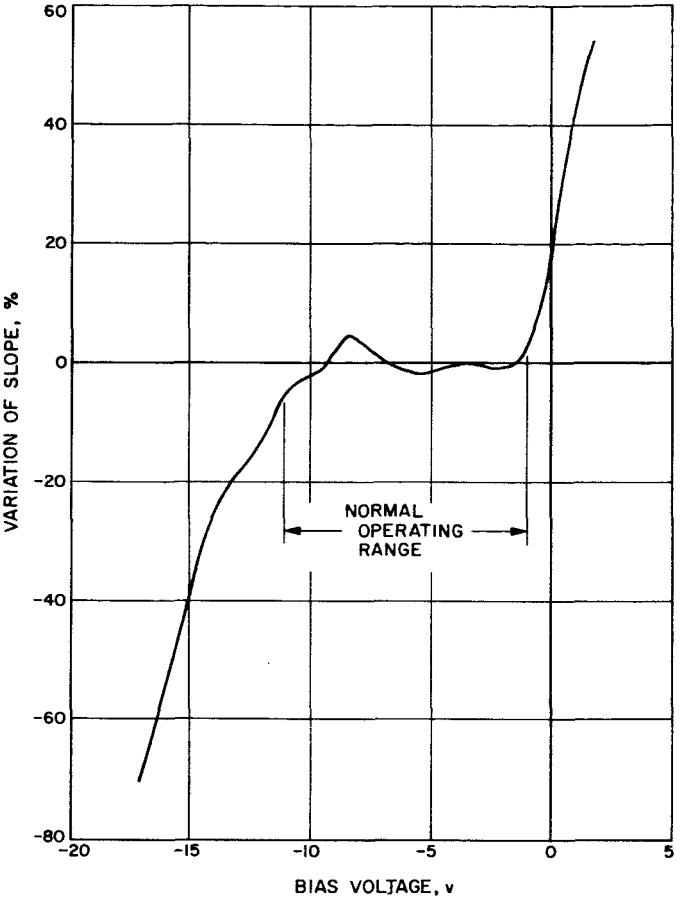

Fig. 4. Sensitivity curve slope variation

analysis using sampled-data control system theory. The following uses this theory to synthesize the computer control equations of a frequency control feedback system known as the programmed exciter. A root locus analysis is then made to determine the effect of subsystem gain changes on the stability and transient response of the overall system.

a. Physical system. A block diagram of the physical elements which comprise the programmed exciter is shown in Fig. 7. The block labeled "digital computer" contains that part of the computer program which operates mathematically on the difference or error frequency. In the actual system, generation of the reference frequency and the differencing operation are also programmed computer functions. The output of the digital computer is converted to an analog voltage by means of the digital-to-analog converter. This voltage is then integrated by the integrating operational amplifier and becomes the control input voltage to the voltage controlled oscillator. Thus, the number out of the digital computer determines the rate at which the output of the integrating amplifier changes. For a computer number of zero, the voltage out of the integrating amplifier would remain constant.

The VCO produces a frequency proportional to the input control voltage. This block also includes the actual multipliers, dividers, and mixers required to bring the frequency to a range suitable for system use. The output of the VCO is sampled by the frequency counter which provides an updated count to the computer each sample time.

b. Mathematical model. Fig. 8 shows the mathematical equivalents of the physical blocks in the form of a Laplace transform block diagram. The reference frequency R, and therefore the error frequency E, is assumed to be the output of a sampling process. The digital computer equation is the ratio of two polynomials $H(Z)$

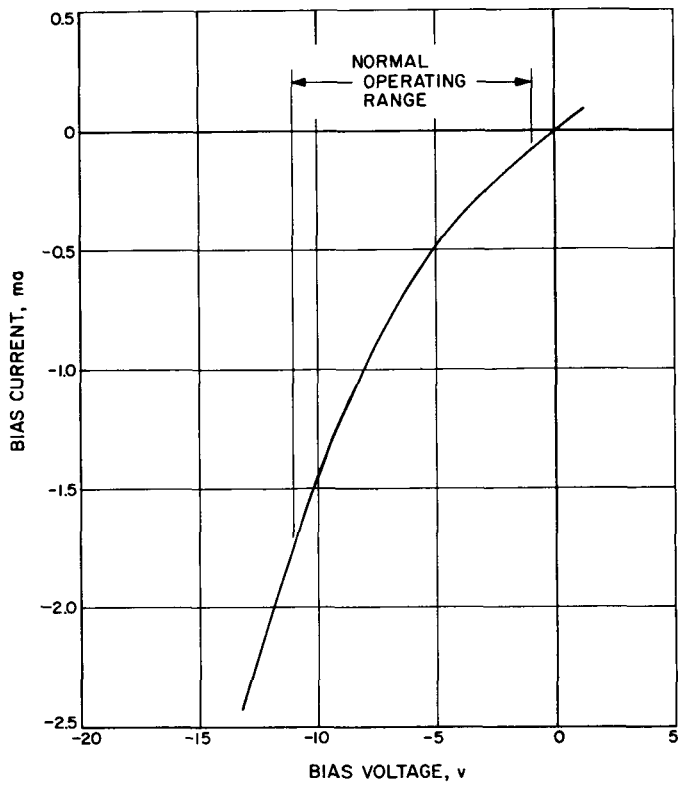

Fig. 5. Voltage–current characteristic of search oscillator bias input

and $L(Z)$, where Z is equal to e^{sT}, e is the Naperian logarithmic base, s is the Laplace transform complex frequency, and T is the sample period normalized to unity for this synthesis. A determination of the degrees and coefficients of these polynomials is the primary purpose of the synthesis procedure. The digital-to-analog converter is the equivalent of the familiar zero hold network in sampled-data theory, and the integrator expression is K_1/s where K_1 is the constant of integration. Since the bandwidth of the signal out of the integrator is much smaller than the dynamic bandwidth of the VCO, the mathematical equivalent of the VCO is simply a conversion gain constant K_2.

An expression for the counter is obtained with the help of Fig. 9, which shows the generalized counting process. The frequency input to the counter varies linearly during the interval between any two system sampled-data times. During a period called the counting interval, the counter is permitted to count the input frequency. At the end of the count, the number in the counter is the average of the frequency during the counting interval, i.e., the frequency at the midpoint of the counting interval. The computer looks at this number at the next sampled-data time. Thus, the effect of the counter is that of pure time delay B, where B is the time from the midpoint of the counting interval to the next sampled-data time. It may

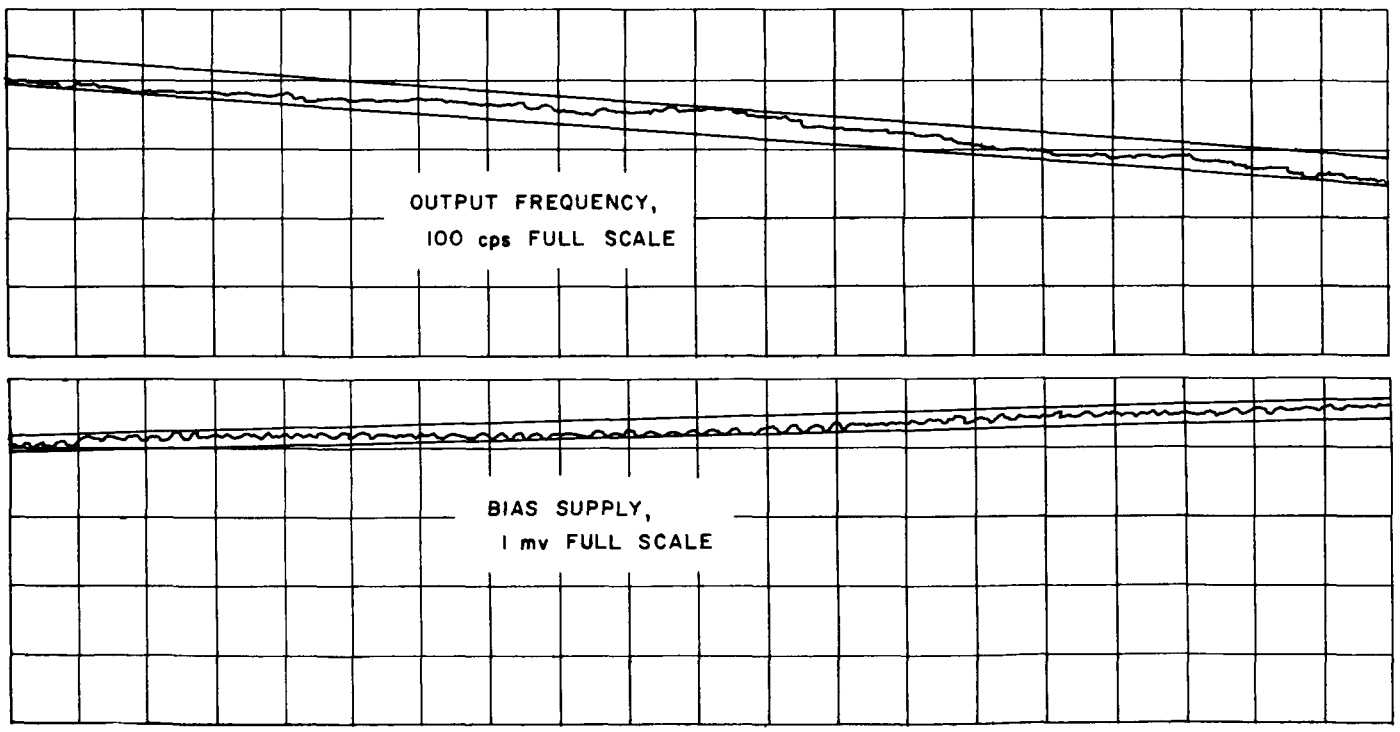

Fig. 6. Search oscillator stability curve at 3.0 Mc

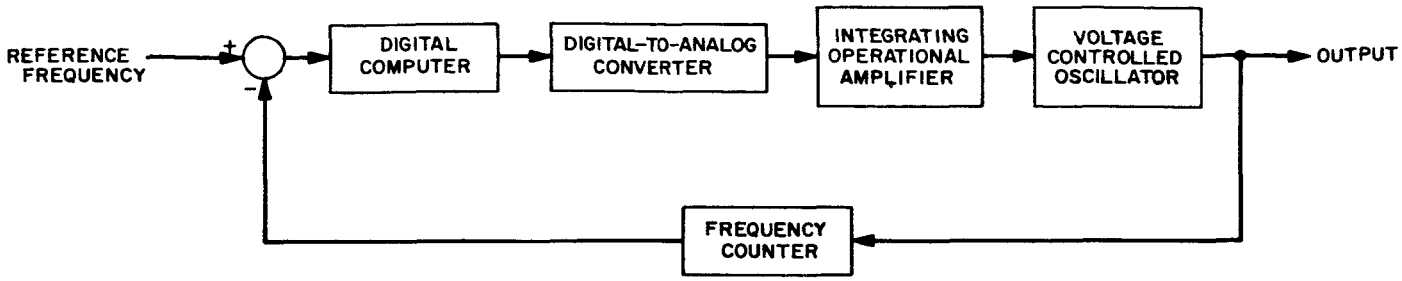

Fig. 7. Programmed exciter block diagram

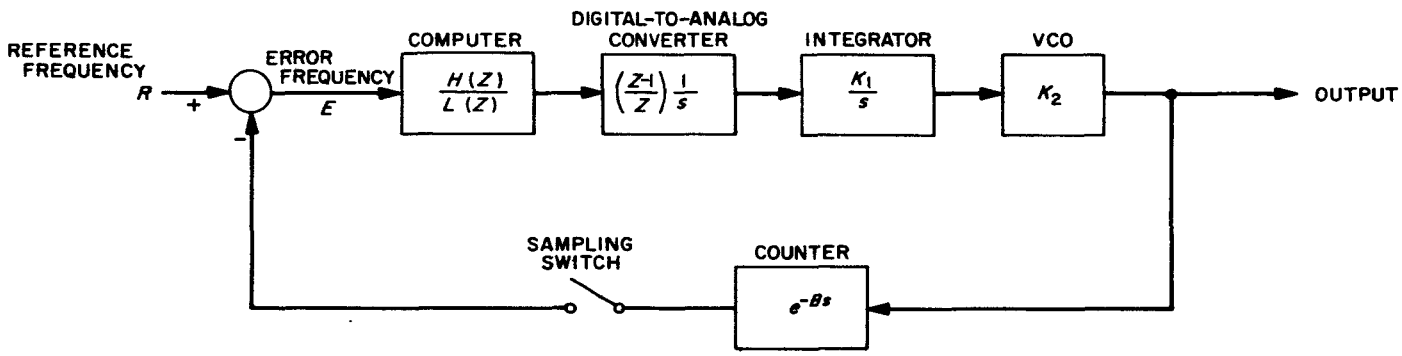

Fig. 8. Laplace transform block diagram

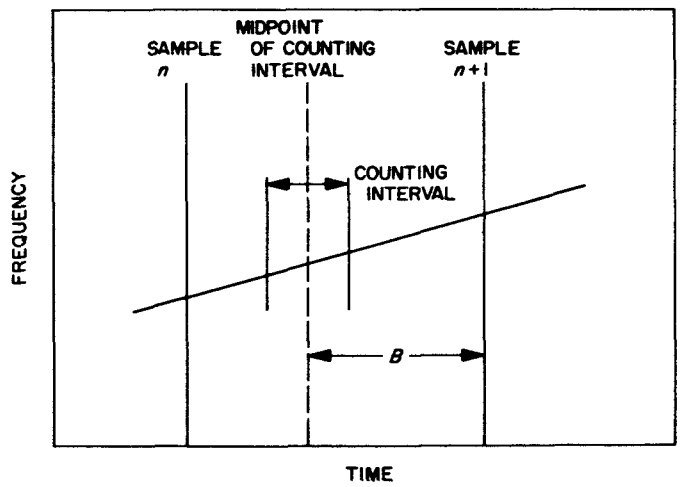

Fig. 9. Generalized counting process

be noted that the length of the counting interval affects only the accuracy of the count but not the mathematical expression. The sampling switch following the counter implies that the counter is read only at the sampled-data times. After being read, the counter is reset to zero in preparation for the next counting interval.

c. Synthesis procedure. It is desired to choose the computer equations H and L so that the error frequency approaches zero for an input reference frequency that is either a constant or a ramp function. A further restriction is that the degree of the polynomial H must not be greater than the degree of L, otherwise knowledge of the future values of E would be required. In order to satisfy the condition of zero error for an input ramp, the Z transfer function of the open-loop gain must have two poles at unity on the real axis of the Z complex plane. The open-loop Z transfer function $G_0(Z)$ of a system containing pure delay B is found by first determining the open-loop modified Z transfer function $G_0(Z,m)$, and then substituting the quantity $1 - B$ for the interpolating variable m. Carrying out the above steps

$$G_0 = \frac{K_3(1-B)H\left(Z + \dfrac{B}{1-B}\right)}{L\,Z(Z-1)} \; ; \; K_3 = K_1 K_2 .$$

Since G_0 has only one system pole at unity, the polynomial L must supply the second pole and

$$L = (Z-1)l,$$

where l is a reduced polynomial.

Final polynomial constants are determined from the transient response consideration of E approaching zero as quickly as possible after the application of an input

step function. The transient portion of E decays according to the term δ^n, where n is the number of sample times after the input step, and δ is the distance to the origin of the farthest pole in the expression of E/R. Since the maximum rate of transient decay is obtained for δ equal to zero, it is desired to cluster the poles of E/R as close to the origin as possible.

Substituting G_0 into the expression

$$\frac{E}{R} = \frac{1}{1 + G_0}$$

results in

$$\frac{E}{R} = \frac{Z(Z-1)^2 l}{Z(Z-1)^2 l + K_3 H(1-B)\left(Z + \frac{B}{1-B}\right)}. \quad (1)$$

Letting the minimal form for the polynomials l and H be

$$l = Z + a$$

$$H = bZ^2 + cZ,$$

and substituting into Eq. (1), gives

$$\frac{E}{R} = \frac{(Z-1)^2 (Z+a)}{Z^3 + F_1(a,b,c,) Z^2 + F_2(a,b,c) Z + F_3(a,b,c)}.$$

The poles of E/R are at the origin if the functions F_1, F_2, and F_3 are made equal to zero. Solving these three functions simultaneously gives

$$a = B(1+B),$$

$$b = \frac{2+B}{K_3},$$

$$c = -\frac{1+B}{K_3};$$

and therefore

$$\frac{E}{R} = \frac{(Z-1)^2 [Z + B(1+B)]}{Z^3}. \quad (2)$$

The computer equation becomes

$$\frac{H}{L} = \frac{(2+B) Z\left(Z - \frac{1+B}{2+B}\right)}{K_3 (Z-1) [Z + B(1+B)]}.$$

d. Root locus analysis. Unfortunately, the simple system expression E/R derived above exists only if the exact value of K_3 is programmed into the computer equations. At the current state of the art, the gain of a high-stability, low-phase-noise VCO may vary over the output range by as much as ±5% from any given nominal value. It, therefore, becomes desirable to examine the stability and transient response of the programmed exciter under the condition of VCO gain variation. This is readily done by means of a root locus analysis.

The location of the poles of E/R as a function of VCO gain is determined from the root locus of the poles of the open-loop transfer function G_0.

$$G_0 = \frac{K C\left(Z - \frac{1+B}{2+B}\right)\left(Z + \frac{B}{1-B}\right)}{(Z-1)^2 [Z + B(1+B)]};$$

$$C = (2+B)(1-B)$$

where C is the system normalizing constant, and K is the normalized VCO gain. When K is unity, the poles of E/R are at the origin and Eq. (2) holds. As K varies from unity, the poles of E/R disperse away from the origin. The farther the poles go from the origin, the longer will be the transient decay time. If a pole goes beyond the unit circle boundary, the system will be unstable.

Figs. 10, 11, and 12 show the root locus plots for three values of B. Since the plots are symmetrical about the real axis, only the upper half plane is shown. Fig. 10 shows the plot for B equal to zero. This condition is approached for a very small counting interval taken just before the system sampling time. The left-hand pole–zero combination shown in Figs. 11 and 12 has moved into the origin and cancelled each other out as B approaches zero. The maximum δ for a 5% deviation in K is 0.2791.

A plot for B equal to 0.2 is shown in Fig. 11. This condition is similar to that which exists for the programmed local oscillator (*SPS 37-20*, Vol. IV, p. 110), where the counting interval is the last 4 sec in a 10-sec sampling period. The maximum δ for 5% deviation in VCO gain is 0.2648 and occurs for reduced gain as opposed to the increased gain maximum δ for Fig. 10.

In Fig. 12, the plot is shown for B equal to 0.5, a condition which exists when the counting interval lasts for the duration of the sampling period. The maximum δ for a 5% deviation is 0.3584 on the increased gain side. In this case transients occurring when the VCO gain increased 5% would take 30% longer to decay than for the equivalent condition of Fig. 11.

e. Conclusion. Computer control equations for the programmed exciter have been synthesized to provide the capability of following an input ramp function with zero error and maximum rate of transient decay. A root locus analysis shows that the system is stable for VCO gain variations well beyond the expected limit of ±5%.

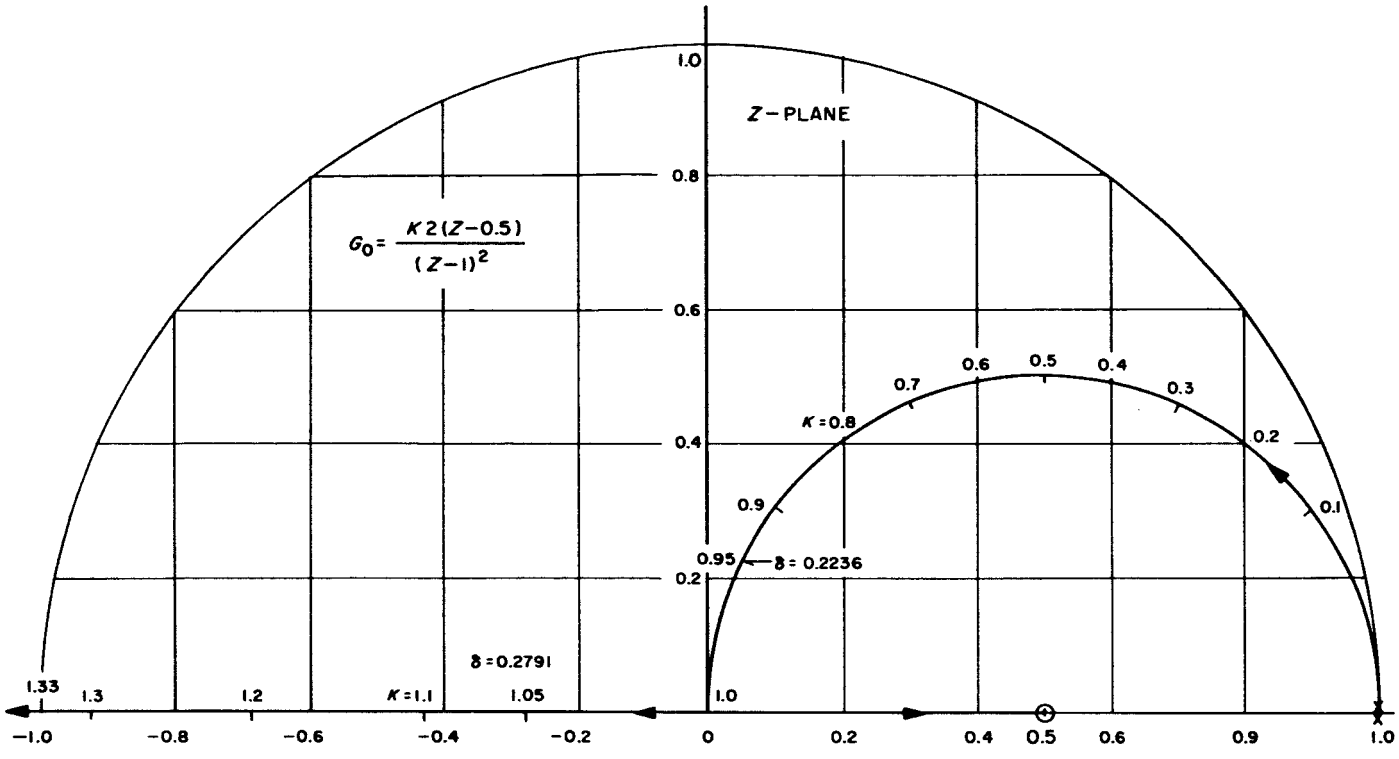

Fig. 10. Root locus plot: $B = 0$

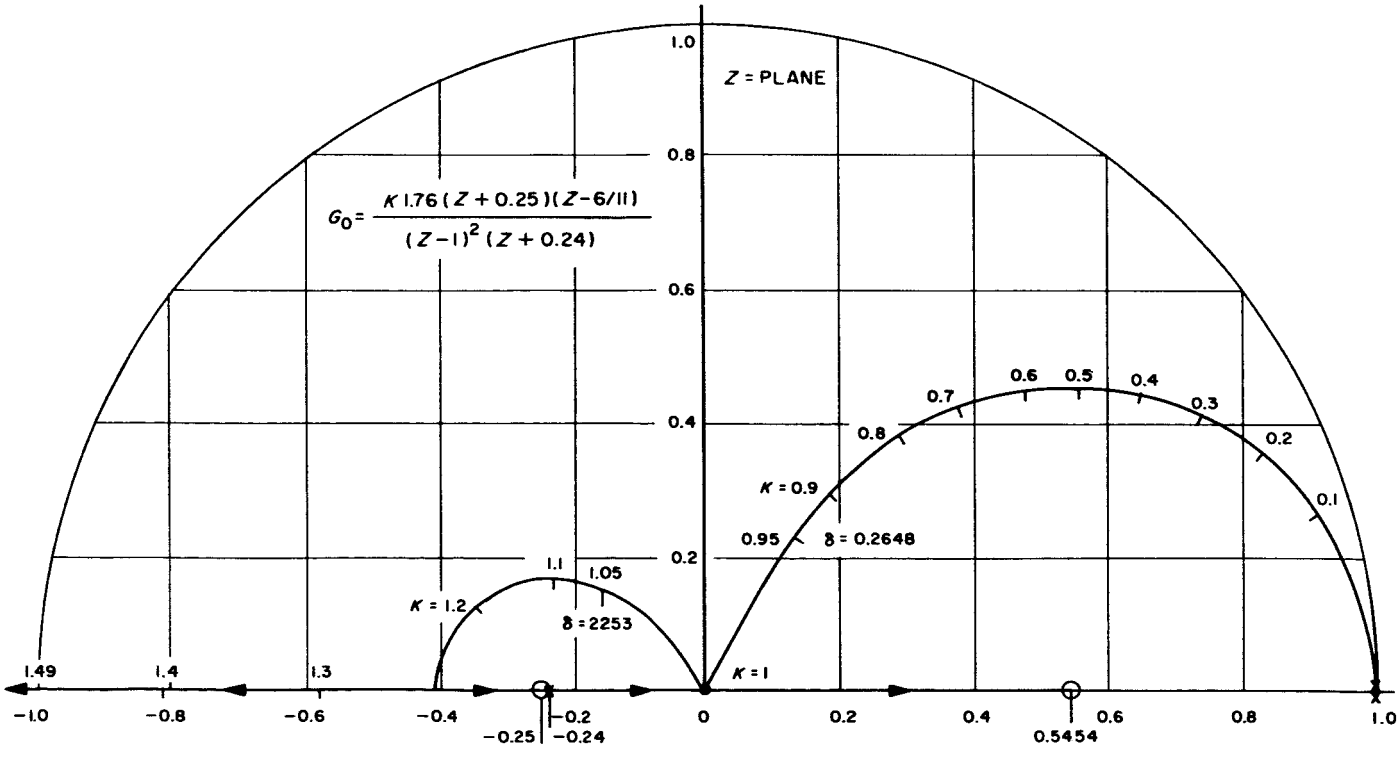

Fig. 11. Root locus plot: $B = 0.2$

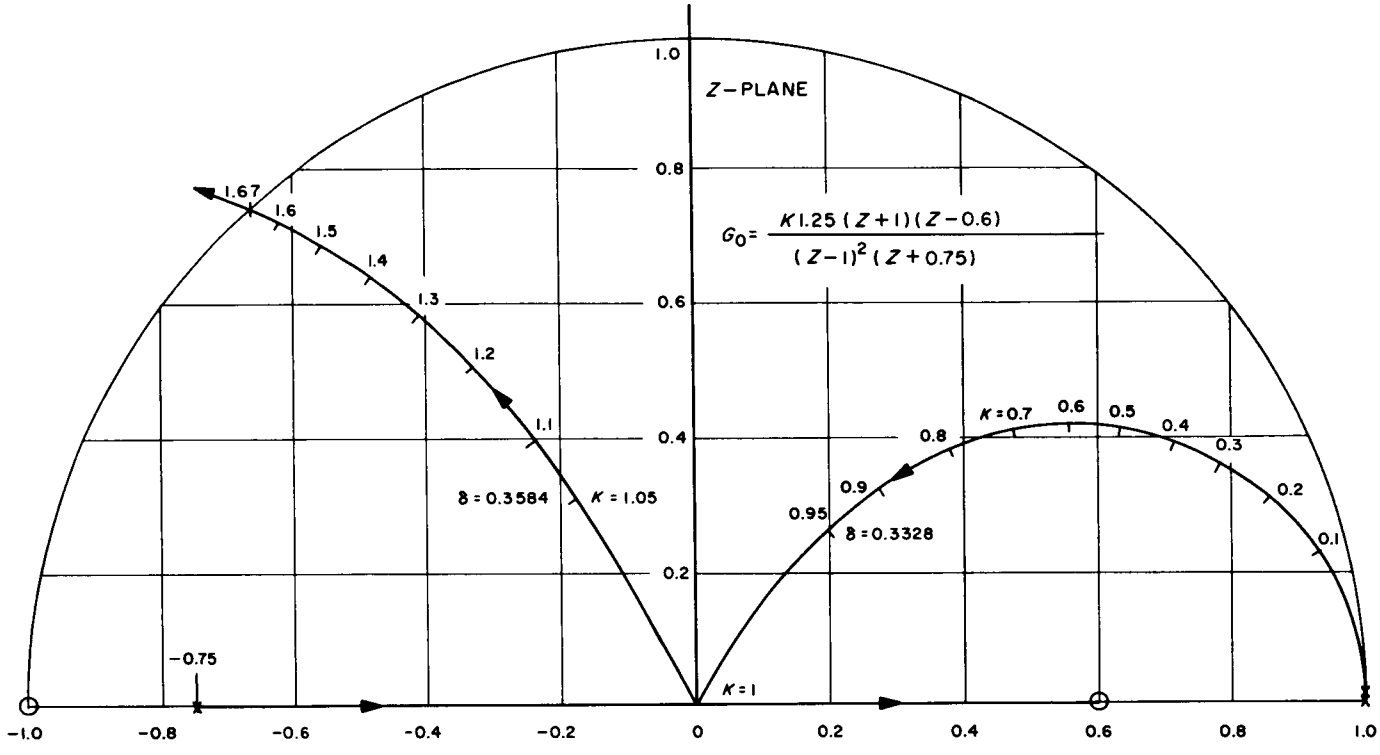

Fig. 12. Root locus plot: $B = 0.5$

3. S- and X-Band Central Frequency Synthesizer

The central frequency synthesizer has been organized into four areas of construction: Areas 1, 1A, 2, and 3.

In Area 1, the fabrication and procurement of two cabinets, five cold plates, slider alignment and modification, cable guides and termination, installation of 60- and 400-cycle power wiring, water cooling system completion, dc power supply procurement and installation, and partial wiring of the dc power distribution system are complete (Fig. 13).

Area 1A consists of the fabrication of the voltage vigilant unit, Rb 87 frequency standard and alarm installation, an RF monitoring junction, and completion of Area 1 minor details.

Area 2 consists of fabrication of established RF modules such as distribution amplifiers, design and development of new modules such as the synthesizers and new up-dated phase detectors, special RF components, modifications of existing hardware, final test, and installation of all RF modules as acquired.

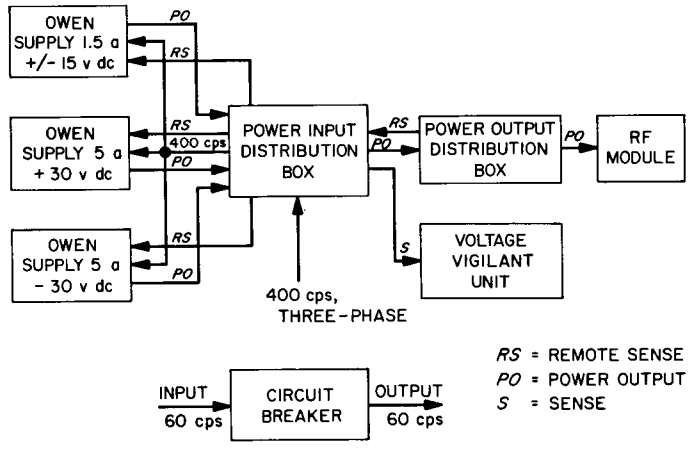

Fig. 13. Power supply diagram central frequency synthesizer

In Area 3 the assembly, calibration, and testing of all completed primary and secondary RF and dc systems, complete modifications, documentation, and implementation of all improvements to the system will be performed.

Area 1 is now 90% complete. Area 2 has 15 completely tested modules (20% of total). They include six balanced

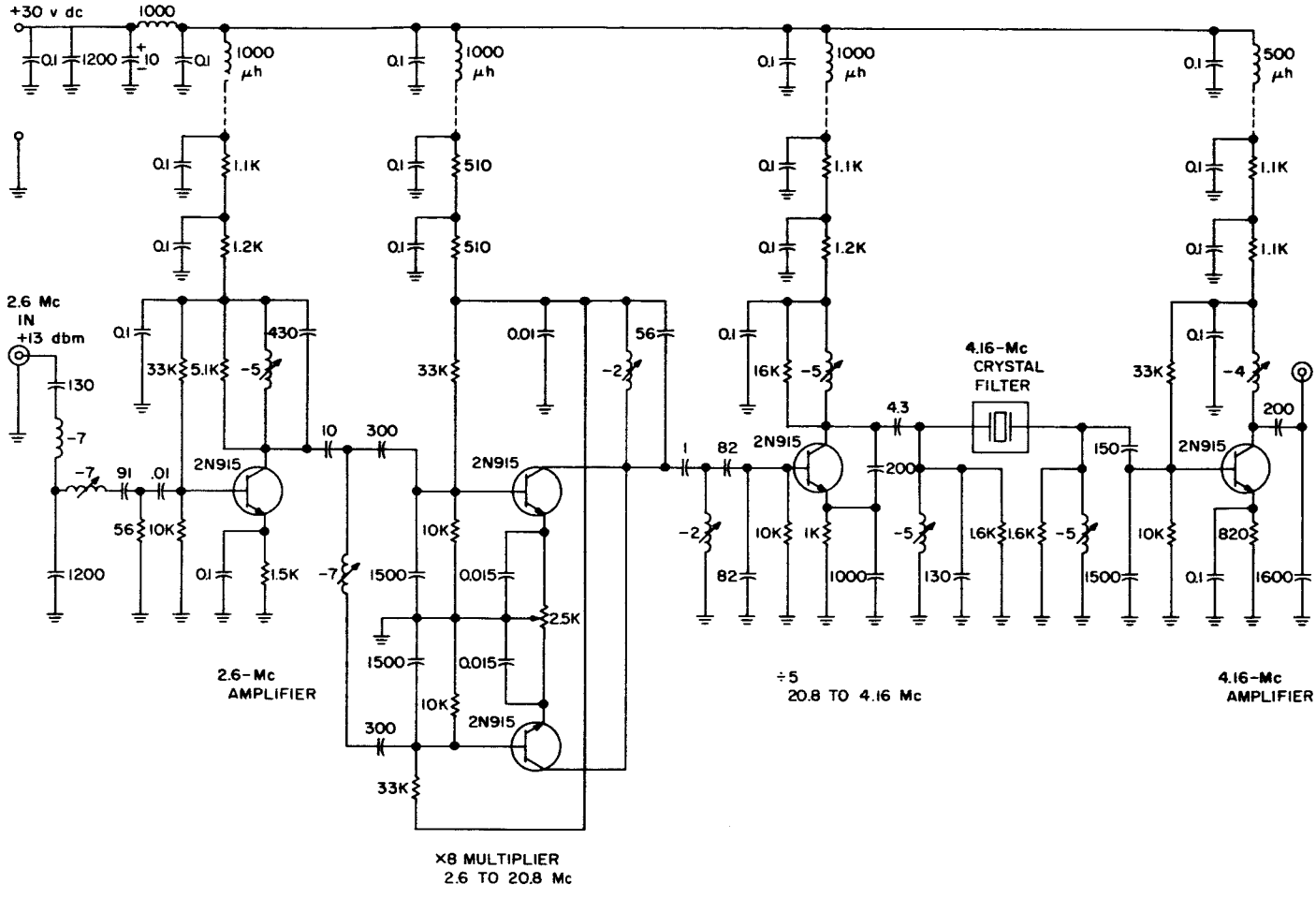

Fig. 14. 4.16-Mc synthesizer

mixers (procured from an external vendor) that have been tested and one mixer developed in-house (*SPS 37-27*, Vol. III, p. 92). A 4.16-Mc synthesizer has been developed. Three tracking filters and three in-lock detectors have been constructed from existing hardware. Modification of the 1.0-Mc crystal filter has been completed. The multipliers, dividers, synthesizers, and a phase detector are in the development stage. The distribution amplifiers are being fabricated at a local vendor.

a. The 4.16-Mc synthesizer development. This synthesizer was developed to provide the system with a reference signal for the programmed exciter (*SPS 37-30*, Vol. III, p. 85).

The synthesizer consists of a 2.6-Mc amplifier–limiter input stage, a ×8 balanced multiplier, followed by a ÷5 synchronous oscillator, one crystal filter, and a final 4.16-Mc output amplifier. Fig. 14 is the circuit diagram.

The input impedance was designed for a nominal 50 ohms ±10% at +13-dbm level. Variation of the input level +3.5 db and −6 db maintains the 50-ohm input impedance within the required 10% (Fig. 15).

Variation of 4.16-Mc output level versus power supply voltage is shown in Fig. 16. A 13% decrease of dc input voltage still produces a nominal output of +13 dbm.

The limiting characteristics of this synthesizer are shown in Fig. 17. An input signal loss of 17 db can still produce the desired +13-dbm level.

The bandwidth of the synthesizer, which is determined by the crystal filter, is ±1 kc, ±4% at 4.16 Mc. The bandpass characteristics contain no ripple. The 2.6-Mc input amplifier–limiter has a ±5% bandwidth. The output spectrum contains no measurable 2.6 Mc or 20.8 Mc, and

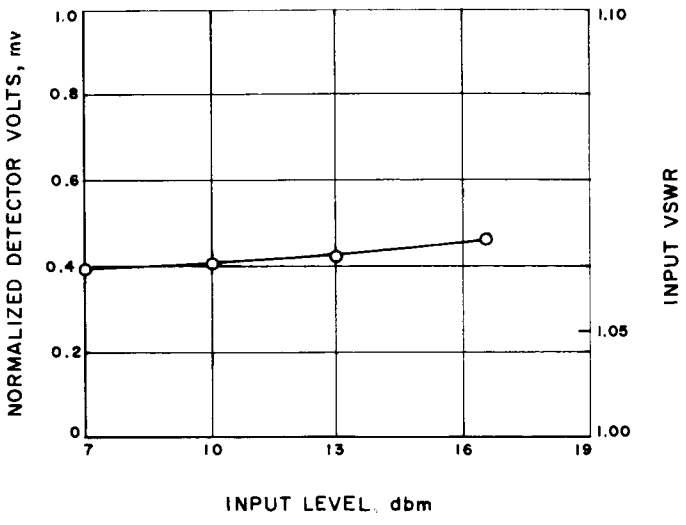

Fig. 15. Input impedance versus level

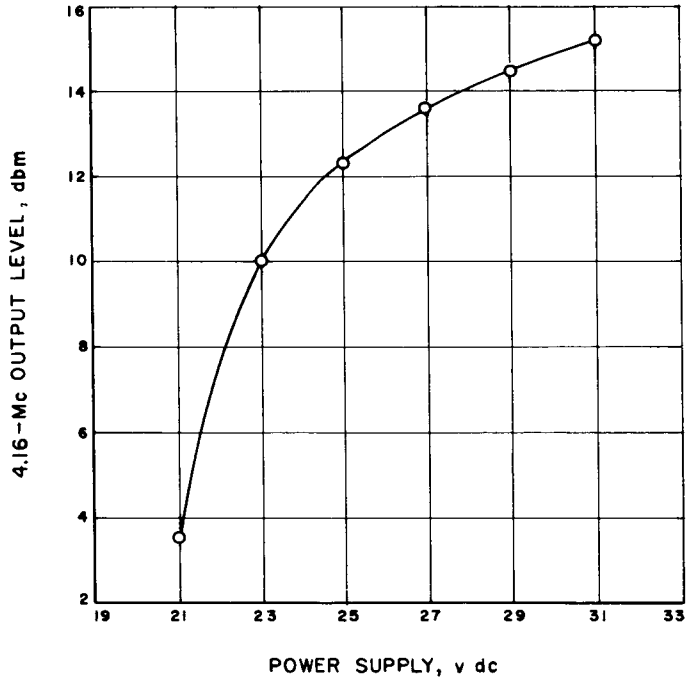

Fig. 16. Power supply variations versus 4.16-Mc output level

no spurious signals were observed. Second harmonic distortion of the 4.16 Mc is 2.5%.

The RF leakage of 2.6, 4.16, and 20.8 Mc was checked at the input and output terminals (TNC connectors), the power line, and all external mechanical junctions. All leakage signals are 0.5 μv. The chassis cavity design and adequate filtering effected the low leakage (Fig. 18).

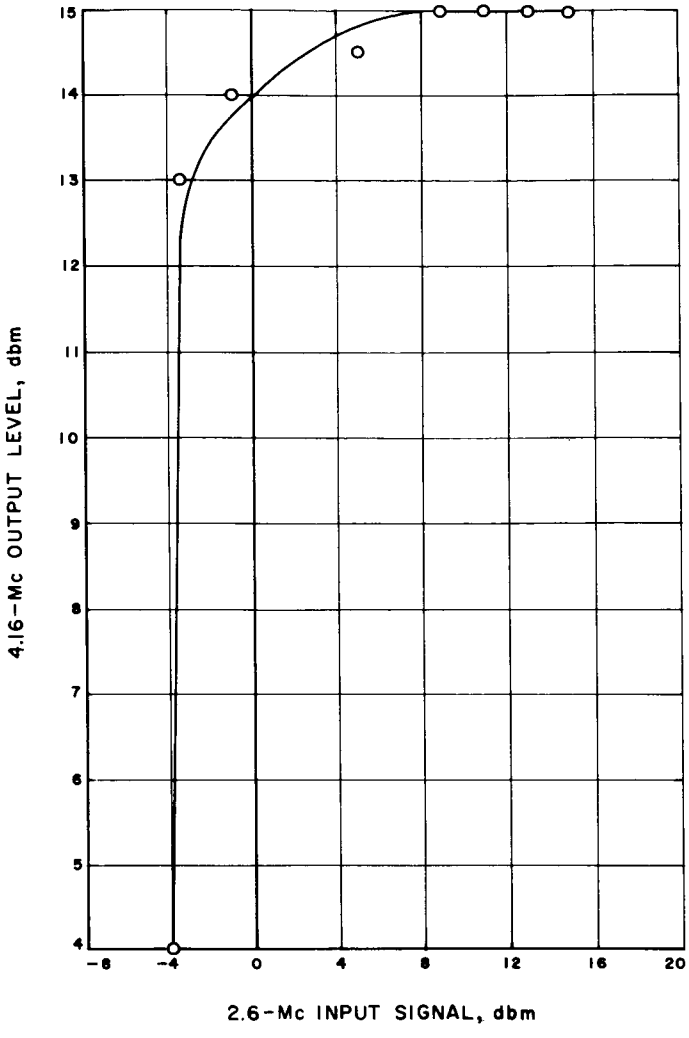

Fig. 17. Limiting characteristics

The synthesizer was subjected to a temperature environment from 0 to +50°C with the results shown in Fig. 19. No thermal runaway was observed.

b. Balanced mixers. Twelve balanced mixers were fabricated by an external vendor to provide the necessary mixers for the central frequency synthesizer (*SPS 37-30*, Vol. III, p. 86) and the programmed exciter system (*SPS 37-30*, Vol. III, p. 85).

RF leakage on the power line and TNC junctions are in excess of 1.0 μv of some units. Adequate filtering and tighter mechanical joints will cure this problem.

Spurious signals are present on some outputs and are under investigation.

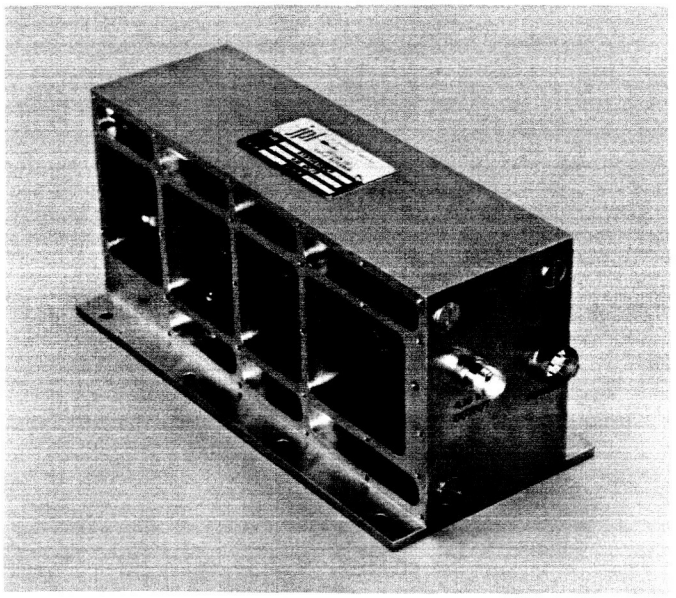

Fig. 18. 4.16-Mc synthesizer

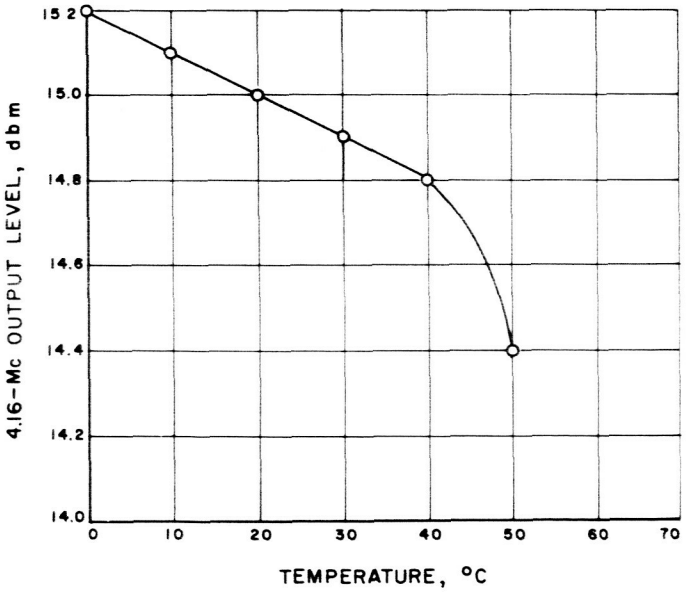

Fig. 19. Temperature versus output

D. Information Systems

1. Design of an Arbitrary Sequence Generator

The design of a sequential machine is sought such that any arbitrary sequence of n-tuples of length m, $1 \leq m \leq 2^n$, can be generated with the same machine. If there are no "repeats" allowed, the machine would be capable of generating

$$\sum_{i=0}^{2^n} (2^n - i)! \binom{2^n}{i} \approx 2^n!\, e$$

different sequences.

A good design of such a machine is one that results in maximum versatility through simplest programming, yet uses a minimum of hardware. In Refs. 1 through 14[1], numerous examples show how to derive fixed (rather than variable) sequences of m n-tuples using a minimum of memory and decision elements. (The Huffman (Ref. 13) and Mealey (Ref. 14) minimization techniques are used.) However, in designing a machine by which any one of these sequences can be easily programmed, the minimization tools mentioned above cannot conveniently be applied. A design must first be conceived as a sequential machine in an intuitive fashion.

What is sought is a free-running sequential source, that is, a recursive circuit with no external inputs. The classical block diagram of such a circuit is shown in Fig. 20. The output is shown derived from a *combinatorial network*. Fig. 21 expresses the design notion that the desired machine is derived by dividing the combinatorial network into two parts which are interconnected via a *programming device*. The programming device is visualized simply as consisting of patch cords between the two combinatorial networks. These two networks in turn are visualized as *code converters*. One code converter is visualized as a network which derives 2^n discrete outputs from n variables, and the other as a network which derives one n-tuple from any one of 2^n possible inputs.

[1] See also *SPS 37-27*, pp. 97–112; *RS 36-10*, Vol. I, pp. 27–31; and *RS 36-14*, Vol. I, pp. 54-55.

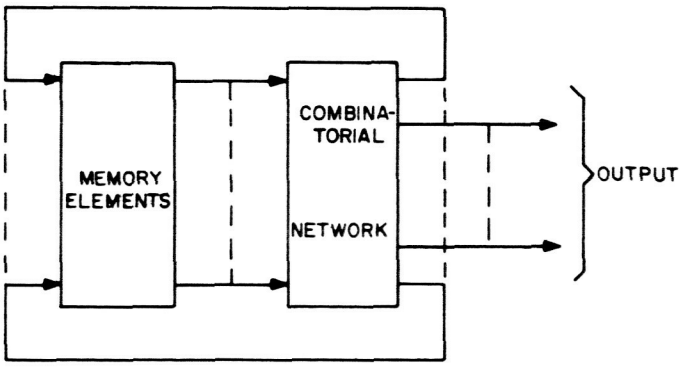

Fig. 20. Sequential source

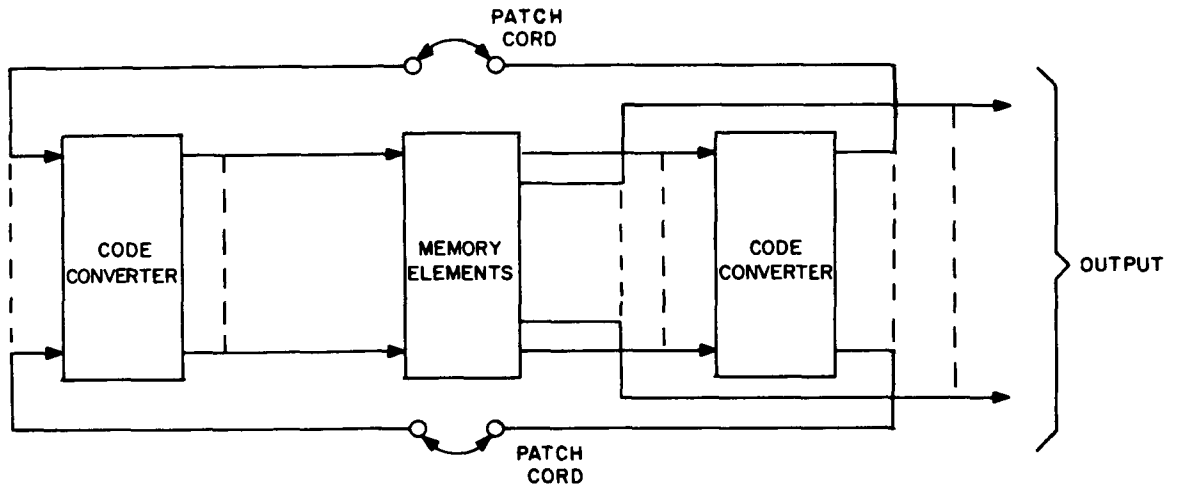

Fig. 21. Programmable sequential source

The output is derived directly from the n memory elements. The change from one n-tuple to any other requires a single connection (patch cord) from the output of one network to the input of the other; in a synchronous arrangement, this change is assumed to occur at clock time. Only sequences of different n-tuples are obtainable with this machine; they can have any period p whatsoever, $1 \leq p \leq 2^n$

As a secondary feature, the n-tuples can be transmitted serially to produce a sequence of length up to $n \cdot 2^n$. There are again about $2^n!$ e such sequences possible. An arbitrary single bit serial sequence of length l, $1 \leq l \leq 2^n$, bits is a third easily programmable output. There are $2^{2^n+1}-2$ such sequences possible.

a. Detail implementation. The design of an arbitrary sequence generator for $n=6$ shall now be described. From the expression above, it is seen that about 3.45×10^{89} different sequences of from 1 to 64 6-bit words are easily programmable with such a generator. The generator consists of a *program patch board*, two *diode matrices*, and a *flip-flop register* as the only basic components. For the secondary output, a 6-bit *serial output* device must be added; and for the third output a simple *AND/OR* network must be added.

As shown in the block diagram (Fig. 22), the arbitrary sequence generator consists of a 6-bit register which is decoded as a binary register to 64 discrete positions. An 8×8 diode *matrix decoder* is used. Each decoded output is terminated on a patch board. Corresponding positions on a second patch board are encoded into binary terms, which are then applied to the input of the very

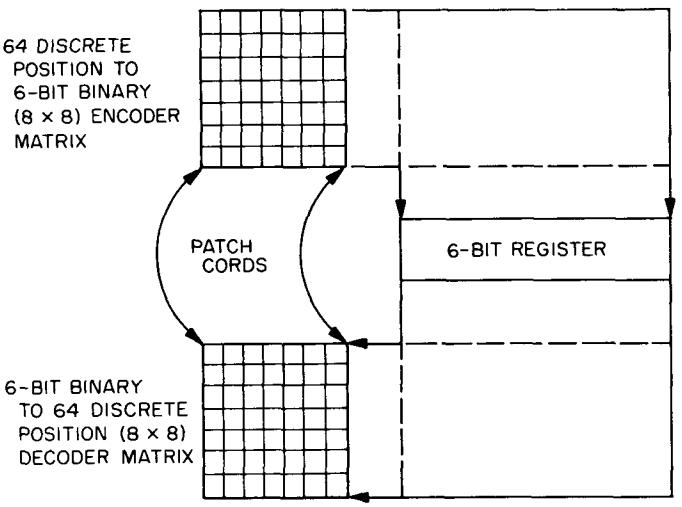

Fig. 22. Arbitrary sequence generator for $n=6$

same register. The encoding is performed in accordance with the same matrix scheme as is the decoding. The two patch boards are labeled in a decimal notation, with the decimal number referring to its equivalent binary word.

The programming procedure is explained by the following example. The short sequence shown in Table 2 is desired. With the two patch board sections labeled D (decoder) and E (encoder), the patch cords to be inserted to derive the desired sequence are listed in Table 3.

b. Serial output. Any of the following three methods can be used to derive the serial output of $n2^n$ bits; for $n=6$, this yields length 384.

Table 2. Sequence example

a_5	a_4	a_3	a_2	a_1	a_0	Decimal
0	0	0	0	0	0	0
1	1	0	0	1	1	51
1	0	1	0	0	1	41
1	0	0	1	0	0	36
0	1	0	0	1	0	18
0	0	1	0	0	1	9
1	1	0	1	0	0	52
0	1	1	0	1	0	26

Table 3. Patch board connection for sequence example

D	E
0	51
51	41
41	36
36	18
18	9
9	52
52	26
26	0

Gates can be used to disconnect the encoding–decoding matrices from the register, and instead connect the register to recycle. Depending on the size of such a rearrangement network, the word can alternately be transferred to a second parallel-input serial-output register, or the original register can be interrogated by a sequence scanner arrangement.

The third program which provides complete serial flexibility (any sequence) for a sequence of $2^n(64)$ single bits will now be described. By controlling the word sequence as discussed for the word sequencer, a completely arbitrary serial-by-bit sequence network requires a minimum of hardware; also, the programming is simple. In this connection, reference should be made to Refs. 12 and 13, which describe a single-bit sequence generator that generates any sequence of *zeros* and *ones* of length 63 or less, but which is somewhat difficult to program.

The idea here is as follows. The output is taken from a gating structure instead of directly from the counter flip-flops. One gate has only 1 bit as its input and will activate (insert zeros) for half of the counts. If this gate is *OR*-ed with another gate with two inputs, the second gate will insert zeros for one-quarter of the possible counter positions. The same reasoning is applicable for gates with 3, 4, 5, 6 inputs to enable 8, 4, 2, or 1 zeros to be inserted. All inserted zeros are disjoint, so that a set of six switches allows insertion of any amount of zeros from 1 to 63. Table 4 shows the binary numbers which insert zeros when the proper switch is thrown.

Table 4. Binary numbers used to insert zeros in a single bit sequence

Number of zeros inserted	Binary numbers used
32	0 to 31
16	32 to 47
8	48 to 55
4	56 to 59
2	60, 61
1	62

As an example, suppose a sequence with five *zeros* and 50 *ones* is desired. With the zeros in positions 1, 2, 5, 10 and 15, switches 1 and 4 are thrown to insert the 5 zeros, and from the table we find the binary equivalent of the zeros to be 62, 56, 57, 58, 59. The program counter is now wired in any sequence of length 55 that has 62, 56, 57, 58, 59 in positions 1, 2, 5, 10, and 15 and any other 50 numbers in any sequence whatsoever.

c. Applications. An arbitrary sequence of m different n bit parallel or serial words, as well as any sequence of l single bits ($1 \leq l$, $m \leq 2^n$) obtainable through simple patch board programming, can be used in a general purpose test instrument for information processing systems. Thus, this sequence generator will find applications in data-handling systems wherever a limited stored program is required and this program is subject to frequent changes (fixed program stored in a memory is equivalent to a sequence generator, but must first be loaded or programmed). The arbitrary sequence generator described here can thus be considered as being at the same time both the programming device and the memory.

The sequence generator design described in this article has these key features: For parallel as well as serial sequences, it is very economical in hardware. Conceptually the design is very simple, and therefore the programming is simple. The serial by single bit sequence is completely arbitrary, but limited in its length. The parallel and serial sequence by word is conversely limited in that a word appears only once in a full sequence.

Often this limitation is of little or no concern. However, if it were of concern, the following design extension is

offered: By decoding and encoding 1 more bit, each word can appear twice; by adding 2 bits every word appears four times, for 3 more bits eight times, etc. The additional decoding and encoding matrices are identical to the original ones; therefore, such an extension would be easy to implement.

2. Quantile System

The theory of data compression by quantiles was first introduced in *SPS 37-17*, Vol. IV, pp. 74–78, and further developed in Ref. 15. The design of the quantile system was discussed in detail in *SPS 37-27*, Vol. III, pp. 103–112. This system allows an approximate reconstruction of histograms, previously generated on board a spacecraft, from the values of only a few *sample quantiles*, or percentage points, of the histogram. Large data compression ratios, coupled with high statistical efficiencies, were discussed in Ref. 15. This article discusses the experimental system and associated tests on random data.

a. Statistical review. Some of the results from Ref. 15 will now be reviewed. Let $G(x)$ be a probability distribution function. In the case of empirical data, $G(x)$ is defined to be the fraction of experimental outcomes below x. Then the quantile of order p, Z_p, of the distribution $G(x)$ is defined as the largest value of x satisfying $G(x) \leq p$. In the case in which $G(x)$ is continuous, Z_p is the value below which X lies with probability p. For the discrete case, Z_p is the largest value just before the fraction of samples jumps above p.

The sample quantiles, being random quantiles, have probability distributions of their own, with the useful property in most cases of interest that as n approaches infinity, the joint distribution of any number of quantiles approaches a known multivariate normal distribution. Thus, for a sufficiently large sample size, if the limiting normal distribution of the sample quantiles is assumed when a statistical analysis is based on quantile values, the error involved in doing so will be small. Since experiments on board a space probe often involve large numbers of observation (1000 samples is not uncommon), the assumption of normality is amply justified.

Estimates of the parameters of the distribution associated with a population and the results of tests of statistical hypotheses are two of the important types of statistical information desired from experiments performed on board a space probe. Using a small number of quantiles to obtain this information means that only a few numbers need be transmitted to Earth instead of all the sample values, resulting in a high data compression ratio. This compression ratio would be of little value, however, if there were a proportional loss of statistical information in quantiles as compared to all the data. That such is not the case accounts for the advocacy of the use of quantiles. In fact, by using only four optimally chosen quantiles, the estimate of the mean of the population can be calculated with an efficiency of 90.8% compared to the calculation using all the sample values, and the estimate of the population standard deviation can be calculated with an efficiency of 73.5%. These four quantiles are $p = 0.067$, 0.291, 0.709, and 0.933.

b. Review of functions performed by quantile system. It is evident from the definition of sample quantiles that no arithmetic unit is needed on board the spacecraft to obtain the quantiles from raw data. It is this simplicity of the compression equipment which makes the quantile system feasible for flight hardware.

One kind of experiment envisioned is a particle counting experiment. Particles arrive at the spacecraft and the number per unit time is counted. This number is the raw input data, and 1024 samples of counts per unit time constitute a histogram. It is assumed that not more than 255 counts arrive per unit time. Once the histogram has been stored, the following four numbers are to be found: ζ_1, the smallest count such that 69 or more of the 1024 counts had at most that value. The same is done for ζ_2, using 299; ζ_3 using 726; and ζ_4 using 956. Due to the method used for storing the histogram, where a unary system is used to store sample values, the calculation of the quantiles is reduced to counting and coincidence detection.

c. Experimental results. Upon completion and checkout of the quantile system, known distributions generated by the random pulse generator (*SPS 37-27*, Vol. III, pp. 112–115) were sampled and displayed by the quantiler display networks. Figs. 23 and 24 show the three displays: the sample histogram, the sample cumulative function, and the four sample quantiles, displayed in octal, superimposed on one picture. Fig. 23(a) and (b) shows histograms of data taken from a population with a binomial distribution (which is close to being normal) but with different means. Fig. 24 shows a bimodal distribution obtained by changing the sample population about halfway through the sample. The effect on the quantiles in this case is that there is a much larger gap between the second and third quantiles than in the unimodal case.

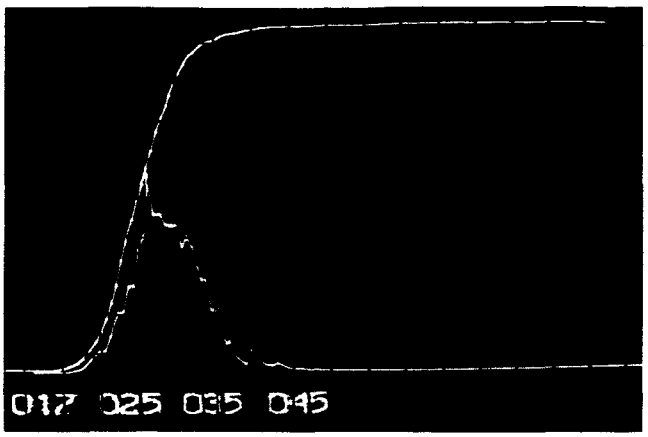

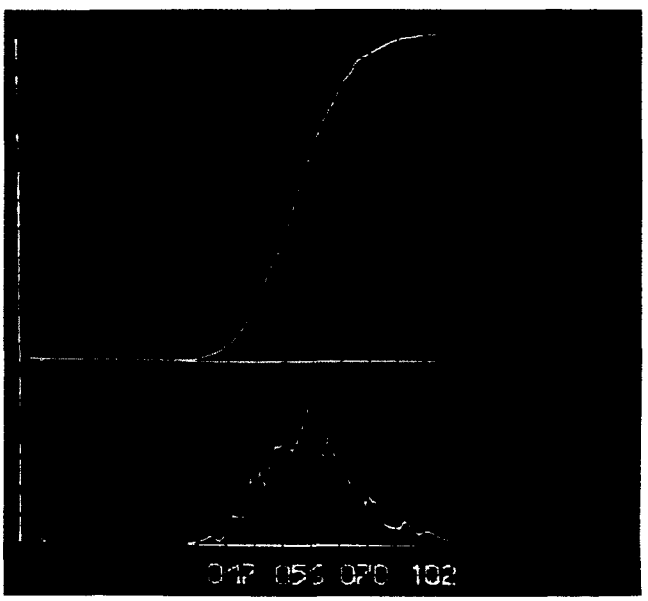

Fig. 23. Histogram: cumulative function and quantiles for binomial distribution

Fig. 24. Histogram: cumulative function and quantiles for bimodal distribution

Tests were then performed to determine the mean and standard deviation of known distributions by sampling and computing these parameters from the observed quantiles. The estimates of these parameters were calculated by the following formulas from Ref. 15:

$$\hat{\mu} = 0.141\,(\zeta_1 + \zeta_4) + 0.359\,(\zeta_2 + \zeta_3)$$

$$\hat{\sigma} = 0.258\,(\zeta_4 - \zeta_1) + 0.205\,(\zeta_3 - \zeta_2).$$

The results of these tests are given in Table 5. It is observed that in all cases the agreement between the observed and theoretical values is excellent. In fact, in the case of the "renewal" data, the variance calculated from the quantiles disclosed an error in the calculation of the theoretical variance!

3. Teletype Coding Experiment

When transmitting messages over a teletype line, one notices errors getting into the message. Symbols are changed or deleted to result in an error message. When the context is clear, it is often possible to correct some of these errors. When the message is a spacecraft command, an error may not be easily corrected. If an error is noticed, a retransmission of the corrupted message is called for. However, messages can be encoded with sufficient structure to enable a decoding apparatus to correct certain errors which may occur during the transmission.

In *SPS 37-26*, Vol. IV, pp. 223–225, a code is described for use in transmission over an interstation teletype channel. The actual implementation of the decoding operation is discussed in *SPS 37-29*, Vol. III, pp. 95–99 and *SPS 37-29*, Vol. IV, p. 299. The code chosen for the operation was a Bose–Chaudhuri (63,18) code. The code had the capability to correct up to 10 teletype symbol errors in each block of 63 symbols, and the probability of an uncorrected error dropped to less than 10^{-8}. While no one knew what the exact characteristics of the channel were, the above code seemed to be perfect for a certain model of the channel. A symbol error probability of no greater than 0.02 with errors occurring equally often among the five channels which make up the symbol was assumed. The only question which remained to be answered was: "Is the model of the channel a good one?"

a. Investigation of the channel. In order to investigate the characteristics of the channel, a long maximal-length shift register message was encoded and sent over the DSIF communication links. The received message and transmitted message could be compared and any discrepancy noted. A computer program to run on the SDS 910

Table 5. Comparison of experimental and theoretical mean and standard deviations

Known distribution	Sample quantiles				$\hat{\mu}$	$\hat{\delta}$	$\bar{\hat{\mu}}$	$\bar{\hat{\delta}}$
Binomial $\mu = 50$	43	47	52	59	49.9	5.15		
$\delta = 5.0$	43	47	52	58	49.8	4.89	49.8	4.90
	43	47	52	57	49.6	4.64		
Binomial $\mu = 125$	109	118	130	140	124.1	10.46		
$\delta = 10.825$	109	118	131	142	124.8	11.18	124.5	10.71
	109	119	130	141	124.6	10.51		
Overlapping windows, 111	104	116	133	149	125.1	15.10		
$\mu = 125$	103	116	133	149	124.9	15.35	124.99	15.29
$\delta = 15.31$	104	116	132	151	125.0	15.41		
Overlapping windows, 101	106	117	132	149	125.4	10.00		
$\mu = 125$	106	116	131	145	125.1	10.51	125.22	10.25
$\delta = 10.45$	106	117	132	147	125.2	10.25		
Renewal process, 111	61	67	75	82	71.9	7.06		
$\mu = 71.43$	61	67	75	83	71.3	7.32	71.47	7.23
$\delta = 7.19$	61	67	75	83	71.3	7.32		

computer at the Venus site at Goldstone was prepared to compare the transmitted and received tape (*SPS 37-31*, Vol. III, pp. 76–78).

The actual operation of the test was as follows: On a daily basis, a shift register message of length 16,000 bits (3200 teletype symbols) was sent from Goldstone to DSIF Stations. The messages were sent over the *Mariner* link so that the system could be checked during standard mission-status operation. When the message reached its destination, two things were to take place:

(1) The operator at the receiving site was to resend the message back to Goldstone as he had received it.

(2) He was to send the tape he received from Goldstone by air carrier back to Goldstone.

This way one could make checks on both the one-way and two-way operation of the channel.

When messages were received, they were compared against the transmitted message. Checks were made to determine the number of teletype symbol errors, and it was determined in which of the five channels the errors had occurred. Further, the program made provisions for counting the length of a string of teletype symbols, all of which were in error. This was used to test the burst error probability of the channel. The channel was, however, found to be "non-bursty" on the symbol level.

Sending of messages began on December 14, 1964, and the first return messages were received a few days later. From the beginning, certain features, some expected and some unexpected, were observed. It was noticed that binary errors (i.e., 0→1 and 1→0) were occurring with reasonable frequency, but that longer strings of symbol errors than expected had occurred. In general, it was determined that the long strings of errors were in fact due to synchronization errors. Symbols had been deleted from the message; this resulted in errors between the two tapes. This synchronization problem was totally unexpected, and it was decided that ideas about error correction should be changed to take care of this kind of error.

Although the bit error probability was within acceptable limits, it was found that, in some messages, 60 to 70% of the errors were occurring in Channel 5. Table 6 shows the frequency of errors occurring in the five channels. It was thought that the high rate of error in Channel 5 was due to a surging effect; i.e., since Channel 5 is the last hole punched on the tape, any build-up in electrostatic charge would cause most errors to occur in that channel. It was felt that, by not encoding information for Channel 5, the error probability could be dropped to a sufficiently low level as to make coding at the reduced rate of 80% of information per symbol feasible. Channel 5 could then be used as a parity check channel.

There were basically two types of errors occurring among the symbols:

(1) Single errors, i.e., those in which one channel in five was found to be in error (these were the most prevalent).

(2) Multiple errors in which more than one channel was in error in a single symbol.

It is thought that these two kinds of errors are basically different in nature. The difference in the errors is in the period of the travel where the errors are inserted.

Table 6. Errors for the channels in 29 message tapes in which no synchronization errors occurred

Channel	Number of errors	Errors per channel, %
1	29	6.2
2	39	8.3
3	41	8.7
4	89	19.0
5	271	57.8

Overseas messages travel through a regular channel. They are first routed through New York or San Francisco depending on whether the destination is east or west. While the message is within the United States, there is no means for detecting errors in transmission. Before overseas transmission, the teletype symbols are encoded in a "4 *ones* in 7 bits" code. The system is called the Van Duuren ARQ System, and any single errors are detected on transmission. When errors are detected, retransmission is requested automatically by the ARQ system. However, an error which inserts a *one* and deletes another *one* will go undetected. Symbols which have been corrupted by this kind of error have no relation to the intended symbol. It is concluded that these are the multiple errors.

The single errors most probably occur while the message is yet uncoded into the ARQ system, i.e., still within the continental United States. Most errors are single errors. Multiple errors occur whenever a symbol is deleted or changed. Of this second type of multiple error only a small number has been observed. In four tapes there were six double errors and one quintuple error. On one tape, which had been transmitted to Johannesburg, an error pattern of (17,4,9,1,0) was observed indicating 17 single errors, 4 double, 9 triple, 1 quadruple, and no quintuple errors. Most of the ARQ errors occur on messages to Johannesburg, which verifies the DSN experience that links to Johannesburg are least reliable.

Another phenomenon which has been noticed, but for which there is no explanation because of an insufficient supply of data, is that the tapes which have been received by mail (i.e., those which correspond to a one-way message) have almost all of the errors in them, and almost no errors occur in the return message. This may be due to some atmospheric conditions prevailing at the time of the original message, or the quality of the associated sender or receiver, or some other effect yet unnoticed. When more data becomes available, this situation will become clearer.

Other problems have arisen which are unrelated to the problem of error detection and correction. On some messages, all occurrences of blank symbols were deleted. The location at which these deletions have occurred has not been determined. However, after a notation to bypass the communications processor at Goddard was affixed to the message, these deletions have not been observed.

b. Results of the investigation. Since the *a priori* conception of the channel was not borne out too closely by the investigation conducted, certain changes were felt to be necessary in the codes used for our mission. Also, it was felt that further investigation into the workings of the channel should be conducted. Now transitions of *zeros* into *ones* and *ones* into *zeros* will be considered different and counted in separate counters. It is possible that this information could prove valuable when discussing error-correcting capabilities.

The biggest result of the investigation of the channel is that the code used for error correction must be changed. It is the phenomenon of a synchronization error which causes us to change the code. There has to be some automatic method for detecting and correcting errors which occur as a result of an insertion or deletion of a symbol. The next part of this article discusses a code which has good error-correcting capacity and handles the problems of insertions or deletion of a symbol. That there is a need to correct errors which result after the insertion or deletion of a symbol is clear from the data. In 47 messages, 18 had at least one deletion or insertion of a symbol occurring.

c. New solution for problem. In the previous part of this article, it was seen that a new code is necessary. The three problems to consider in choosing a code are:

(1) Satisfying a reasonable error-correction rate for the channel.

(2) Dealing with the problem presented by the high error rate in Channel 5.

(3) Correcting the problem of synchronization errors.

The code chosen to meet these criteria is the Reed–Solomon (15,9) code[2], a code over the four element field. The code words are of length 15, and can be generated by a shift register given 9 information symbols. The entries in the sequences are elements in the field of 2^4 elements, and the code corrects 3 symbol errors. As previously mentioned, since only 4 of 5 channels are used for encoding information, the fifth channel is to be used as an (odd) parity channel. A spot check would be made of the fifth channel to determine channel bit error statistics.

The problem of insertion or deletion of symbols will now be discussed. The code can be thought of as being made up of a word of length 14 with an extra symbol affixed to act as a synchronizing symbol. When this synchronizing symbol is noted to be out of position, a procedure for determination of the symbol deleted and its position can be determined[2]. The best choice for the synchronizing symbol is one which maximizes the distance between it and other code symbols.

In particular, there is a group of symbols for which the distance between the group and the synchronizing symbol should be maximized. This group contains the 4 symbols: *figures, H, letters,* and *blank* symbol. The reason that these symbols should be avoided is a characteristic of the teletype system. In normal operation, when the sequence of symbols *figures, H, letters* is transmitted, the receiving machine is turned off. This is a hard-wired feature and a fact-of-life which has to be accepted when communicating over the teletype system. If we make the synchronization symbol (in fact, all code symbols) as far from these three symbols as possible, the probability that a message segment will be corrupted into the "offensive trio" will be minimized. The reason for avoiding the *blank* symbol is clear from the earlier discussion of the blank symbol suppressions. The odd parity for the fifth channel avoids having the 5-tuples for *figures, H,* and *blank.*

The problem of finding the synchronization symbol is complicated by the fact that all symbols have two representations. They are encoded as a 5-tuple for the teletype code for transmission in the continental United States, and they are re-encoded into the ARQ 7 unit code. The synchronization symbol should maximize the distance from these symbols in both encodings.

[2]To appear in *SPS 37-33,* Vol. III.

Blank is encoded in the two systems as 0 0 0 0 0 and 0 0 0 0 1 1 1; *Figures* is encoded as 1 1 0 1 1 and 0 1 0 0 1 1 0. *H* is encoded as 0 0 1 0 1 and 1 0 1 0 0 1 0, and *letters* is encoded as 1 1 1 1 1 and 0 0 0 1 1 1 0. For the 7-unit Moore encoding, it can be shown that given 4 symbols *A, B, C, D* with the distances

$$d(AB) = d(AC) = d(BC) = 2 \text{ and } d(AD) = d(CD) = 4,$$

a fifth symbol *E* can be added that has the distances $d(AE) = 6$, $d(BE) = d(DE) = 4$, and that no symbol can be found to increase these distances. Among the possible symbols *E* that can be chosen, we take the one which maximizes the distances $d(AC)$, $d(BE)$, $d(CE)$, $d(DE)$ in the 5-tuple teletype code. The symbol which maximizes these distances is encoded 1 0 0 0 1 and 0 1 1 0 0 0 1. Thus, 1 0 0 0 1 is chosen as the synchronization symbol.

The encoding and decoding schemes or the (15,9) code, discussed above, have been worked out. A computer program for the SDS-910 is being written to do the encoding and decoding and will be ready shortly for operation on experimental spacecraft command messages.

E. S-Band Planetary Radar Project

1. 1-Mw Solid-State Rectifier

The installation of the solid-state rectifier has been completed. Preliminary data on the system was recorded under test conditions. The full 1-Mw test will be conducted in the near future. A circuit diagram of the rectifier is shown in Fig. 25.

The solid-state rectifier is fully protected against all normal hazards. An oil temperature interlock in the rectifier tank will shut down the large generator in the event of abnormal oil heating. Low oil flow will also shut down the main generator, and thereby remove the primary voltage from the power transformer. The oil level gage and the over-pressure relief valve each have an interlock. Closure of either of these interlocks will show a warning light on the transmitter control panel and shut off the oil circulating pump; the flow interlock will shut down the main generator. Shutdown of the oil pump,

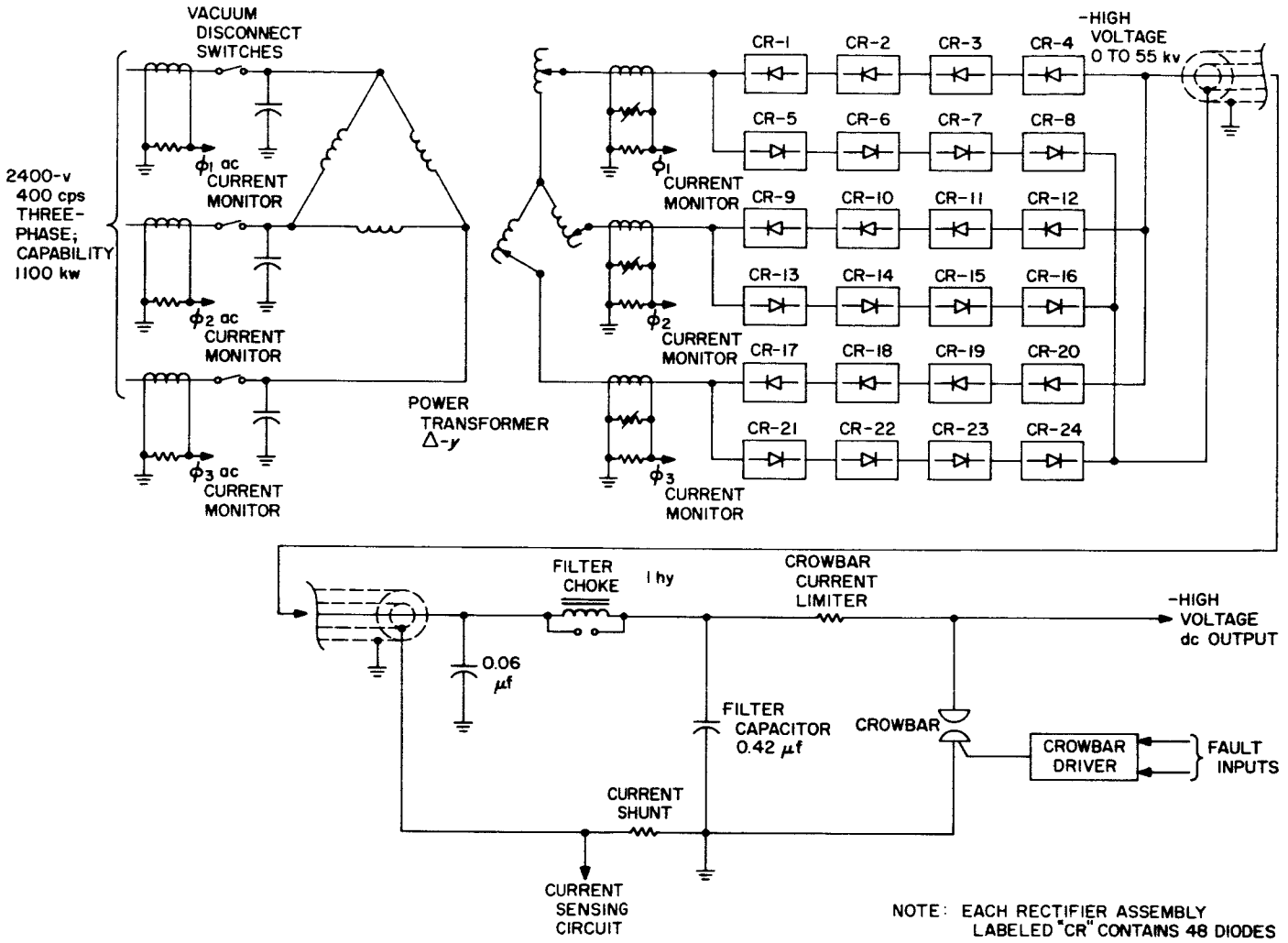

Fig. 25. Circuit diagram of solid-state rectifier

when the pressure relief valve has opened, is necessary to prevent a large loss of oil. Over-current and over-voltage protection are provided by the existing system equipment.

Switching from the vacuum tube rectifier to the solid-state rectifier is accomplished in approximately 1 hr and requires the following procedure: The three input phases and the high-voltage dc output cable are transferred to the solid-state rectifier. The water valves are closed on the vacuum tube rectifier and opened on the solid-state rectifier heat exchanger. The switch for the oil pump is turned on, and the switch on the interlock control panel (Fig. 26) is turned from the vacuum tube position to the silicon-rectifier position. The system will then turn on and cycle to the *operate* condition in the normal manner. Fig. 27 is a schematic diagram of the oil and water system.

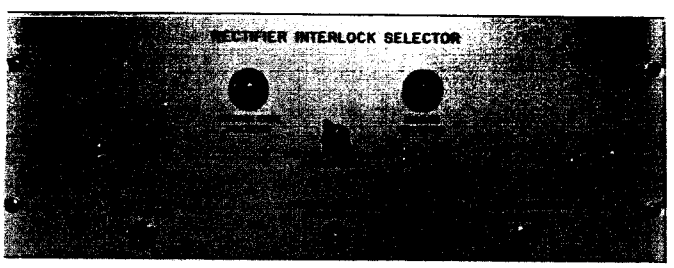

Fig. 26. Interlock panel

As soon as the rectifier tank was filled, the oil was tested for breakdown. Residue and foreign material in the system caused the breakdown to fall from 50 kv dc to 16 kv dc, under ASTM test conditions (0.1 in. between ball electrodes; see *SPS 37-30*, Vol. III, p. 82, Fig. 50). The oil was circulated through a filter press for 1 day,

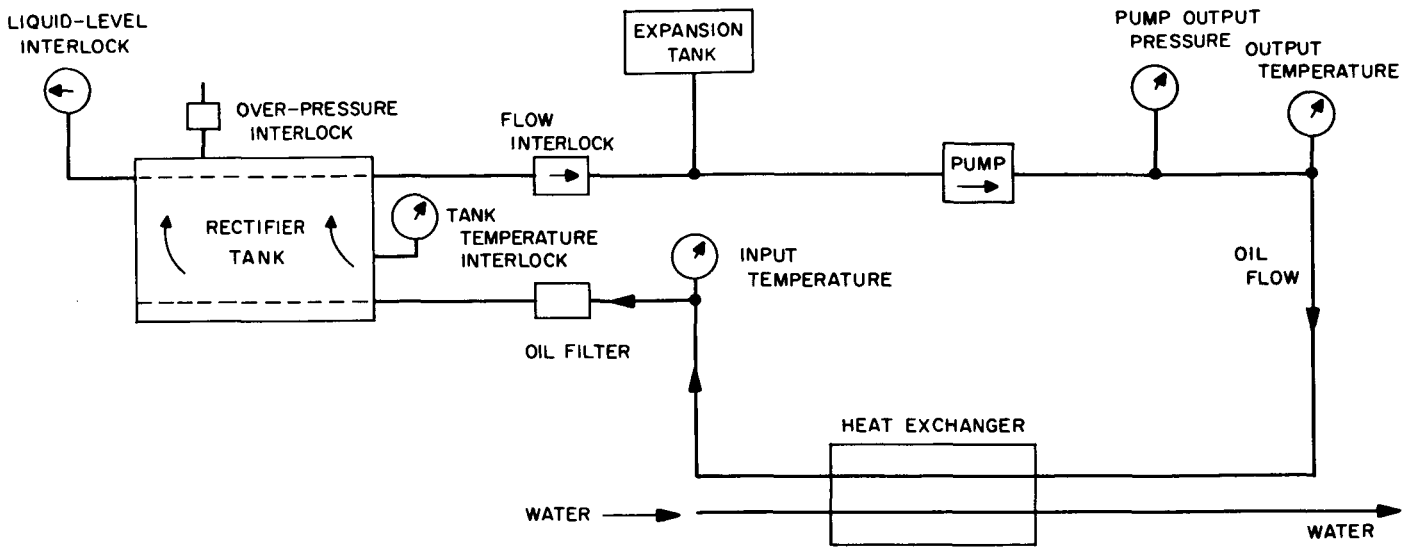

Fig. 27. Oil and water system (1-Mw solid-state rectifier)

and the breakdown voltage point was thereby raised to an adequate 40 kv dc.

The rectifier was terminated into the dc water load, and power was then applied. The dc output voltage was changed in steps of 5 kv beginning at 4 kv and ending at 39 kv. Subsequent tests were conducted up to 55 kv under no-load conditions.

Following this test, the new rectifier operated satisfactorily on the 100-kw S-band transmitter. The tube potential was 32 kv and, with the normal drop in the series limiter, the power supply voltage was 39 kv. After a 16-hr test, and with the system sustaining a few routine crowbars, the primary lines to the power transformer showed a 10% phase unbalance. The rectifier legs were then tested for forward voltage drop under a nominal test current and for reverse resistance. The results indicated conclusively that one leg of the bridge was breaking down. Testing was suspended, and the manufacturer is supplying four new rectifier assemblies.

Fig. 28 gives the distribution of diodes versus resistance readings for the remaining rectifier assemblies. Fig. 29 gives the distribution of diodes versus resistance for the new assemblies. Rectifier cells below 25K ohms are being replaced in the five remaining legs of the bridge. Fig. 30 gives the cumulative percent of diodes equal-to or less-than the back-resistance on the abscissa. Data was also taken wherein the reverse current was recorded for a given potential.

The test results, after showing the weakness of one leg of the bridge and several individual cells, do not in any way detract from expectations of eventual success and high reliability from the solid-state rectifier. A new series of tests will be scheduled in the near future when the rectifier cells and the rectifier legs will have been placed in first-class condition.

2. *Transmitter Power Stability*

This report describes the work which has been done to reduce power variations in the output of the 100-kw Venus transmitter. These variations in power are accompanied by variations in phase as a consequence of the phase pushing that is experienced to some degree in all klystron amplifiers. The main cause of the power and phase variations was determined to be the variations in dc supply voltage applied to the klystron. This phenomenon was reported in *SPS 37-29*, Vol. III, p. 70.

Recent maintenance of the high-voltage dc power supply has included the machining of the commutator in the main dc generator and replacement of the brushes on both the main generator and the amplidyne. The power factor automatic controller for the 60-cycle motor, which drives the main generator, was found to be improperly connected by the contractor. Satisfactory operation was noted following correction of the wiring.

A test was subsequently run on the 1-Mw power supply to determine the extent of the presently existing output voltage variations and to isolate the device causing

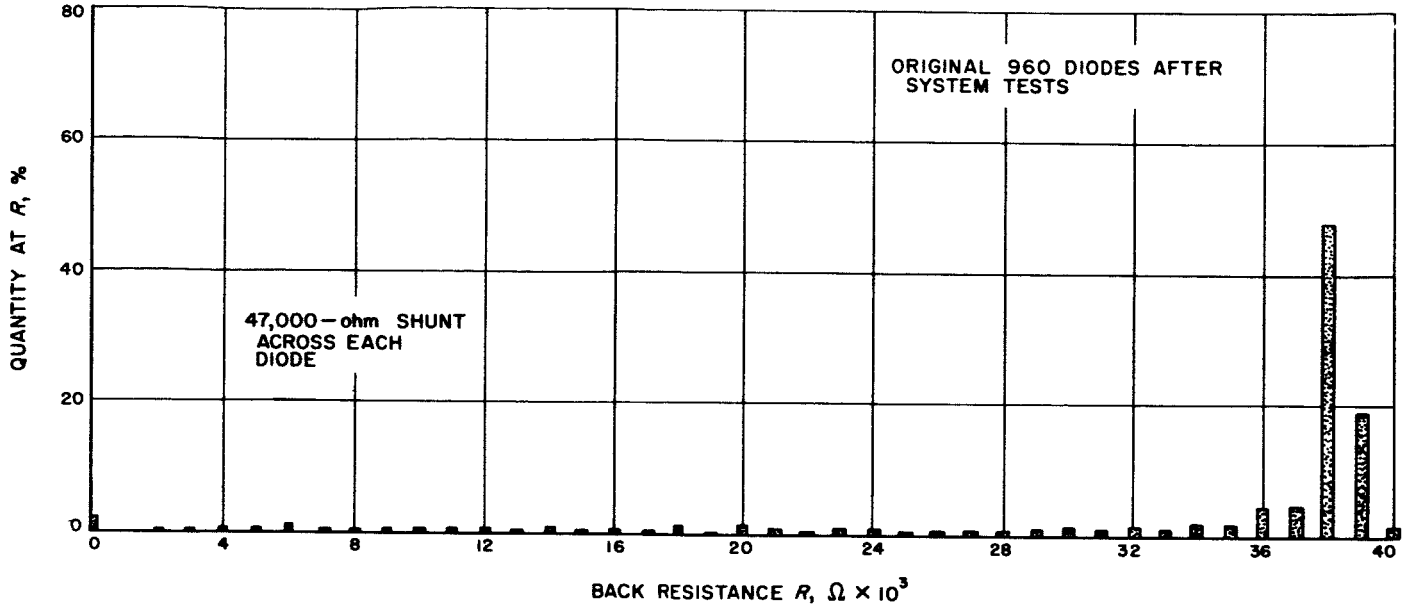

Fig. 28. Resistance distribution of 960 diodes in 1-Mw rectifier

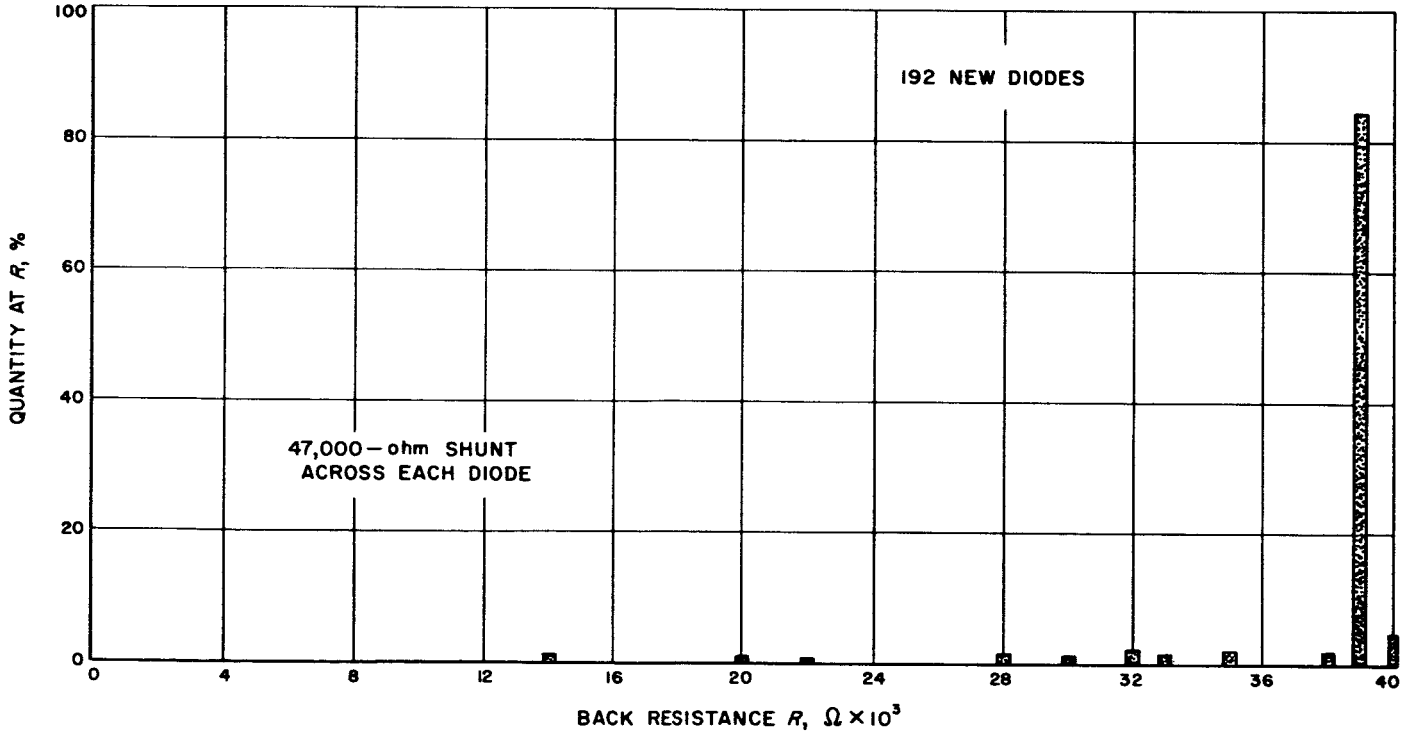

Fig. 29. Resistance distribution of 192 new diodes in 1-Mw rectifier

the disturbance. Fig. 31 shows the recording of the power supply dc output when using the electronic control on the amplidyne. Fig. 32 shows the dc output voltage recording taken when the amplidyne was excited with dc from the internal power supply in the manual mode. The absence of electronic control in the manual mode is evidenced by the level drift. Fig. 33 shows the dc output when the main generator field was excited from a fixed dc source. In the latter case, the amplidyne was completely removed from the circuit. As can be noted in the

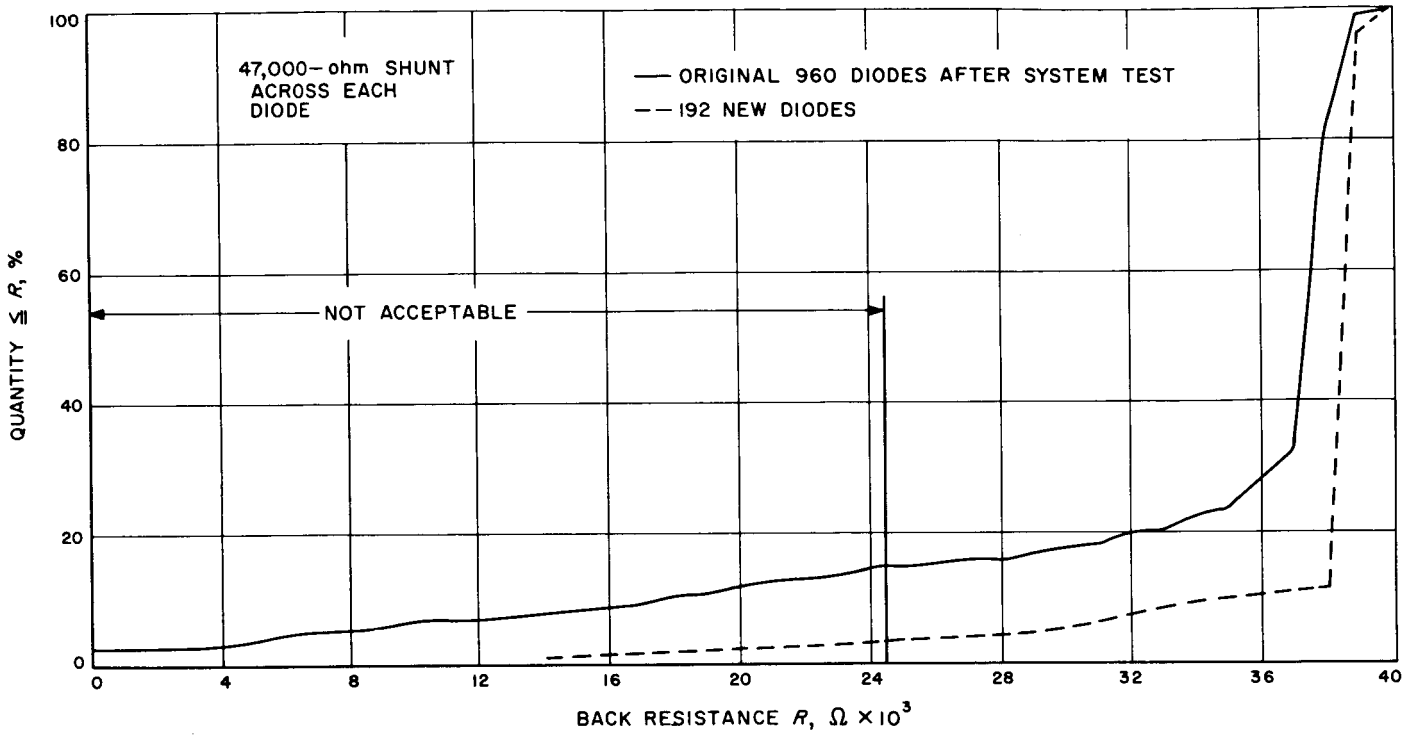

Fig. 30. 1-Mw solid-state rectifier: cumulative distribution of diodes by resistance

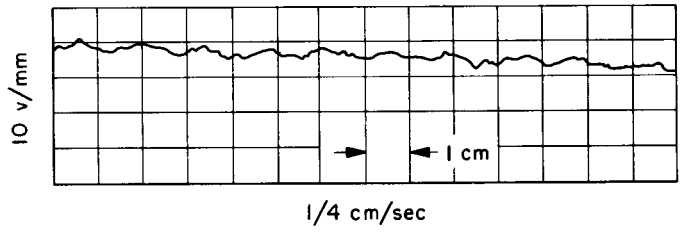

Fig. 31. Power supply voltage ripple: electronic regulation with amplidyne, 24 kv dc at power supply

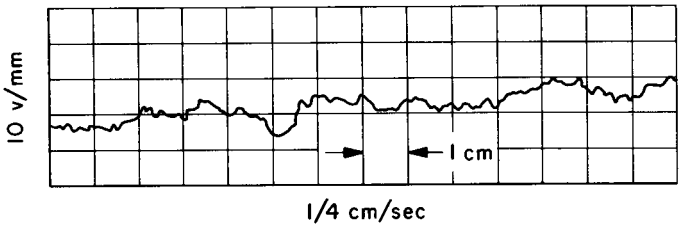

Fig. 32. Power supply voltage ripple: manual excitation with amplidyne, 24 kv dc at power supply

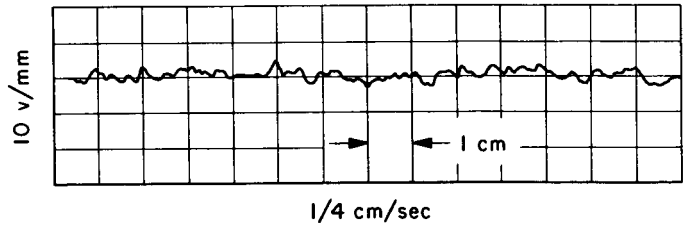

Fig. 33. Power supply voltage ripple: battery excitation at main generator field, 24 kv dc at power supply

various figures, the dc output is essentially the same when the main generator field is excited by the amplidyne or the special dc supply. The conclusion is that the variations evident in the recordings are due to the main generator. Since these variations are of the order of 50 v out of 24,000 v, and would produce a phase modulation of only 1.8 deg, the machine is considered to be working satisfactorily. The variations before the modifications were made were ten times as great as those of this test.

3. *Multiplier Chains*

Since last reporting (*SPS 37-31*, Vol. III), module development and documentation have been completed for the procurement of solid-state chains to replace the vacuum tube units in the S-band exciter and receiver. Both digital phase modulators have been installed at the Goldstone Venus site, and procurement of the balance of the units required for S-band replacements and for S- and

X-band test chain spares is well underway. Booster and distribution amplifiers have been added to the transmitter monitor so that up to three additional coherent outputs of −10 dbm are now available for ranging and experimental use at the Venus site. The basic three-stage amplifier developed for this requirement has been standardized for use in all VHF amplifier procurements.

a. Procurement. Module development has been completed and procurement initiated to meet the following requirements:

(1) *X-band lunar radar project.* Two complete test chain spares, excluding keyers and phase modulators.

(2) *S-band vacuum tube replacement.* Four complete chains, one each for receiver and exciter replacements, and two for test chain spares.

(3) *Mariner vacuum tube VHF amplifier replacement.* Two VHF amplifiers for the receiver.

b. Booster and distribution amplifiers. In order to extend the usefulness of the S-band coherent monitor, booster and distribution amplifiers have been added. A schematic diagram of the distribution amplifier is shown in Fig. 34, and photographs of each side of the unit with cover plates removed are shown in Fig. 35. The basic three-stage amplifier used in both units has resistively loaded band-pass coupling elements which provide an

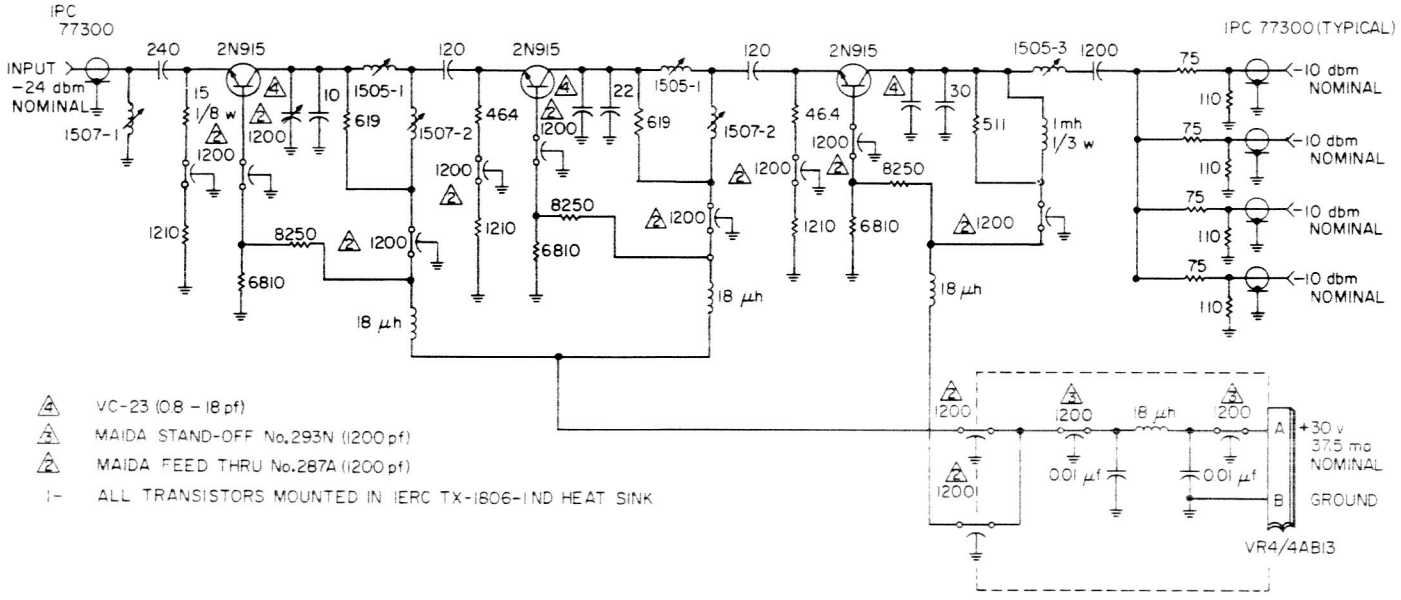

Fig. 34. Schematic diagram of 30-Mc distribution amplifier

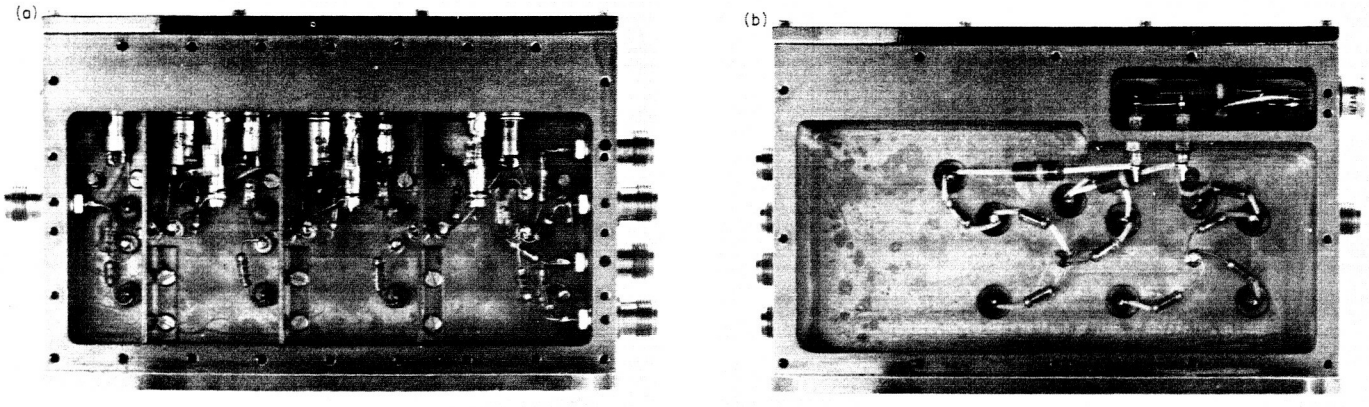

Fig. 35. 30-Mc distribution amplifier (both sides)

over-all bandwidth of 37% at the 1-db points and 46% at the 3-db points. The isolation between each of the four −10-dbm outputs provided by the distribution amplifier is 25.5 db.

c. Digital phase modulator. Two digital phase modulators have been adjusted for S-band use and installed in the Venus receiver and exciter chains at Goldstone for evaluation. In an effort to simulate "worst" operating conditions, "limit" clock generating cards, especially made for the purpose by the Digital Projects Group, were substituted for the normally operating card. Under these conditions the carrier suppression was degraded to as low as 37 db, but the carrier could, in any case, be suppressed to better than 50 db by readjustment of the phase modulator. However, it is considered unlikely that such limit cards need ever be used in the equipment and even more unlikely that any one nominal card would exhibit such degradation of symmetry. Stability tests over 12-hr periods have been conducted. At a carrier suppression of typically −53 db, the maximum variation has not exceeded 1 db. Sideband symmetry is good and the amplitudes of the first two even sidebands are typically −27 db and >40 db.

4. S-Band Cone Signal Generator

During the recent conversion of the R&D S-band cone, the cone signal generator (previously described in *SPS 37-18*) developed a malfunction and was returned to JPL for repair and recalibration. This consisted of initial generator testing, individual module testing, and/or redesign. Included at this time was a series of tests to determine amplitude stability and resetability of the calibrated attenuator.

Table 7. Test results of ×5 multiplier and VHF amplifier

I.	Power: 30 vdc
II.	Gain
	Input: +13 dbm
	Output: +26 dbm
	Total gain: 13 db
III.	Bandwidth
	Input (3-db points): 3.8 Mc
	Output (3-db points): 19 Mc
IV.	Input level versus output change
	Input change: from +13 dbm to 0 dbm
	Output change: from +26 dbm to +25 dbm
V.	Harmonic suppression
	At 159.2 Mc: 0 db
	At 127.36 Mc: −36 db
	At 95.52 Mc: −61 db
	At 63.68 Mc: −70 db
	At 31.84 Mc: −61 db
	All others: >−70 db

a. Initial generator and module testing. The signal generator (Fig. 36) was connected to a spectrum analyzer (Panoramic Model I-4A), which displayed a randomly modulated carrier. This modulation was traced to the ×5 multiplier phase modulator module. The module was put through a rugged mechanical and electrical test which pointed to two interrelated reasons for the failure of the unit. The unit was constructed on a glass epoxy board with gold flash on each side, and the threaded ground lugs did not hold in the glass board, thus providing intermittent ground paths. The common base transistor amplifier used in the electrical design was of an unstable nature. This module was redesigned both electrically and mechanically (Fig. 37). The internal phase modulator was removed with provision for use of an external modulator when required. Test results of the new ×5 multiplier and VHF amplifier are shown in Table 7.

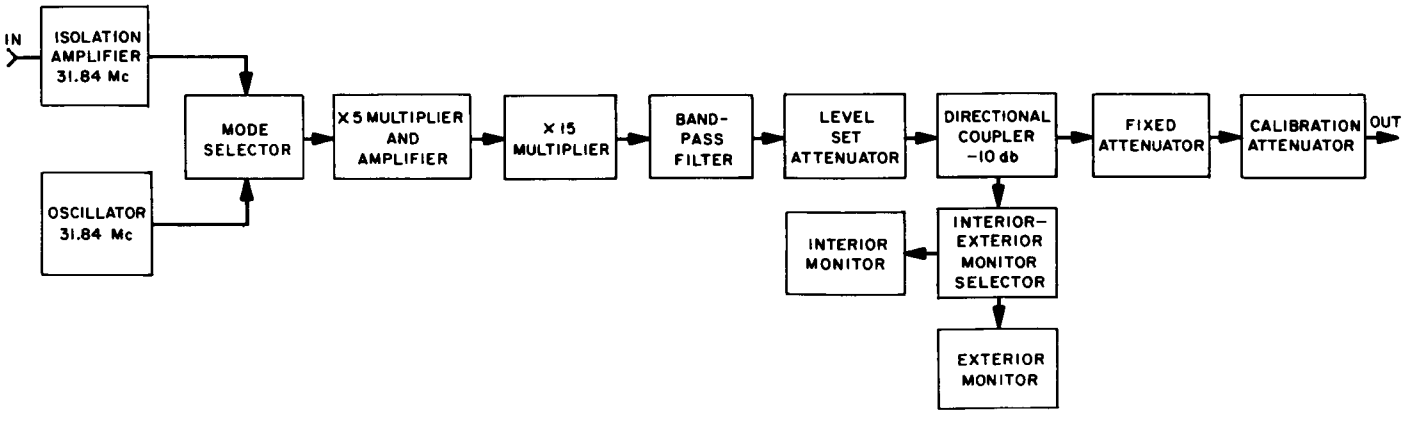

Fig. 36. Block diagram of S-band signal generator

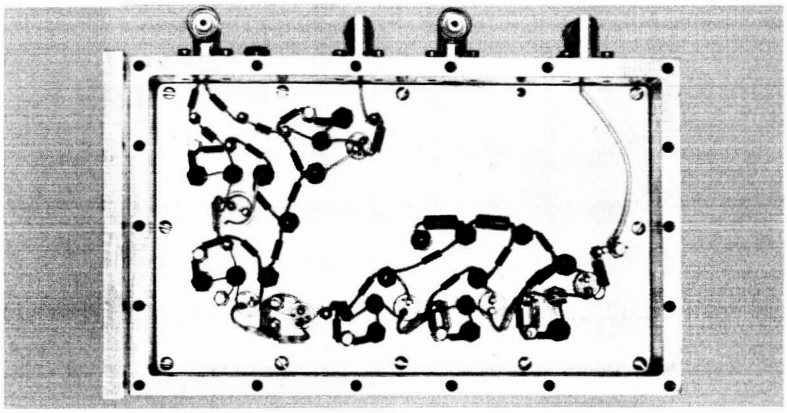

Fig. 37. View of × 5 multiplier and VHF amplifier

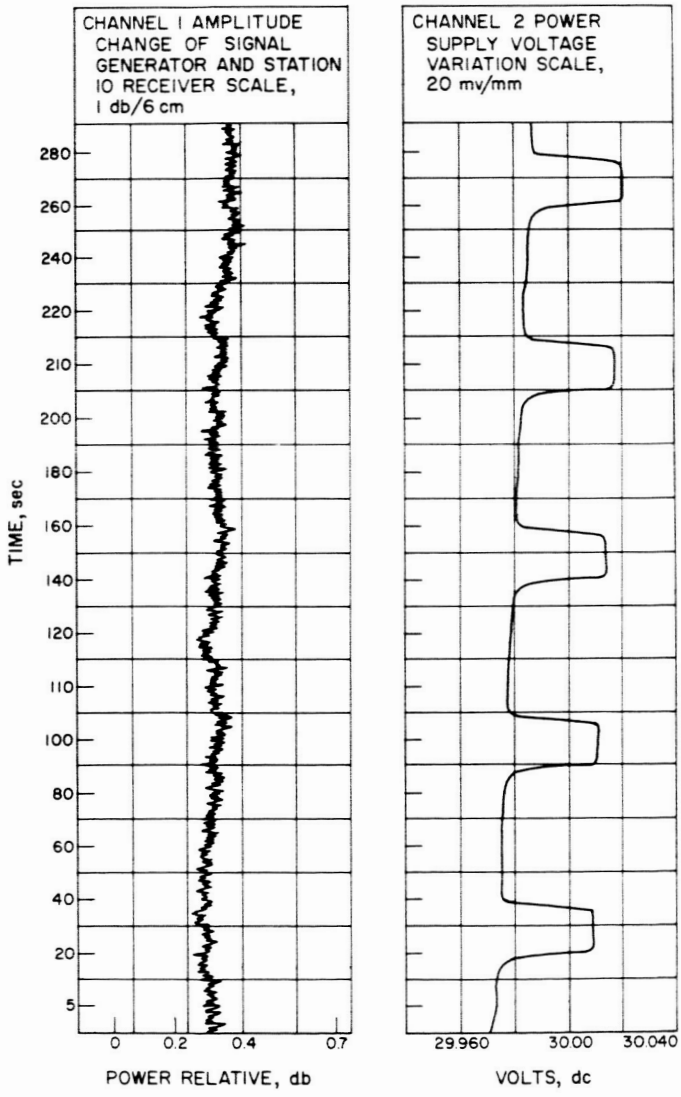

Fig. 38. Generator amplifier stability versus dc power supply change

After installing the new multiplier/amplifier in the generator, a preliminary amplitude stability test was made while monitoring the dc power supply voltage of the signal generator. Results are shown in Fig. 38. The dc voltage variations were attributable to the oscillator oven cycling. This module was disassembled, and it was discovered that the oven oscillations were due to the thermistor not being firmly fastened to the oven wall, thus creating a thermal delay in the oven feedback loop. This condition was corrected by fastening the thermistor to the oven wall using an epoxy cement.

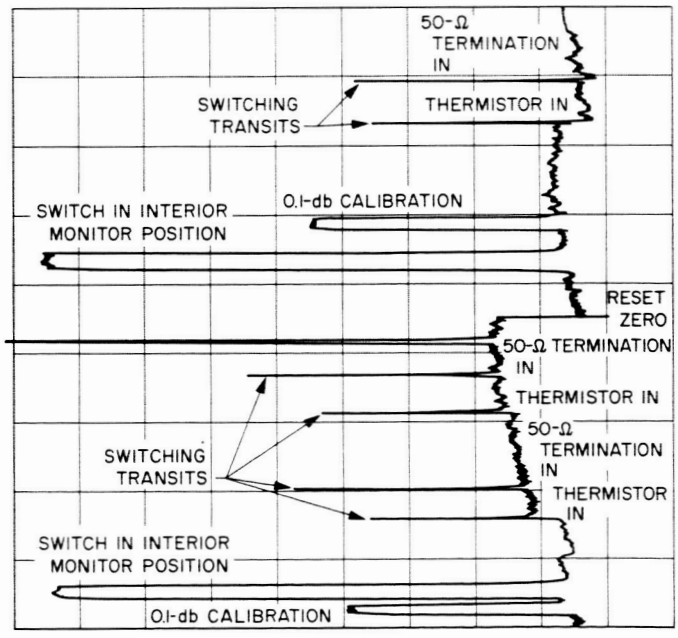

Fig. 39. Test results of internal–external monitor, also 50-ohm termination versus thermistor

b. Signal generator stability and resetability tests. A test was made to determine the effect of the internal monitor switch position on generator output power calibration. The results shown in Fig. 39 indicate definite resulting errors in output calibration. Because of space limitations in the RF compartment, no attempt will be made to improve this situation. All receiver measurements will be made with the internal–external monitor switch in the *external* position.

A test was conducted to determine the effect of substituting the thermistor mount for the external monitor termination on the output power of the generator. The results of this test are also shown in Fig. 39 and indicate the errors introduced by this method to be negligible. An attenuator resetability test was made at this time using Bendix and JPL personnel. With the signal generator attenuator adjusted to −80 dbm, the operator moved the attenuator to −90 dbm and then reset the attenuator to −80 dbm. Results are shown in Fig. 40. They confirm that the attenuator can be reset to better than 0.01 db.

A short stability run was made at Goldstone using the Mod IV receiver and the maser instrumentation. The results given in Fig. 41 show a stability better than 0.01 db for 1 hr.

The signal generator testing is complete at this time, except to determine effect of cleaning up of the 60-cycle line supplying the generator by use of a transformer. This test will be completed in the near future.

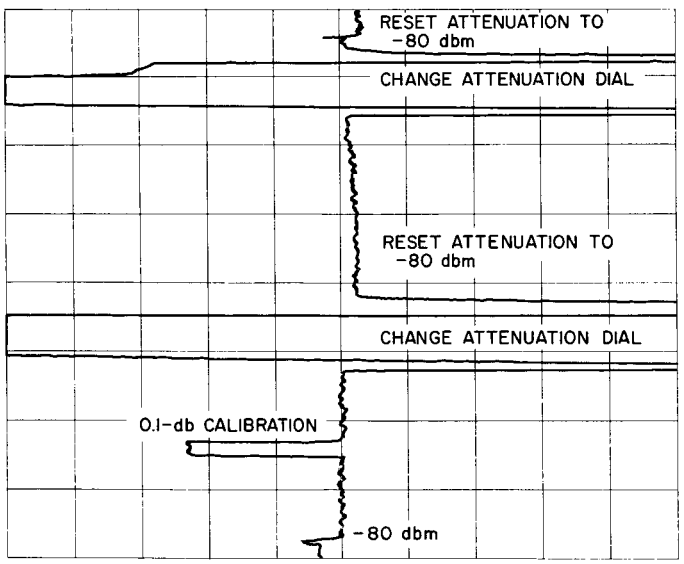

Fig. 40. Test results of calibrated attenuator resetability

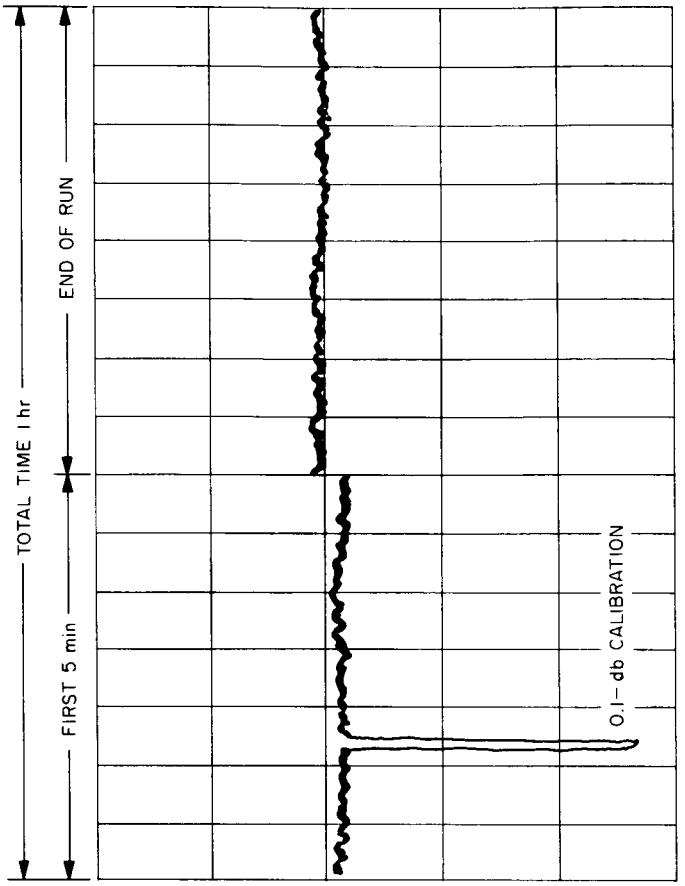

Fig. 41. Test results of amplitude stability run on S-band signal generator

F. S-Band Transponder Ranging Station

Initial planning for the conversion of the L-band system, known as the 890/960 Mc transmit–receive system, to S-band for use in further ranging experiments was reported in *SPS 37-20*, Vol. III, p. 50. However, before the task was fully underway, the scope of the effort was redefined to include the following:

(1) Permanent integration of the sideband discriminator subsystem (*SPS 37-22*, Vol. III, p. 38) already used for RF acquisition tests under computer control (*SPS 37-24*, Vol. III, p. 69).

(2) Modification for complete computer control of all operating functions.

(3) Adaptation for coded telemetry experiments.

(4) Reduction of *integral* test instrumentation.

(5) Incorporation of new module and circuit improvements in the general areas of IF amplifier dynamic range and operational amplifiers used for isolation of instrumentation.

1. Computer Control

The desired control philosophy includes not only computer control of all switching functions and analog inputs (via digital-to-analog converters) but also elimination, or at least complete bypassing, of all local, operator accessible, controls. As an interim solution, it was decided to equip all modules for full remote control and sensing, but to retain the existing control panels for subsystem operating capability. However, the original functional intent has been fully achieved by means of complete redesign and replacement of the cabling and junction box system to include choice of local (operator panel) or remote (computer) control.

Fig. 42 depicts in a simplified manner the control and sensing arrangement used for both analog and switching functions. The local/remote relay contacts are duplicated for each controlled function and are gang switched in such a way that inadvertent repositioning can be avoided. The purpose of "computer sense of operator input" is two-fold: In the case of a complex computer program, a preset or operator aided parameter can be sampled for further processing or, simply, selective operator control may be retained in this manner. Additional acccess for recording purposes is obtained by connection to "computer sense."

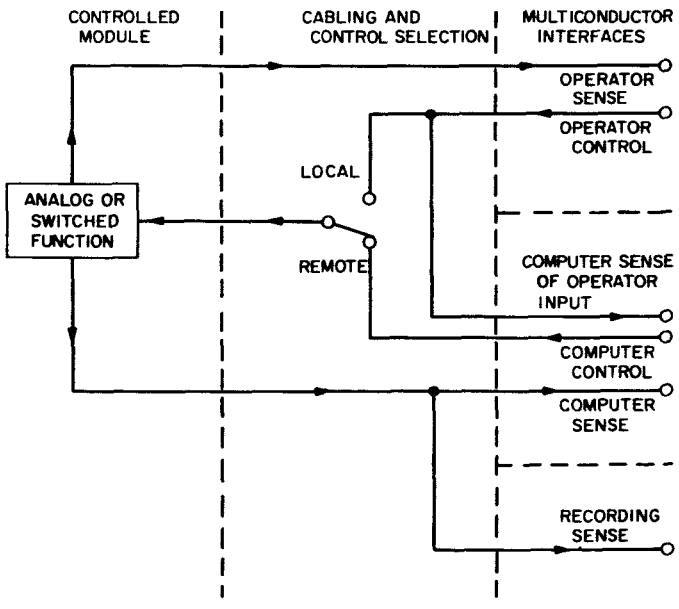

Fig. 42. Remote control and sensing

In addition to the sensing associated with each control, all available internal functions are similarly brought out for operator, computer, and recording sensing. Typical examples include loop phase errors and lock indicators. All of the above-mentioned connections are made by means of multiple conductor cables. A number of critical "signal" connections (such as ranging code inputs, doppler output, etc.) are retained on coaxial cables.

2. Coded Telemetry

Aside from the precision ranging and RF acquisition experiments, this system has been adapted for use in connection with telemetry experiments scheduled for mid-year 1965. A complete channel has been added for detection of wide-band PM modulation. The associated telemetry system requires a coherent RF reference signal at both the point of transmission (transponder) and at the receiver. Suitable outputs have been selected, and frequency dividers are being developed to provide references at a nominal frequency of approximately 2.4 Mc.

In order to obtain this coherent signal from the receiver, the frequency synthesizer must be somewhat revised. As originally conceived (*SPS 37-20*, Vol. III, Fig. 35), a fraction ($\frac{1}{96}$) of the drift of the 30-Mc reference oscillator is present in the receiver (VCO) output, but is compensated for in the doppler detection system through the *subtraction* of 312.5 kc (30 Mc $\times$ $\frac{1}{96}$) from the doppler reference. The intended solution is to *add* the 312.5 kc to the VCO output prior to doppler detection instead. This will provide a coherent RF receiver output signal (without 30-Mc drift) for telemetry purposes while retaining equivalent VHF doppler capability for ranging purposes.

3. Status

With the exception of the telemetry reference frequency dividers mentioned, essentially all the procurement, modification, and rebuilding have been accomplished. Specifically, the computer control cabling and interfaces are complete and have been checked on an individual basis. Loop parameters such as noise bandwidth, phase detector constants, and loop filter time constants are yet to be verified or adjusted. Preliminary testing is underway on

the multiplier chains and first mixer. It is expected that complete check of the system will be compatible with both the June telemetry experiment schedule and with occupation of the new Telecommunications Building early this year. A potential scheduling conflict exists, however, in that the recently defined Venus site *Mariner* receive capability has pre-empted the local oscillator multipliers and front end converter hardware from the ranging station. Replacement hardware has been procured, however, and will be integrated as schedules permit.

G. Venus Site Operations: Experimental Activities

During the past 2 mo, the planetary radar on the 85-ft antenna was used to perform spectrum analysis experiments on Mars, Jupiter, and Venus at S-band (2388 Mc). Additionally, extensive modification of the *Mariner 1964* Cassegrain cone was performed to provide a receive capability in addition to the previously provided transmit capability. Certain changes were made in the S-band R&D Cassegrain cone to provide increased water flow through the radio frequency water load.

After preliminary measurement and testing on the antenna during the *Mariner* spacecraft pass of February 13, 1965, one-way lock was acquired on the spacecraft-to-ground link at 00:45 hr GMT on February 14, 1965 from the Venus site. Inasmuch as the final receiving system is not available at this time, the "suitcase receiver" was installed in the *Mariner 1964* cone and performed excellently. Telemetry data received was transmitted to SFOF via a microwave link through the Pioneer site; it was tested by SFOF and found to be essentially identical in quality to that provided by the other DSIF Stations utilizing a standard receiving system. After verifying the capability of the Venus site to support the *Mariner* mission during the *Ranger VIII* and *IX* missions, the *Mariner* cone was removed and the S-band R&D cone was reinstalled for further planetary radar work.

A summary of the activities at the Venus site during this period is tabulated in Table 8.

Table 8. Summary of Venus site experimental activity (December 20, 1964 through February 15, 1965)

Activity	Hours
Primary experiments	
Planetary radar	
(1) Jupiter	122
(2) Mars	90
(3) Venus	23
Secondary experiments	None
Testing, calibration, construction, and maintenance (scheduled)	944
Downtime, (equipment failure; includes unscheduled maintenance)	89
Holidays	100
Total hours	1368

1. Preliminary Experiment Results

The 23-Gc radiometer experiment, using the 30-ft antenna with Jupiter as a target, was concluded on January 31, 1965. On conclusion of the experiment, calibration measurements were taken of antenna patterns and on noise sources. The data from this experiment was reduced daily, using the SDS-910 computer at the Venus site which is also used to point the antenna. An analysis of this data is presently in progress, and no results are available at this time.

A radar experiment is now in progress with Mars as the prime target. A continuous wave signal of 100 kw at 2388 Mc is being transmitted for one round-trip time. During a transmit cycle, noise from the receiver is being correlated to obtain an estimate of the noise spectrum. The receiver is then turned on for one round-trip time, and the signal return plus noise is correlated to obtain an estimate of the signal plus noise spectrum. These spectra are then subtracted to obtain the signal spectrum. As in the previous Jupiter radar experiment, the results are divided according to the longitude of the target planet. Preliminary analysis of the composite spectra shows that a reflected signal is being received from Mars.

2. Subsystem Performance

a. 100-kw transmitter (operation). The transmitter for this reporting period has been operating at 100 kw about 12 hr/day with the exception of the shutdown time for the *Mariner 1964* Cassegrain cone testing. During this time the transmitter has caused a total of 59 hr and 33 min of lost tracking time, due to system shutdowns caused by reflected power amplifier transients, klystron

tube "out-gassing," series limiter filament potentiometer failure, waveguide pressure leaks, water line break, breakdown of high-voltage cable and connectors, and circuit breaker and waveguide switch failures.

b. System improvements and modifications. The time used on the antenna for the testing of the *Mariner* cone was used to modify the water load input fittings and to replumb the S-band R&D cone so more water flow could be obtained through the water load and the transmitter. The water connections for both cones were made alike at this time.

New instantaneous trip relays and current transformers have been obtained for replacement of a thermal breaker relay on the 100-hp starting motor. This relay has caused difficulty in getting the main motor generator on the incoming line and will be replaced at the earliest shutdown time. Work is being done on the main motor voltage regulator to maintain better stability of the generator voltage and the power factor.

Dual water pressure regulators have been installed in both cones to prevent the breaking of the water load glass during water surges of the system. The water loads are being modified with new O-rings to prevent the seepage of water into the waveguide portion of the loads.

The *Mariner* cone was modified by the installation of a maser, receiver front end, "suitcase receiver," and additional waveguide switches to provide a receive capability.

c. Testing. The *Mariner* 100-kw transmitters have been tested, both on the antenna and in the cone storage area, with a total of 91.7 filament hours and 25.6 beam hours on Amplifier 1, and 87.4 filament hours and 27.4 beam hours on Amplifier 2.

d. Digital subsystems. The only new digital equipment installed at the Venus site during this reporting period was a high-speed Franklin line printer for the Mod III stored program controller. This device has the capability of printing 12 columns of decimal information at the rate of 20 lines per second.

Three new programs have been written and put into regular operation on the SDS-910 computer. These programs are used in the generation of angle, range, and doppler drive tapes. The range and doppler drive tapes are generated by expanding polynomials in time with coefficients supplied from the computer group at Pasadena. Both of these tapes are verified as they are punched by having a small loop of paper tape running from the punch to the reader. After the initial delay has been punched, one sample is punched and then one sample is read. Every hour on the hour the value of the range or doppler is computed and printed out on the console typewriter so that the operator may check this against the printed ephemeris. A running second difference is also computed, and the maximum value is printed out on the console typewriter at the conclusion of the program. The polynomials are supplied from Pasadena on punched cards. They are changed from punched cards to punched paper tape through the IBM-1622 card reader and SDS-920 computer located at the Echo site.

The angle drive tape is produced from data obtained from "The American Ephemeris and Nautical Almanac." The data required is inputted through the console typewriter and consists of:

(1) Sidereal time hour angle (HA) of first point of Aries for 3 successive days.

(2) Apparent right ascension of the source for 3 successive days.

(3) Apparent declination of the source for 3 successive days.

The 3 days are necessary to allow the view period to run over 2400 hr. A three-point fit is made to the right ascension and declination data. After punching, the tape is verified and listed on the SDS-920 computer and line printer at the Echo site.

e. S-band receiver. The S-band receiver operated normally during this period with no lost time due to equipment failures. A new digital phase modulator has been installed in the receiver and is being evaluated by the JPL Project Engineer.

The Resdel signal generator was reinstalled in the R&D cone. Measurement of the system phase jitter disclosed excessive phase or frequency variations in the signal generator. An on-site repair of the generator will be attempted.

Work has been completed to allow receiver operation in the cone storage area. A special test fixture with appropriate control and monitor functions has been constructed and checked out with both the R&D cone and the *Mariner 1964* cone.

All the required cabling for the *Mariner* receiver cone-mounted equipment has been completed. Also, all the cone-mounted equipment, except for the S-band-to-30-Mc converter, has been installed.

f. S- and X-band central frequency synthesizer (CFS). By substituting various rubidium frequency standards for the one normally used in the CFS, a comparison was made of the relative phase jitter contribution due to noise from each unit. It was found that the one normally used in the CFS (LA 33660) was, at some frequencies, the poorest of three checked and twice as bad as the best one checked. A new frequency standard (LA 37985) was installed, but it failed after only 48 hr of operation. (This unit was repaired at Goldstone and is now operating normally.) Table 9 tabulates the relative dynamic phase errors found on the various output frequencies for the three units measured. These measurements were taken by connecting a Sanborn Model 320 two-channel recorder to the dynamic phase error monitoring point on the CFS.

Table 9. Peak-to-peak dynamic phase error for rubidium standards

Reference loop frequency, Mc	Normal R&D standard (LA 33660), mv	New R&D standard (LA 37985), mv	Mariner standard (LA 55139), mv
30.455	100	50	50
31.440	60	22	26
31.840	55	30	24

At present, there are two operating rubidium frequency standards at the Venus site. There is also one on loan from JPL, Pasadena, in a standby status.

g. Programed local oscillator (PLO). No failures occurred, and no modifications were made to the radio frequency portion of the PLO during this period.

Several intermittent troubles were encountered in the digital part, but each time the trouble would correct itself before the cause could be located. Troubleshooting will continue as time and the site operating schedule permit.

A change in the paper tape format has been made to facilitate the production of doppler drive tapes on site. This change removed character number 17 from each block of information. Character number 17 is only a space between blocks and does not contain any information. This change does place a slightly more rigid requirement on the operation of the tape reader, but, thus far, the operation has been satisfactory.

h. Maser. With the exception of a vacuum leak in the refrigerator vacuum jacket, the maser has performed satisfactorily during the past 2 mo, maintaining a nominal gain of 45.5 db. The leak occurred around the cable fitting bringing out the readouts, which monitor the temperatures of the various heat stages in the cryogenic refrigerator. Retightening of the mounting nuts and application of vacuum grease restored the vacuum integrity of the jacket; after suitable vacuum pumping, the maser cooled down normally. Note that this loss of vacuum occurred also on December 8, 1964; at that time it was thought improper O-ring seating was at fault.

Just prior to the conclusion of the planetary radar experiment with Jupiter, the liquid nitrogen-cooled termination was delivered and installed in the R&D Cassegrain cone (*SPS 37-31*, Vol. IV, pp. 283–284). After cool-down and stabilization, the system temperature was measured and recorded on an hourly basis with the maser input terminated with the liquid nitrogen-cooled termination. Using the relationship $T_{system} = T_{nitrogen} + T_{receiver}$, a calculated $T_{receiver}$ of 9.17°K was subtracted from the measured system temperature to obtain the equivalent noise temperature, at the maser input, of the

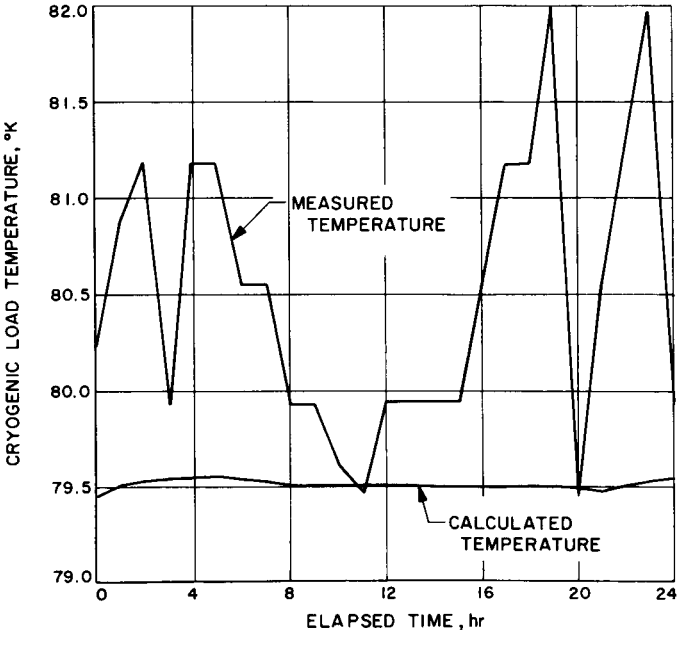

Fig. 43. Equivalent noise temperature of Venus site S-band waveguide nitrogen-cooled load

liquid nitrogen-cooled termination. This temperature is plotted as the curve labeled "measured temperature" in Fig. 43.

Using the relationship $T_{N(°K)} = 71.89 + 0.00894\,T_{0(°K)}$ (*SPS 37-31*, Vol. IV, pp. 283–284), the equivalent noise temperature of the liquid nitrogen-cooled termination was translated to the input of the 26-db waveguide coupler on the maser input and corrected for waveguide temperature. This temperature is plotted as the curve labeled "calculated temperature" in Fig. 43. Inasmuch as, with two exceptions, the measured curve always lies above the calculated curve, it appears that the value of 9.17°K used for $T_{receiver}$ may be in error. However, the agreement between measured and calculated values is fairly good, within the sum of the probable errors of the calculated excess noise temperature of the gas tube and the calculated $T_{receiver}$. Additional calibrations will be performed in an effort to resolve this discrepancy in nominal values.

References

1. Bartee, T. C., et al., *Theory and Design of Digital Machines*, McGraw-Hill, 1962.
2. Caldwell, S. H., *Switching Circuits and Logical Design*, Wiley & Sons, 1960.
3. Gill, A., *Introduction to the Theory of Finite State Machines*, McGraw-Hill, 1962.
4. Humphrey, Jr., and Watts, S., *Switching Circuits with Computer Applications*, McGraw-Hill, 1958.
5. Hurley, R. B., *Transistor Logic Circuits*, Wiley & Sons, 1961.
6. Ledley, R. S., *Digital Computer and Control Engineering*, McGraw-Hill, 1960.
7. Bartee, T. E., and McCluskey, E. J., *A Survey of Switching Circuits*, McGraw-Hill, 1964.
8. Maley, G. A., and Earle, J. J., *The Logic Design of Transistor Digital Computer*, Prentice-Hall Inc. (EE Series), 1963.
9. Marcus, M. P., *Switching Circuits for Engineers*, Prentice-Hall Inc., 1962.
10. Phister, M., *Logical Design of Digital Computers*, Wiley & Sons, 1958.
11. Tornq, H. C., *Introduction to the Logical Design of Switching Systems*, Addison-Wesley, 1964.
12. Warfield, J. L., "Principles of Logic Design," Ginn & Co., 1963.
13. Huffman, D. A., "The Synthesis of Sequential Circuits," E.E. Ph.D. Thesis, MIT, June 1953.
14. Mealy, G. H., "A Method for Synthesizing Sequential Circuits," *Bell System Technical Journal*, Vol. 34, pp. 1045–1079, 1955.
15. Eisenberger, I., and Posner, E. C., "Systematic Statistics Used for Data Compression in Space Telemetry," Technical Report No. 32-510, Jet Propulsion Laboratory, Pasadena, California, October 1, 1963.

V. Advanced Antenna System

A. Synopsis

A 210-ft-diameter Advanced Antenna System (AAS) is being designed and constructed for the Mars Site of the Goldstone Space Communications Station. The operating frequency of the AAS will be at the S-band frequencies of 2.1 to 2.3 Gc.

The AAS is designed specifically for deep space communications and will be integrated with related systems and equipment of the Deep Space Instrumentation Facility (DSIF). Completion of the AAS as an operational receiving station is scheduled for June, 1966.

Work progress has been reported regularly in this *SPS*, along with a series of discussions concerning components of the system. The project continues generally on schedule, and it is anticipated that end dates for erection and project completion will be met. All structural and drive components of the AAS are either being fabricated or are under erection at the Mars Site. Fabrication and on-site erection is being accomplished by Rohr Corporation, Chula Vista, California.

The pedestal, alidade and alidade building structures have been completed, and work on the interior equipment and personnel areas is nearing completion. A discussion of these interior areas has been included in this *SPS*. The instrument tower and windshield have been erected on the AAS. Fig. 1 depicts the wind and thermal shield being lifted and lowered over the insulated steel instrument tower.

The azimuth motion components, consisting of the azimuth radial bearing, the azimuth hydrostatic thrust bearing and azimuth drives, have been installed and are now operational.

On-site erection of the elevation motion components has begun. The elevation bearing assemblies have been installed atop the massive alidade structure (Fig. 2), and the tie truss extending between the two bearing assemblies is being erected. The tie truss assembly will support the elevation wheel and primary reflector structure center hub and will be structurally integrated with the primary reflector structure. Fig. 3 is a photograph of the center section of the tie truss being delivered to the Mars Site.

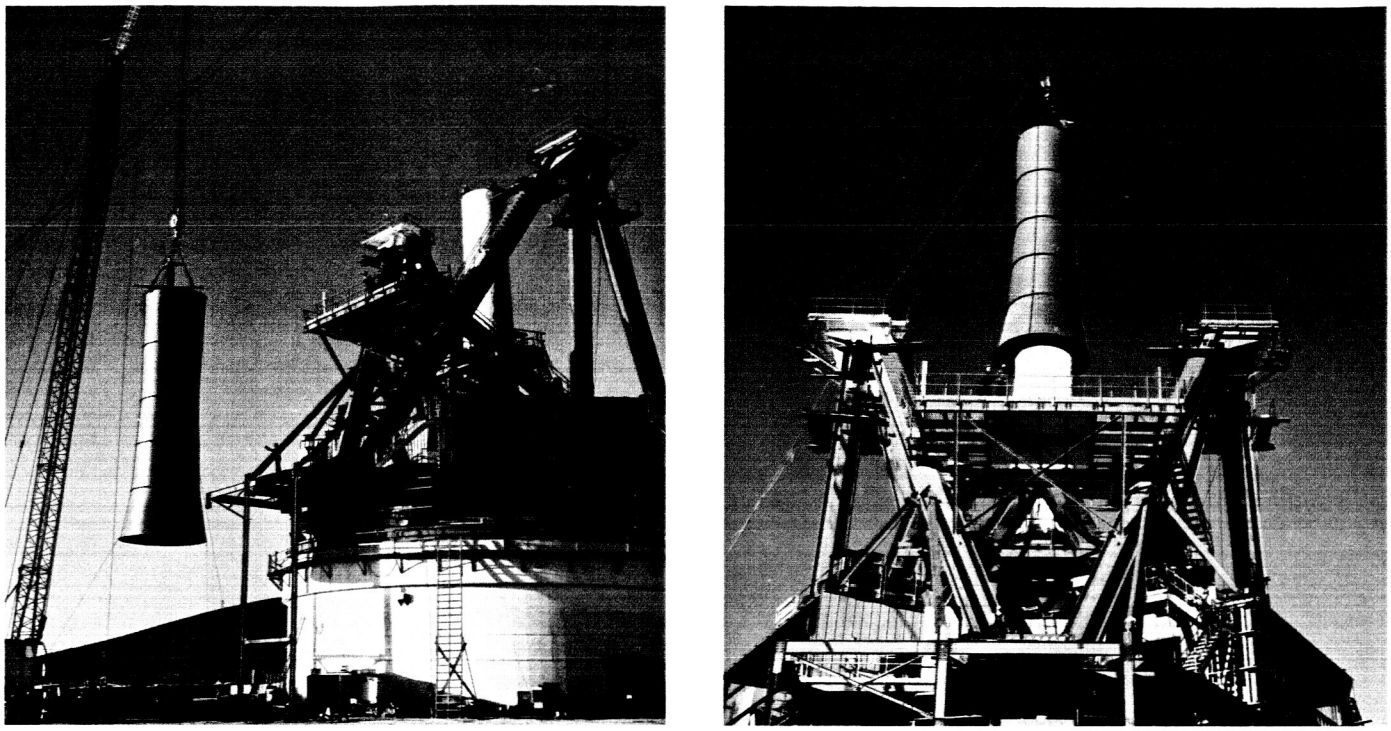

Fig. 1. AAS instrument tower erection

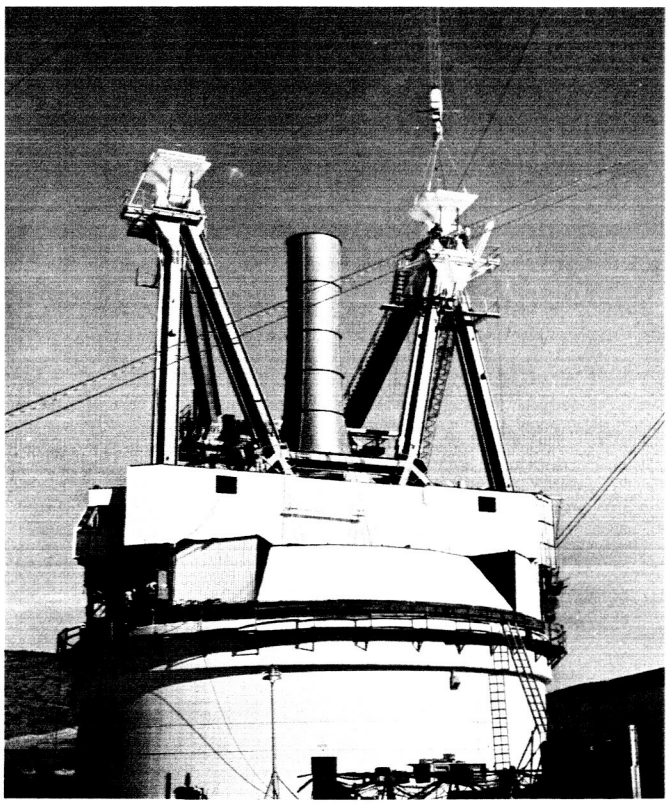

Fig. 2. Erection of the AAS elevation bearing assemblies

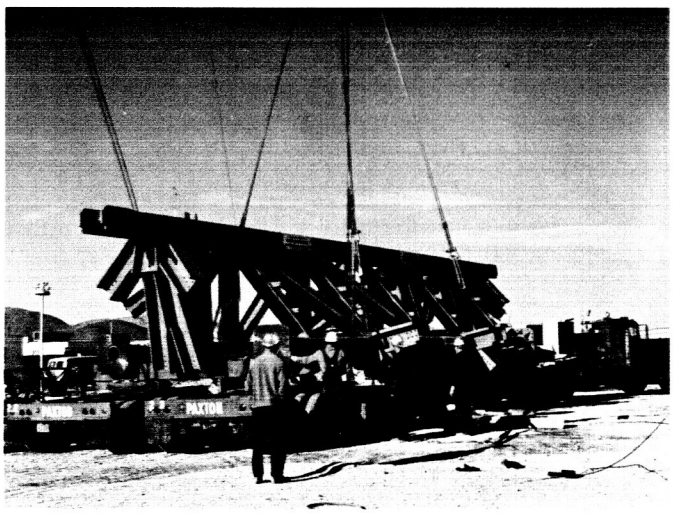

Fig. 3. Tie truss center section

Fabrication of the parts for the elevation wheel assembly and the large 210-ft diameter paraboloidal structure is well underway. As in-plant fabrication is completed, the parts are being shipped to the Mars Site for erection on the AAS. The elevation drives and gears have been transported to the Mars Site and are being prepared for installation. A discussion of this component is included in this *SPS*.

Fabrication of the primary reflector surface panels, subreflector, quadripod support structure and feed cone continues at Rohr Corporation.

The hydraulic components of the servo system are being installed on the AAS. The electronic components of the servo system are being fabricated at Dalmo Victor Company, Belmont, California.

Developmental work and procurement actions are in progress for the site communications, ancillary equipment for test and measurement, the precision angle data system, and standard DSIF electronic equipment necessary to outfit the AAS structure for space communications operations.

B. Interior Areas of the AAS Structure

The AAS equipment and personnel will be housed in the two floors within the pedestal structure and in the alidade building. There are two additional service areas currently under design or fabrication. These are (1) the feed cone, which is a four-level structure housing the receiver and reflector monitoring equipment, and (2) the precision angle data system astrodome, which is to be located atop the AAS instrument tower. The feed cone and astrodome will be discussed in subsequent *Space Program Summaries*.

1. Pedestal Building

The primary purpose of the base pedestal is to serve as an exceedingly stable and rigid support for the rotating elements and to transfer all vertical, horizontal and rotating loads from the antenna through the pedestal and foundation to the soil. The secondary function of the base pedestal is to house service and operating areas. It is this secondary function that is discussed below.

The base pedestal building is separated into two annular-shaped floors of approximately 4400 ft² each. The outer wall is formed by the 42-in. thick reinforced concrete wall of the base pedestal. The inner wall is of stud and plaster construction and is the separation between the main use areas and the loft for the cable wrapup.

a. Second floor of pedestal building. The second floor of the pedestal is used to house the large control and computer room, and also the restrooms, walkways, stairwell, and service hatch. This floor (Fig. 4) is supported entirely from the pedestal structure since foundation loads could not be tolerated adjacent to the instrument tower. The floor is formed by radially oriented steel beams supporting a reinforced concrete deck. The steel beams are supported by corbels on the outer periphery and by steel hangers from the pedestal concrete top deck on the inner periphery. Because of differential shrinkage and possible dimensional changes due to temperature, the second floor concrete is isolated from the pedestal wall by means of expansion joint material. In addition, the radial steel beams rest on low-friction supports.

An access hatch and a 3-ton overhead chain hoist with crane rail into the control room is provided to service the heavy electronic equipment. If required, dependent on future needs, this hoist can be replaced by an elevator.

Where flexible floor coverings are required, vinyl asbestos tile, or sheet vinyl has been selected for durability, fire resistance and easy maintenance. Where special finishes are not required, concrete floor surfaces are treated with a non-dusting hardener.

In the control room, a modular aluminum-panel removable false floor, with vinyl wearing surface, has been provided. This provides a 4-ft high clear area beneath the

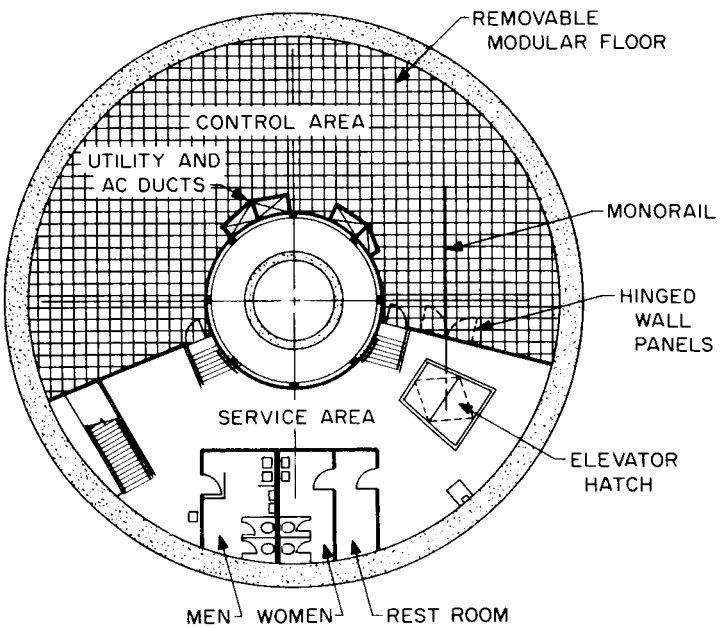

Fig. 4. AAS pedestal second floor plan

false floor, thereby facilitating installation of and access to cabling for the various electronic and computer equipment. This subfloor area also acts as a plenum chamber for the chilled air which is used to cool the electronic racks.

Where practicable, finish ceilings have been eliminated. Where ceilings are required, gypsum board or acoustic tile of mineral fibers is used, providing both fire resistance and flexibility. In the control room, acoustic tile is carried from the ceiling down the wall to four feet above the floor in order to reduce the noise level.

b. Ground floor of pedestal building. This floor (Fig. 5) is divided into three basic areas: an equipment room, a mission-oriented room, and an area to be used for office and laboratory space.

The equipment room on the ground floor occupies approximately 1600 ft². This room contains the water chillers for the pedestal and alidade, the air handling equipment for the base pedestal, and the electrical transformers and switchgear for both the pedestal utility and electronic power circuits.

Adjacent to the equipment room is the mission-oriented room containing approximately 800 ft². It is well lighted and air conditioned but is not acoustically treated. This room is to house special equipment for specific missions. It is adjacent to the truck access door and has cable access openings leading through the ceiling to beneath the control room subfloor. This enables easy tie-in to control consoles and to junction modules—the junction modules being the lower terminal point of the cable windup system which permits power and signal cables to cross from the stationary to the rotating portion of the antenna.

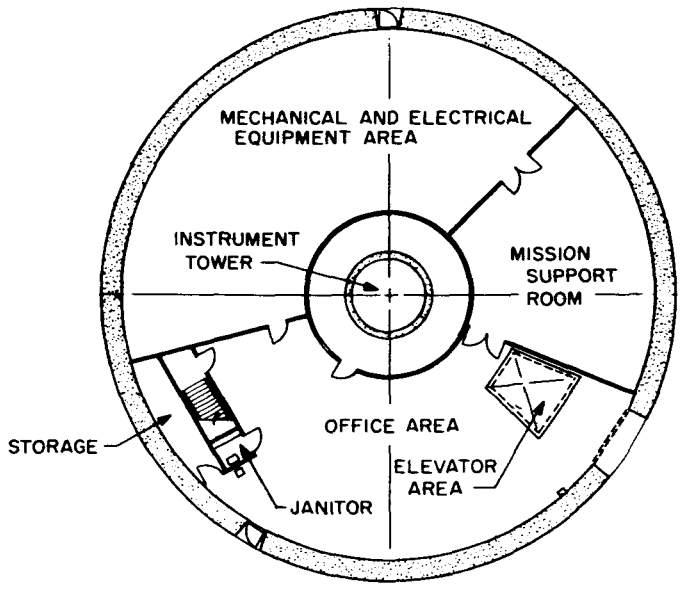

Fig. 5. AAS pedestal first floor plan

The remainder of the first floor area—approximately 1600 ft²—is utilized in service area, truck and man access doors, janitor's closet beneath the stairwell, the stairwell itself and area to be utilized for office and laboratory use as required.

The entire pedestal building is heated and ventilated. With the exception of the equipment room and the cable loft, the building is fully air conditioned. The equipment room is air cooled only. Humidity control is provided in the control and computer room. Incandescent lighting is used throughout.

2. Alidade Building

The alidade is defined as that portion of the antenna which rotates in azimuth and which supports the tipping parts. The alidade is constructed of exceedingly heavy steel members in the configuration of a space frame pentahedron. This steel framework also supports the azimuth and elevation drives, the instrument tower wind and thermal shield, and the alidade building.

The alidade building (Fig. 6) is supported on the triangular base of the alidade. The building, a trapezoid in plan, is approximately 70 × 50 ft with a clear height of 10 ft. The floor system is made of structural steel members supported or cantilevered from the alidade base. The structural steel roofing is supported in part by the upper alidade members, and in part by independent steel columns from the alidade base triangle. The stationary instrument tower projects through and is isolated from the alidade building floor and roof. The 53-ft high wind and thermal shield which encloses the instrument tower above the alidade building roof line is cantilevered from the alidade roof structure.

The design of the alidade building was dictated by the plan configuration and base support available for the structure. Since the structure is larger than the triangular base support, the building floor structure is cantilevered on two sides. Where the cantilever length becomes excessive, hangers are used which frame back to the heavy alidade legs. Hangers are also used to stiffen the support

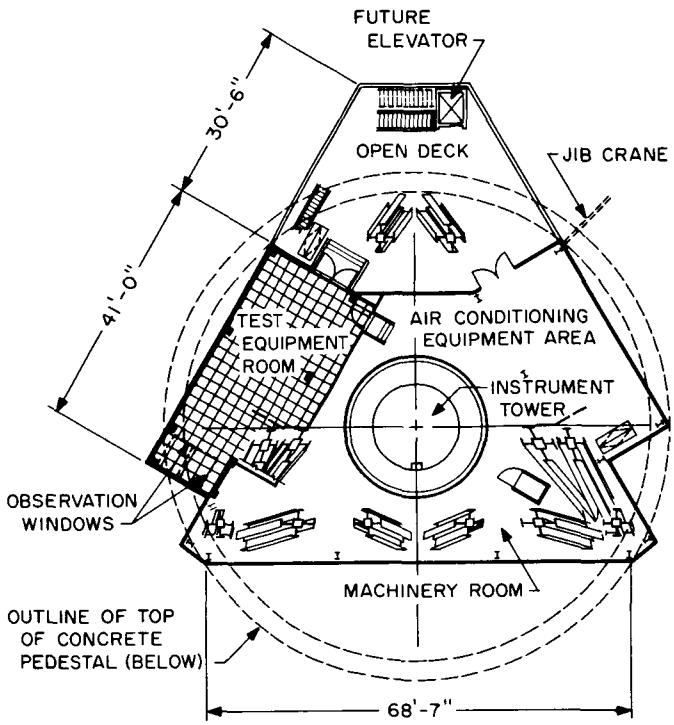

Fig. 6. AAS alidade building plan

of the stair and future elevator well which lead to the ground. Wind loads of the windshield require heavy beams in the roof system to limit deflections of the windshield. The wind shear delivered to the roof level is transferred by bracing to the floor diaphragm which in turn transfers the loads into the alidade base triangle.

The alidade building exterior walls are field-assembled, metal-insulated sandwich panels, providing noncombustible weathertight construction and thermal insulation. The roof is of the built-up insulated type on steel decking. The floor of the alidade building is a steel plate diaphragm welded to steel floor beams. This floor has a non-skid finish. A sound-deadening partition is provided between the equipment machinery area and the test equipment room. In the test equipment room, a removable modular floor provides power and instrument cable access and plenum chamber for underfloor equipment cooling. Doors in the alidade building are hollow metal with glazed upper panel and insulated lower panel. Acoustic type insulated metal decking is utilized for the ceiling in the equipment and machinery areas to reduce the noise level in these areas. A suspended acoustic ceiling is utilized in the test equipment room. Exposed construction, except that which is prefinished, is painted with enamel or vinyl paint.

The alidade building is used to house all of the hydraulic drive pumps and accumulators, the hydrostatic bearing pumps, the electric, electronic and utility bus substation for the rotating structure, the rotating portion of the cable windup system and the upper terminals of cables and water lines.

In the alidade building, there is approximately 1500 ft^2 of usable area in the equipment and machinery room, and about 750 ft^2 in the test equipment room. In addition, equipment, piping, and cabling is hung beneath the equipment room floor. This area is accessible through hatches. The roof of the alidade building, on the equipment machinery room side, has been used for mounting the electrical substation. The test equipment room has been designed to permit the addition of another room immediately above the present room if future requirements dictate such addition.

The equipment and machinery room is heated, ventilated and air cooled. The test equipment room is air conditioned rather than air cooled, and is provided with humidity control. The entire alidade building is pressurized to minimize dust.

Access ladders, platforms and walkways are provided to all use and maintenance areas. All these items comply with California Safety Code regulations. Platforms are designed so as to support any equipment items that may be normally placed on them for installation or repair. A 5-ton hoist and jib crane has been provided on the alidade building roof adjacent to the rear platform. This hoist will provide service from the ground to the alidade building rear platform.

Present access to the alidade building is provided by a stairway which is cantilevered from the back of the alidade structure and rotates with the antenna. The height of the alidade building above the ground is equivalent to a fifth-floor level. Because of this, the structure has been designed to accommodate future installation of a 6000-lb electric elevator.

C. AAS Elevation Gears and Drives

The AAS elevation gears and drives component has progressed through design and manufacture, and the

component is now at the Mars Site awaiting installation on the antenna. Detail design and fabrication of the component was accomplished by Philadelphia Gear Corporation, King of Prussia, Pennsylvania, under subcontract to Rohr Corporation. The on-site installation will be accomplished by Rohr. The function of the elevation drive system is to convert electrical and hydraulic servo signals to elevation rotation of the antenna. The rotation of the tipping parts of the antenna structure about the elevation axis is accomplished by four elevation gear reducers attached to the alidade. Pinions on the output shaft of the reducers mesh with each of two bull gears mounted on the elevation wheels (Fig. 7).

1. Elevation Bull Gear

The elevation bull gear consists of 22 segments, 11 on each of the two wheels. The bull gear segments are bolted and doweled to double angle brackets welded to the elevation wheels (Fig. 8).

The bull gear is an 83-ft pitch diameter spur gear, L-shaped in cross section, with the toothed leg of 4140 steel welded to a 1020 steel mounting plate. The teeth are 3.5-in. circular pitch, 25-deg pressure angle, 9.75-in. face width, and hardened to 245-285 BHN.

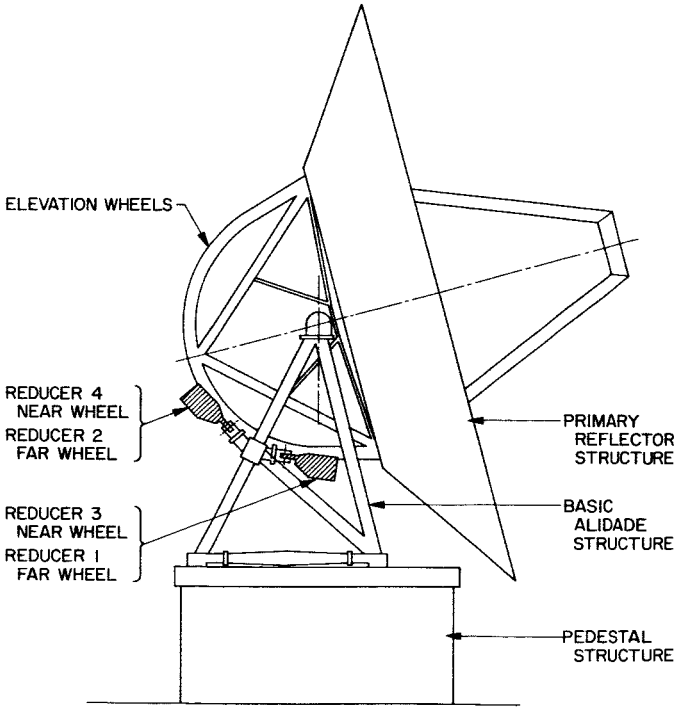

Fig. 7. AAS side view showing elevation drive reducer location

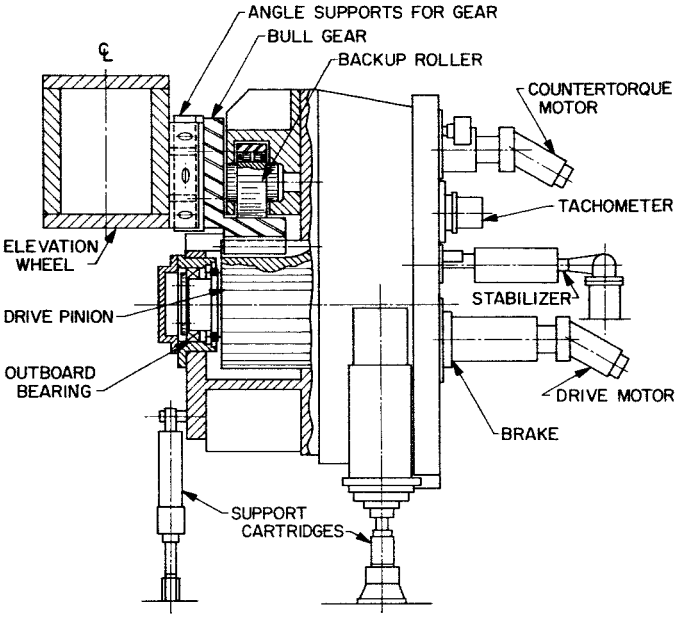

Fig. 8. Section through AAS elevation reducer, showing backup roller

2. Elevation Reducer Mounting

To achieve the requisite gear reducer stiffness and to provide proper final gear mesh alignment, the four elevation gear reducers are mounted with a linkage and backup roller arrangement. The reducer is restrained tangentially by means of a tangential link connection to a hard point on the alidade (Fig. 9). Radial restraint is accomplished by a backup roller integral with the reducer housing and rolling on a machined surface on the back of the bull gear (Fig. 8). The tangential link connection to the reducer has a spherical joint to allow the roller and the reducer to follow variations in the bull gear (Fig. 9). The tangential component of the tooth loading is taken directly into the alidade by simple tension or compression. The gear separating force is taken by the backup roller through its supporting bearings into the housing.

The major portion of the deadweight of the elevation reducers is supported by pairs of adjustable compression spring cartridges (Figs. 8 and 9). The supports are designed to maintain a minimal amount of deadweight on the backup roller in order to assure roller contact under the most adverse conditions.

3. Elevation Reducers

Each of the four reducer assemblies consists of a welded steel housing; four-stage gear reduction exclusive of the

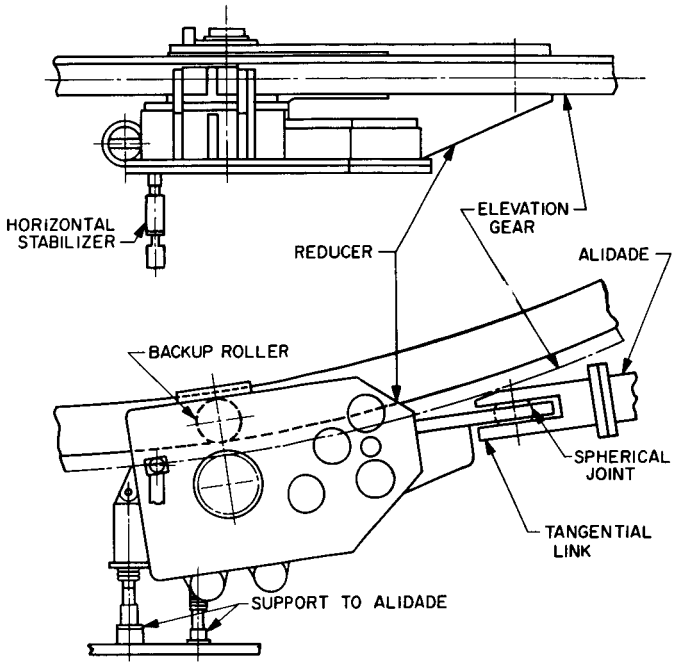

Fig. 9. AAS elevation drive reducer

final pinion-to-gear mesh; associated shafts, bearings and seals; final drive pinion and backup roller; and an integral pressure lubrication system. Each reducer has provisions for mounting hydraulic motors, a hydraulic-release spring-set brake, and a tachometer. These components are part of the servosystem. The total weight of an assembly is approximately 22,000 lb.

The first two stages in the reducer are helical gearing, while the final two meshes and the pinon-to-bullgear mesh are spur gearing. The pressure angle in all gearing is 25 deg. The ratio within the reducer is 514-to-1, which, in combination with the final pinion-to-bullgear ratio of approximately 56-to-1, makes the total ratio from motor to antenna axis 28,730-to-1. The output pinion is integral with the low-speed shaft of the reducer and has 16 teeth, 17.8-in. pitch diameter, hardened to 285-325 BHN. The backup roller is 12-in.-D and 5.5-in.-width, manufactured of 4320 steel and case-hardened to 55-60 Rc.

Maximum reducer output torque is 69,000 ft-lb and occurs with the antenna reflector at approximately 55 deg elevation, pointed downwind in a 70-mph wind. Strength and wear ratings of the gearing have been calculated according to the American Gear Manufacturers Association standards. The calculated life of the gearing exceeds the 22,000-hr (10 yr at 25% usage) design requirement established at the beginning of the project.

Lubrication within the reducers is supplied by a force-feed pressure system. This system has two pumps for redundancy; in the event of a failure of one pump, the system is switched to a standby pump.

4. Design Background

Alternate methods of mounting the reducers on the alidade were explored. The tangential link-backup roller concept was adopted for stiffness and to avoid excessive dynamic loads and the resultant stresses caused by the relatively large bullgear pitch-radius errors expected.

In elevation, a tie between opposite reducer pinions was investigated to determine if it would result in higher overall stiffness. Since it did not appreciably increase stiffness, it was discarded. Investigation was made as to the possibility of decreasing the pitch radius of the elevation gear so as to match the azimuth gear. It was found that the increased cost of the counterweight and structural changes in the elevation wheel would more than offset the savings in reducer and bullgear costs.

An investigation was made as to the best configuration of backup roller. One-, two- and three-roller systems were explored. The single-roller configuration was chosen since it results in a more desirable load path and minimum deflections.

5. Countertorque System

The countertorque system employed to eliminate the effects of backlash in the AAS elevation drives is the same as used for the AAS azimuth drives. The countertorque system used for the azimuth drives is discussed in *SPS 37-29*, Vol. III, pp. 108, 109.

D. Cassegrain Feed for the Advanced Antenna System

1. Summary

Scale model tests utilizing the 30-ft Venus Site antenna have been presented in previous reportings. Modification of the 30-ft antenna to provide a more accurate and versatile scale model is presently in progress; this work involves installation of a true scale model quadripod, installation of a precision subreflector positioner, and a series of optical tests of the reflector surface. Also during

this retrofit period, a series of scale model tests of the feed system are being performed at the Mesa antenna range. These tests are designed to provide information relating to the performance effects of various small feed system misalignments which may occur on the 30-ft antenna model and on the full-scale Advanced Antenna System.

A new approach for the AAS Cassegrain feed cone assembly has been defined since the last reporting. In this approach the upper AAS cone section will be structurally identical to the existing 85-ft antenna feed cone design, thereby allowing interchangeability of feed systems with the DSIF 85-ft antennas and also providing for direct use of existing feed technology. Three of these upper cone assemblies are being procured for the AAS; a DSIF tracking assembly, a low-noise 2295-Mc listening assembly for evaluation tests, and an ultrahigh performance 2295-Mc/2388-Mc listening assembly which will be a DSIF prototype and will be used for R&D AAS experiments.

Computer studies are in progress relating to the subreflector vertex match plate design and possible minor modification to the beamshaping flange for improved performance.

2. Recent Work

As described above, a new configuration has been selected for the AAS feed cone. As shown in Fig. 10, this configuration consists of the originally conceived bottom two AAS cone sections, an adapter section, and an upper assembly consisting of the existing 85-ft antenna feed cone design. Three upper assemblies are being procured for use with the AAS; the associated schedules and functions are given in Table 1.

Table 1. Feed cone upper assembly fabrication and test schedule

Event	Tracking; AAS acceptance tests; DSIF operations	2295-Mc listening; AAS acceptance tests	2295/2388-Mc listening; DSIF high-performance prototype/ R & D experiments
Award of cone structure contract	February 1965	Existing cone	February 1965
Award of feed contract	May 1965	Existing feed	In-house
Delivery of cone structure	May 1965	—	June 1965
Delivery of assembly to Goldstone	September 1965	June 1965	November 1965

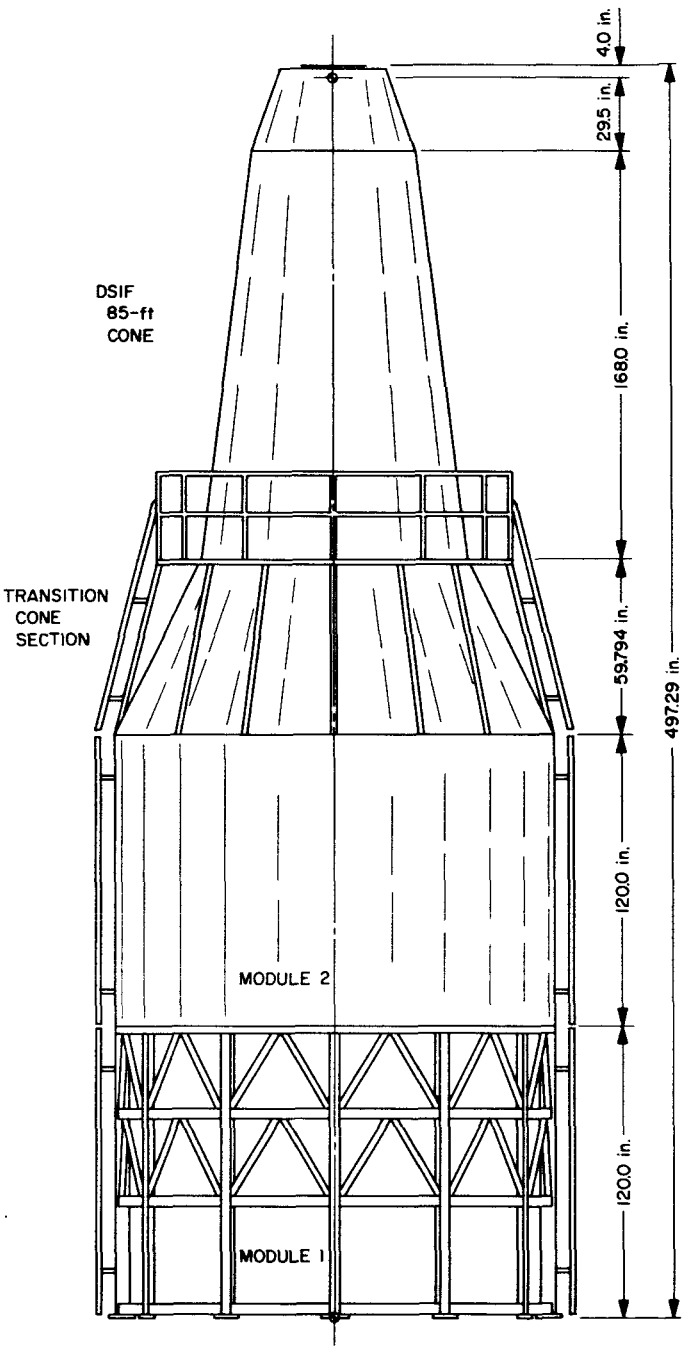

Fig. 10. New AAS feed cone configuration

The tracking assembly will be identical to the S-band GSDS 85-ft antenna feed cones presently used in the DSIF. The 2295-Mc listening assembly is an existing unit with dual-mode conical feedhorn previously used for 85-ft antenna performance evaluation.

Scale model tests of possible multimode feedhorn designs for the 2295/2388-Mc listening assembly have been previously reported (see *SPS 37-26*, Vol. IV, pp. 204–

208). At the time of this reporting, however, it is not certain that all of the existing technical problems associated with this type of horn can be solved in time for its incorporation into the 2295/2388-Mc assembly; the dual-mode type of horn is considered as the backup.

As mentioned earlier, ½-scale models of the AAS tracking feed system are being tested. Recent experimentally obtained scale model feed data includes radiation patterns of the low-noise listening feed, i.e., the horn-subreflector combination. Some data have been collected relating perturbations of the Cassegrain assembly to the radiation patterns. Perturbations accomplished thusfar include: offset hyperbola, offset horn, and tilted horn. The case of a tilted hyperbola has not been tested.

The radiation patterns for the modified suppressed-sidelobe monopulse horn model obtained at the Mesa Antenna Range, are presented in Figs. 11 and 12. These figures are to be compared with *SPS 37-29*, Vol. III, p. 110,

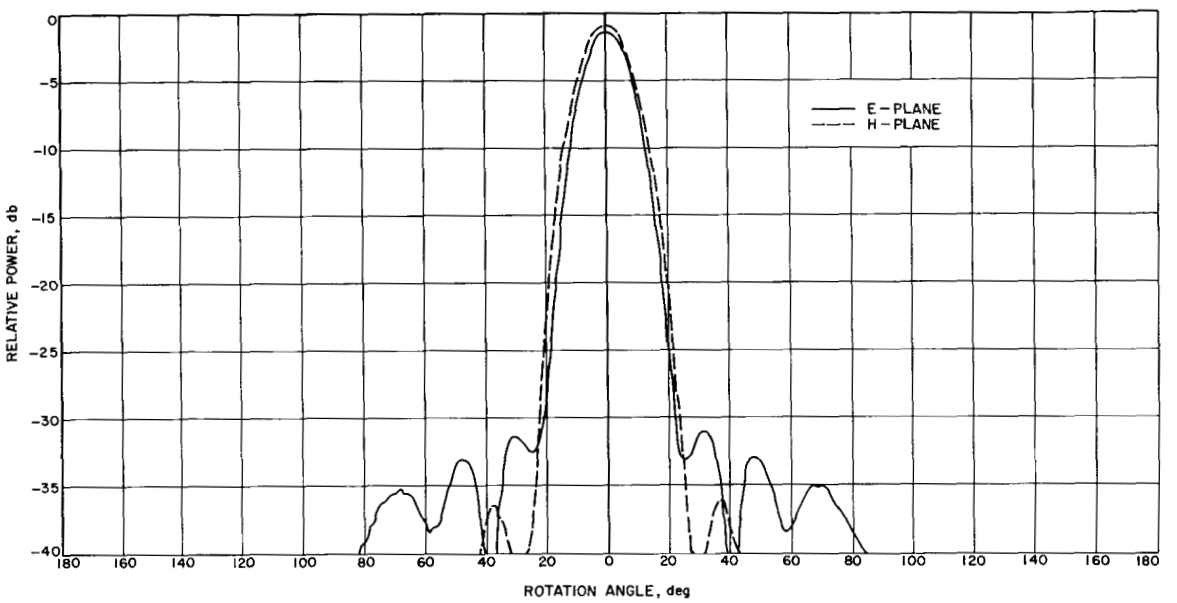

Fig. 11. 16,330-Mc modified monopulse feed sum channels

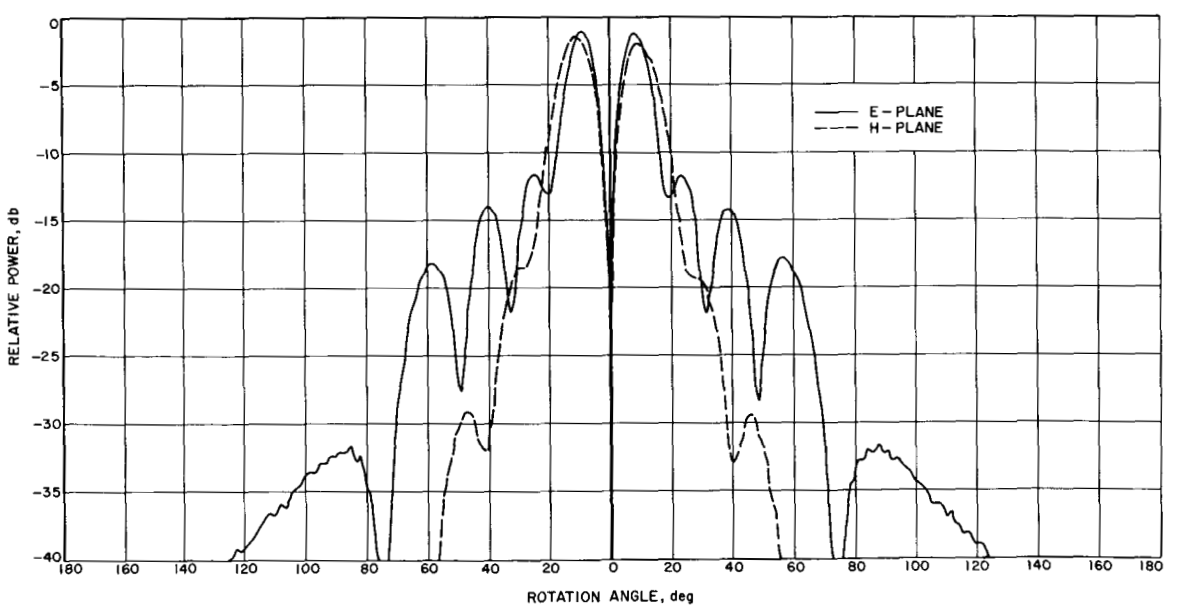

Fig. 12. 16,330-Mc modified monopulse feed error channels

Figs. 11 and 12, which show the patterns prior to sidelobe suppression. It is evident that superior E-plane performance has been achieved. Previously reported boresight null depths for the unmodified feed of 55 and 58 db have changed to 44 and 60 db for the E- and H-planes, respectively, indicating that some slight mechanical asymmetry in the E-plane has occurred.

Phase-front patterns for the suppressed-sidelobe model horn also simulate the prototype. Table 2 compares the

Table 2. Phase centers, inches behind aperture

Channel	DSIF-SCM modified feed	JPL modified feed 16,330 Mc
E-plane sum	4.0 in. avg	0.25
H-plane sum	at S-band	−0.25[a]
E-plane error	0.56 in.	1.25
H-plane error	Scaled	0.75

[a]In front of aperture plane.

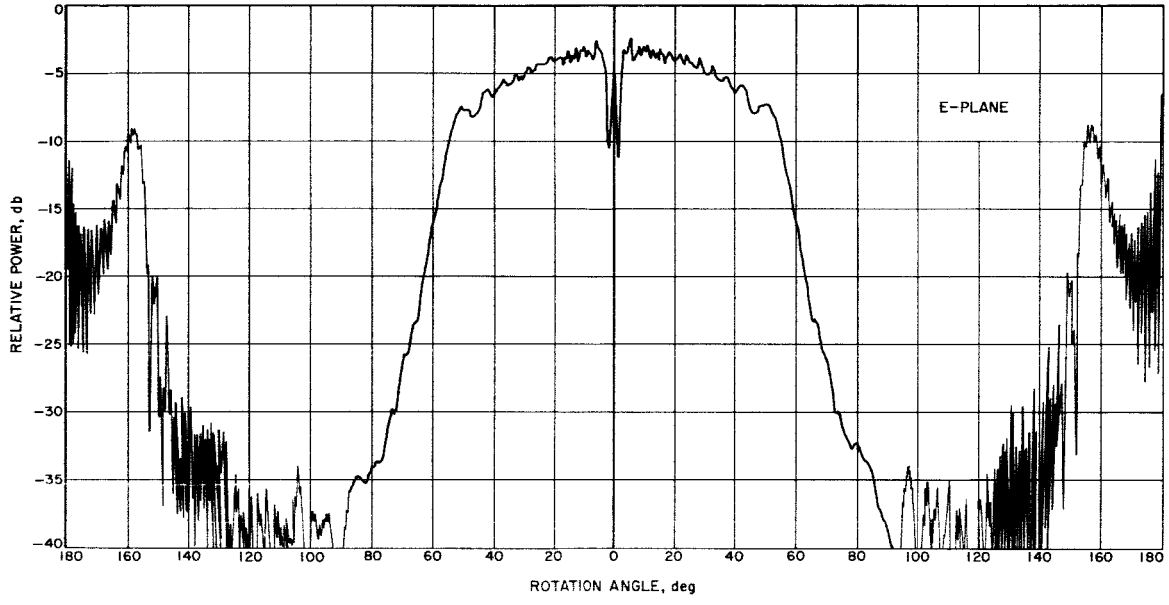

Fig. 13. 16,330-Mc Cassegrain listening feed, no flange

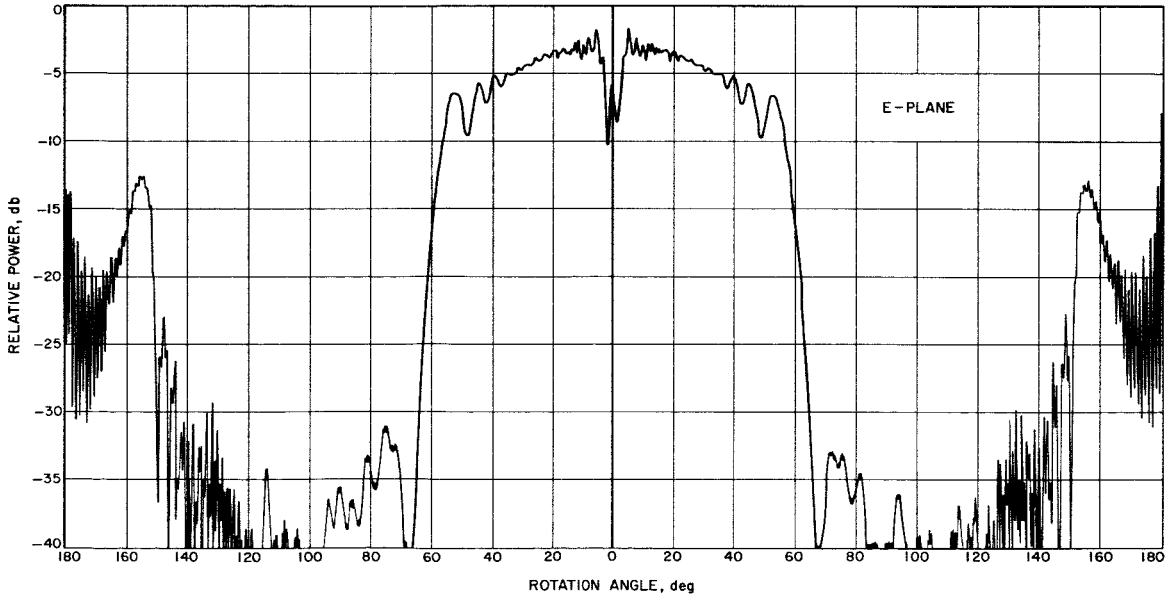

Fig. 14. 16,330-Mc Cassegrain listening feed, with flange, amplitude

DSIF accepted average value of phase centers with that of the JPL modified model. The JPL data represents interpolations believed accurate to ±0.25 in. Averaging the JPL data, in two steps, results in 0.50 in. behind the aperture. Previously reported phase centers for the unmodified feed, reported in *SPS 37-29*, Vol. III, p. 112, can be compared with Table 2; of significance is the improved phase center coincidence for the sum channel.

Subreflector scattered radiation patterns, obtained at the Mesa Antenna Range are shown in Figs. 13–17. These patterns were obtained using the dual listening feed with an optical ($\psi = 60.0$ deg) hyperboloid. Fig. 13 represents amplitude performance without the beamshaping flange, while Figs. 14 and 15 show amplitude and phase performance with the empirically derived AAS flange. The improvement in forward spillover ($140 < \psi < 180$ deg) and

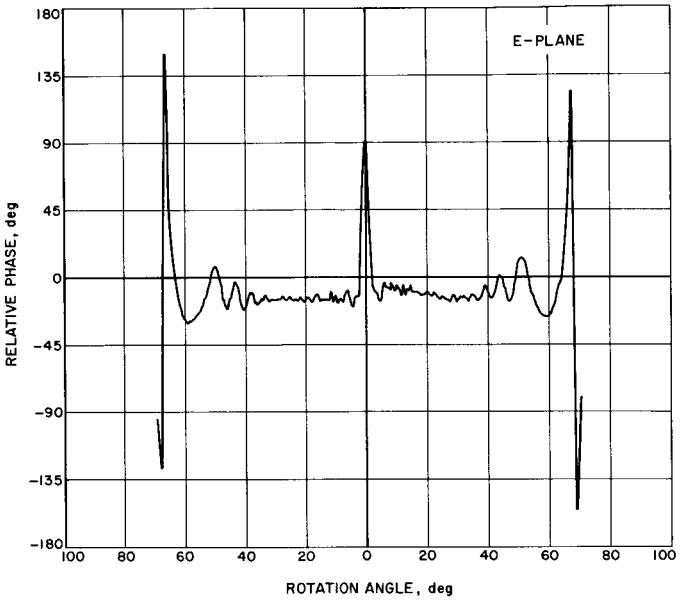

Fig. 15. 16,330-Mc Cassegrain listening feed, with flange, phase

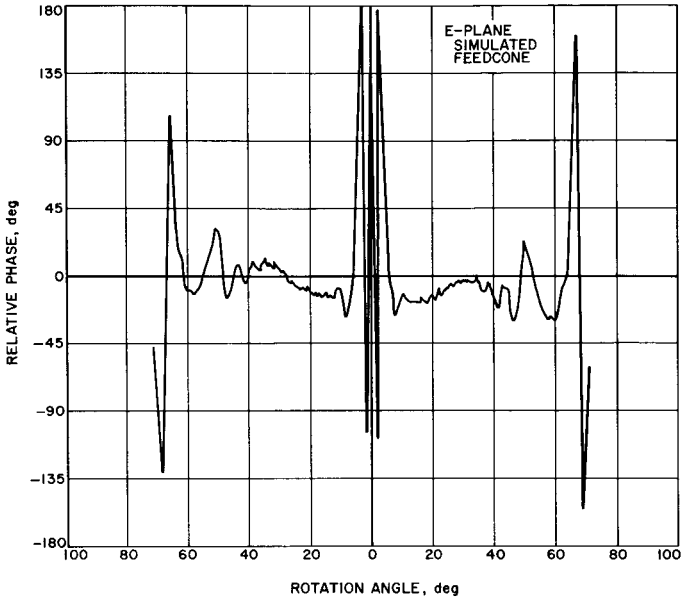

Fig. 17. 16,330-Mc Cassegrain listening feed, with flange and feed cone, phase

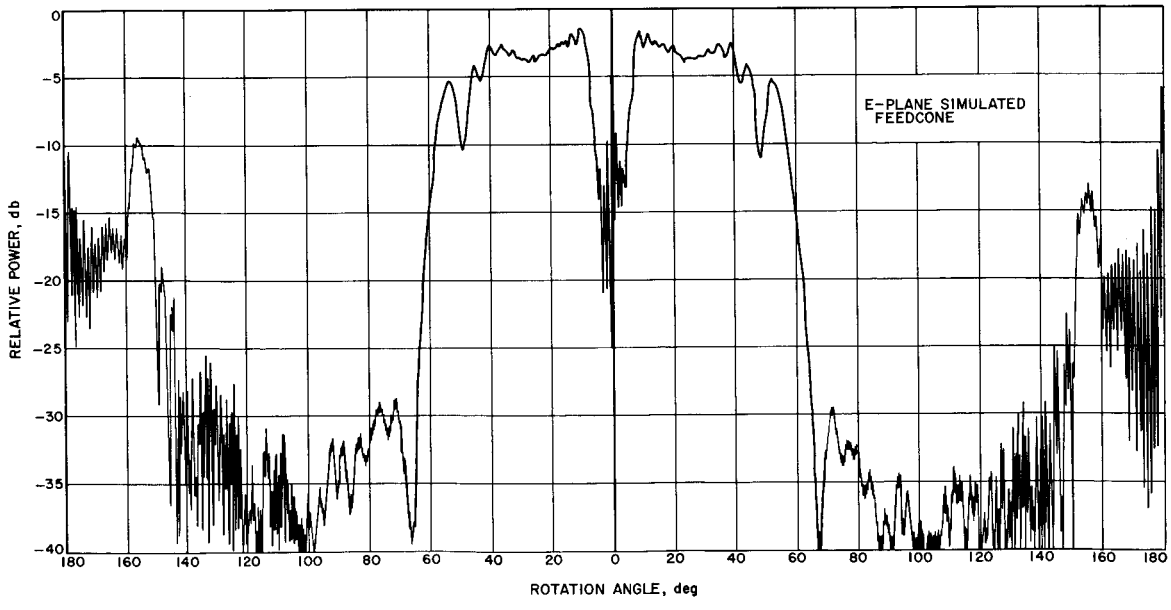

Fig. 16. 16,330-Mc Cassegrain listening feed, with flange and feed cone, amplitude

slope ($\psi \approx 60$ deg) is apparent by comparison of Figs. 13 and 14. The phase front behavior is acceptable; however, distortion is present ($\psi \approx 50$ deg), caused by the beam-shaping flange.

At this point, the question of central region ($\psi \approx 0$ deg) radiation requires some attention. Two matters require resolution; that of subreflector scattered energy intercepted by the feedhorn and subsequent feed VSWR, and that of subreflector scattered energy intercepted by the feed cone top surface and subsequent reradiation towards the subreflector. Feed return loss was directly measured on the model and found to be −31.5 db or approximately 1.06 VSWR, not a totally unacceptable value. Scattered energy intercepted by the feed cone top surface was simulated on a worst-case basis by using a flat plate around the feedhorn equivalent to 11-ft diameter on the prototype. Figs. 16 and 17, by way of comparison with Figs. 14 and 15, clearly show the magnitude of the reradiated field from the simulated feed cone top surface and the perturbations to the phase front.

In referring to Figs. 13–17, the manner of measurement should be clarified. If one were to probe the fields *between* the horn and reflector, the scattered field in the central angular region would not exhibit the oscillatory behavior shown here. As a practical matter, it is necessary to probe the fields *beyond* the horn and reflector, thus the feed horn shadows the subreflector near, and on, the axis. For this reason Fig. 16, for example, cannot be interpreted as having reduced fields near the axis.

Figs. 14–17 clearly show the necessity of a modified subreflector and/or feed horn to reduce near and on-axis radiation while not upsetting the phase front. In the past, empirically derived vertex plates have been used. It is expected that recently available analytical techniques will be valuable tools for vertex plate optimization.

During the past year, an analytical technique for synthesis of ultrahigh performance non-optical Cassegrain-type feed systems has been developed and programmed for the IBM 7094 computer. This technique, described in detail in *SPS 37-31*, Vol. IV, p. 285, analytically develops a prescribed subreflector surface and prescribed feedhorn radiation pattern to produce ultimate overall antenna performance. The type of feed horn pattern generally required is a sector beam, similar to that theoretically obtainable with the experimental multimode feed horn described above. The type of subreflector generated is an infinite surface of revolution which, in the inner region, resembles a hyperboloid with beamshaping flange and vertex matching plate. It has been shown by use of the IBM 7094 Scattering Program (see *SPS 37-31*, Vol. IV, p. 286) that truncation of the ideal infinite subreflector surface to include only the inner region has negligible effect on performance. Thus a technique now exists for

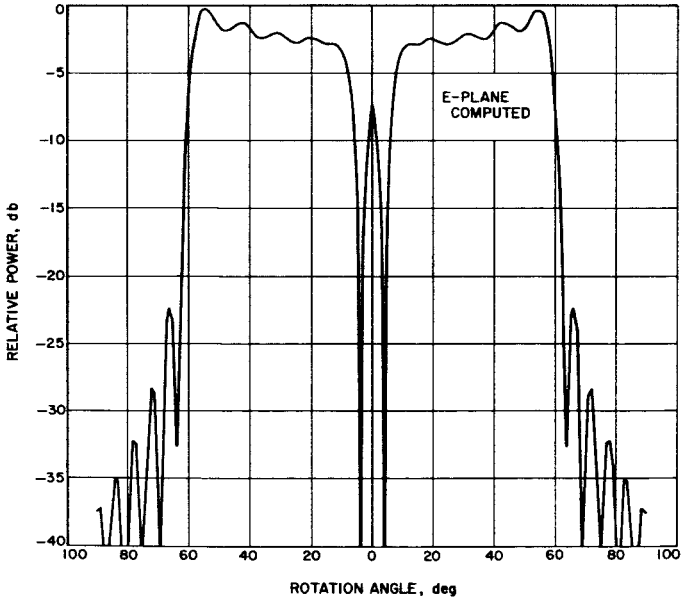

Fig. 18. Synthesized Cassegrain listening feed, ideal feed horn

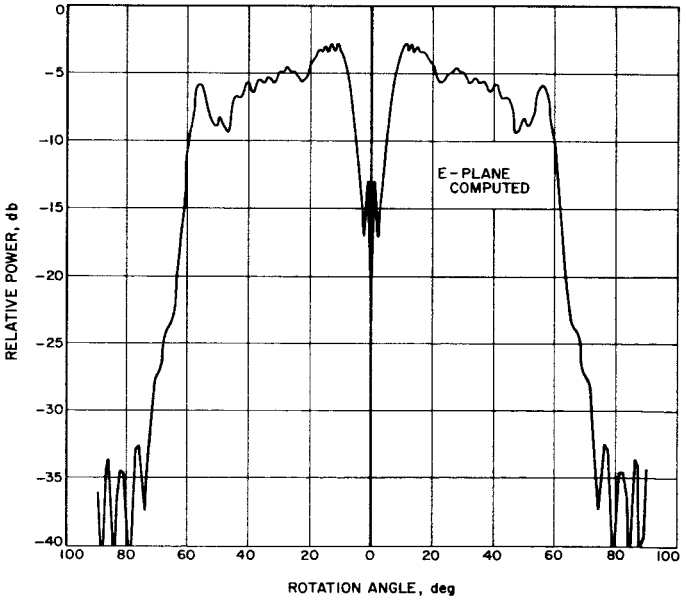

Fig. 19. Synthesized Cassegrain listening feed, dual-mode feed horn

synthesis of a physically practical ultimate performance feed system for the AAS.

The IBM 7094 Synthesis program was used to generate a subreflector surface and physically realizable required feed horn radiation characteristics for a high-quality feed having central region reduced radiation. As shown in Fig. 18, very high performance is indicated.

Because the dual mode horn is an existing medium performance feed horn, and since the generation and control of higher order waveguide modes, necessary for production of the ideal horn pattern has proved difficult, the dual mode horn is an AAS listening system backup design. Consequently, analytical work of a hybrid nature is being conducted. The Synthesis program is used to generate a prescribed subreflector surface and prescribed feed horn. The IBM 7094 Scattering program is next used with input describing the previously synthesized subreflector surface, but illuminated by a dual mode horn, rather than the ideal Synthesis pattern. Fig. 19 shows the scattered pattern of the dual mode horn-synthesized subreflector hybrid. It is encouraging to note the retention of the central reduced radiation from Fig. 18.

Fig. 20 is a specific comparison of the present AAS optical hyperboloid ($\Delta R = 0$) with empirically derived beamshaping flange and the synthesized reflector used to produce Figs. 18 and 19. It is apparent that a vertex plate and slightly different flange are called for.

Because this work is of a hybrid nature by way of utilizing a non-prescribed feed horn, it is of interest to compare the required horn performance with what is now available and what may soon be available. Fig. 21 shows the radiation patterns of three successively more sophisticated feedhorns: the dual mode horn, a four mode horn, and the Synthesis program prescribed horn, physically realizable with a presently unknown large number of waveguide modes.

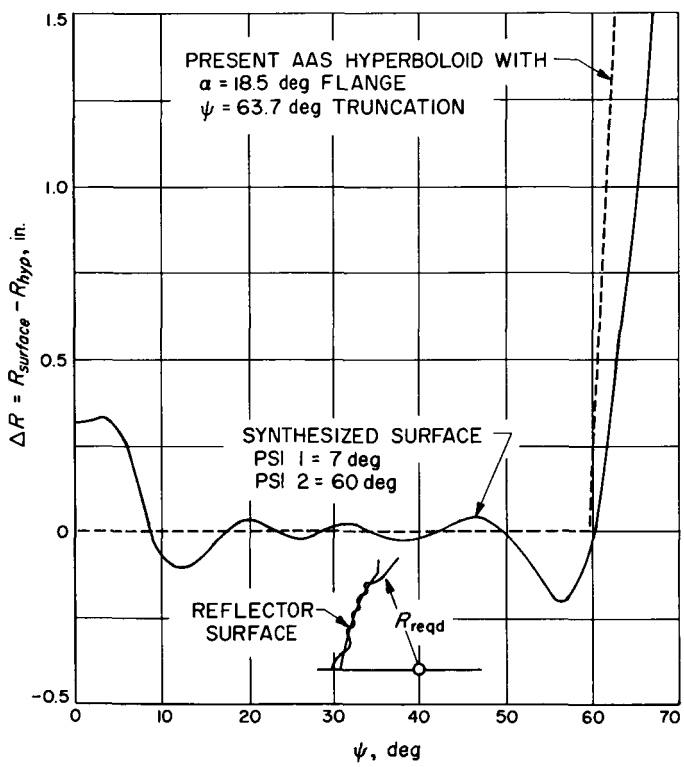

Fig. 20. Required and actual reflector surfaces

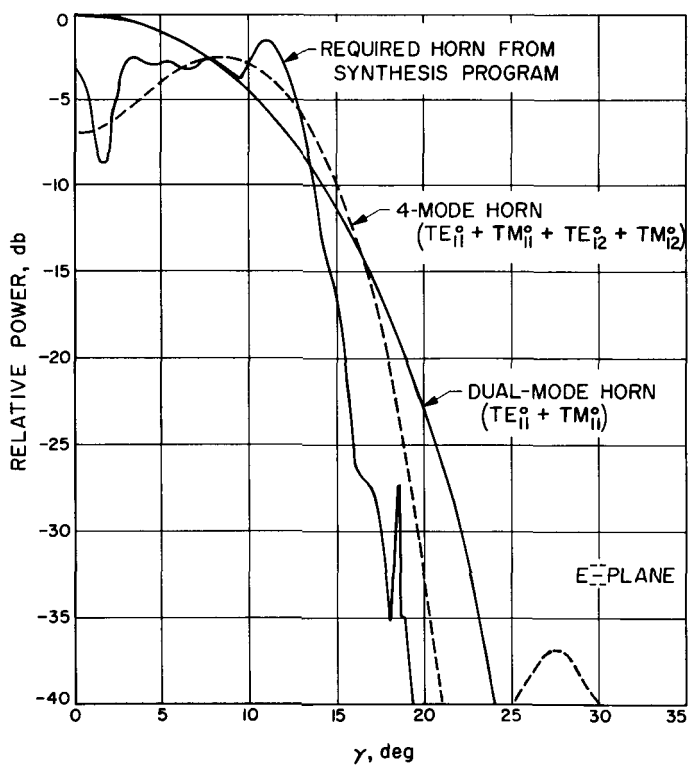

Fig. 21. Required, 4-mode and dual-mode feed horn patterns